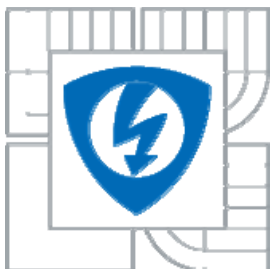# VYSOKÉ UČENÍ TECHNICKÉ V BRNĚ
BRNO UNIVERSITY OF TECHNOLOGY

FAKULTA ELEKTROTECHNIKY A KOMUNIKAČNÍCH TECHNOLOGIÍ
ÚSTAV FYZIKY

FACULTY OF ELECTRICAL ENGINEERING AND COMMUNICATION
DEPARMENT OF PHYSICS

STUDY OF SCATTERING AND POLARIZATION IN BIOLOGICAL TISSUE
STUDIUM ROZPTYLU A POLARIZACE V BIOLOGICKÝCH TKÁNÍCH

DOKTORSKÁ PRÁCE
DOCTORAL THESIS

AUTOR PRÁCE   HAMED MOHAMED ABUBAKER, MSc.
AUTHOR

VEDOUCÍ PRÁCE   Prof. RNDR. PAVEL TOMÁNEK, CSc.
SUPERVISOR

BRNO 2013

Abstract

Tissue optics becomes a rapidly expanding field of great interest and a precise knowledge of optical properties of biological tissues is essential for biomedical investigation and food quality control.

If the sample of tissue is illuminated, the multiple scattering occurs. In the case of the postmortem tissue (meat) the cell dimensions are larger than the wavelength. Mie scattering of transmitted or reflected light arises and produces various polarization states.

Polarization properties of light scattered from a scattering medium have been studied with experiments and modeling. Two modified experiments were performed: scattering of polarized light passing twice the sample (forward and backward) and only transmitted light. The measurements of scattered light display depolarization and rotation of polarized light, which depend both on orientation of the muscle fibers and ageing process of meat. Theoretical description of turbid biological tissue and computing of radiative transfer equation by modified Polarized Light Monte Carlo (PLMC) method has also been executed.

It is shown that the degree of polarization is sensitive to the optical properties of the turbid medium. The results demonstrate that polarized light scattered from a scattering medium is sensitive to the state of input polarization and the optical properties and thickness of the tissue during the ageing. The correlations of polarization changes and freshness of meat, as well as dynamic behavior of the polarization in ageing meat are shown.

Keywords

Abstrakt

Tkáňová optika nabývá rychle na významu a přesná znalost optických vlastností biologických tkání je podstatná pro výzkum v biomedicíně i pro kontrolu kvality potravin.

Jestliže je vzorek tkáně osvětlen, dochází k mnohonásobnému odrazu světla. V případě postmortem neživých tkání (maso) je rozměr buněk větší než vlnová délka použitého světla. Dochází k Mieovu rozptylu prošlého nebo zpět odraženého světla, v důsledku čehož se objevují různé polarizační stavy světla.

Polarizační stavy světla rozptýleného na difúzním prostředí jsou experimentálně zkoumány a modelovány. V práci jsme provedli dva modifikované experimenty: rozptyl polarizovaného světla, které dvakrát prochází vzorkem (vpřed a vzad) a jen světla, které jen prochází vzorkem. Měření rozptýleného světla ukazuje, že dochází k depolarizaci a ke stáčení polarizační roviny, což obojí závisí na orientaci svalových vláken a stárnutí tkání postmortem. Mimo experimentů byl také proveden teoretický popis difúzní biologické tkáně a byla vypočtena radiační přenosová rovnice pomocí modifikované Monte Carlo metody, která zahrnuje polarizační stav světla (PLMC).

Je ukázáno, že stupeň polarizace podstatně závisí na optických vlastnostech rozptylového prostředí. Výsledky ukazují, že stav polarizace světla na výstupu závisí na stavu polarizace světla před vzorkem a na optických vlastnostech a tloušťce vrstvy prostředí v průběhu jejího stárnutí. Je také provedena korelace změn polarizace na čerstvosti masa, i popis dynamického chování polarizace při stárnutí masa.

Klíčová slova

Biologická tkáň, světlo, rozptyl, polarizace, Stokesův vektor, Muellerova matice, Monte Carlo, stárnutí, výpočet, měření

Affirmation

I declare that my thesis "Study of scattering and polarization of light in biological tissues," was elaborated by myself under professional leadership by my supervisor, and on the basis of the recommended technical literature, which is completely cited in the References.

Brno, February 25 2013 …………………………………………………

Hamed Mohamed ABUBAKER

Acknowledgments

It would be impossible to thank all the people who have helped me both personally and with this work. However here are a few people to whom I owe my gratitude, and without their tremendous support, I could not have made this journey.

First of all I would like to thank my advisor, Prof. Dr. Pavel Tománek, CSc. A lot of what I learned these past four years, not just academically but as a person, I owe to Prof. Tománek. He was also a great source of motivation and I am lucky to have him as my supervisor and mentor.

I would like to thank Prof. Ing. Lubomír Grmela, CSc., head of the Department of Physics and Doc Ing. Karel Liedermann, CSc. who always gave me advice and encouragement when I needed it the most. It was a pleasure to meet them not only as research colleagues but also as really good friends.

I would also like to thank all other members of the Department of Physics for their help, when I had difficulties with my research, and for their warm friendship.

Last but not least, I would also like to thank Prof. Dr. Carol Chase from Knox College, Galesburg, MI, USA for her willingness to read the text and correct my English in this dissertation.

Finally, I would like to express my thanks to my family who always believed in me and have always been my biggest supporter.

Brno, February 25, 2013   Hamed Mohamed ABUBAKER

CONTENTS

List of symbols

a	scattering particle radius
a	polarization ellipse major axis
b	polarization ellipse minor axis
c	concentration of the absorbing material
c	propagation speed of light
$d_{21}(\Theta)$	element of scattering matrix
g	anisotropy function
k	wavenumber
$\mathbf{k}$	wave-vector
l	photon step size
l^{*}	transport mean free path
l_s	scattering mean free path
m	relative refractive index of the scatterer
$m(\mathbf{r})$	relative refractive index at a point $\mathbf{r}$
n	refractive index
$p(\hat{s},\hat{s}')$	scalar Mie phase function
$p_{11}(\Theta)$	element of scattering matrix
$p_{21}(\Theta)$	element of scattering matrix
$\mathbf{r} = \mathbf{r}(\theta,\phi)$	direction of propagation of scattered wave
r	distance from scatterer
r_λ	reflection loss
$\hat{s},\hat{s}'$	direction of propagation unity vectors
$s_{21}(\Theta)$	element of scattering matrix
t	time
x	thickness of the sample
$x = kD/2$	size parameter
z	propagation direction
A	amplitude
A	cross section of particle
A_i	mixing coefficient
A_{km}	Kubelka-Munk absorption coefficients
D	diameter of the scatterer
DP	differential path-length
DPF	differential path-length factor
$\mathbf{E}$	electric field

E	electric field wave amplitude
G	additive term due to the scattering loss
I	intensity of transmitted light
I	total intensity
I_0	intensity of incident light entering the material
$I(r,t,\hat{s})$	radiance
$\mathbf{J}$	Jones matrix
$J(r,t)$	photon flux
$\mathbf{K}$	identity matrix
L	optical thickness of slab
$\mathbf{L}(\sigma)$	rotation operator
$\mathbf{M} \equiv \mathbf{M}(\Theta)$	Mueller matrix
$\mathbf{M}_t$	Mueller matrix of the train
N	number of scatterers
$\mathbf{P}(\mu_2,\phi_2;\mu_1,\phi_1)$	phase matrix
Q	polarization at 0° or 90° to the scattering plane,
$R(\theta,\phi)$	form factor
R	reflectance
R_d	diffuse reflection
$\mathbf{S}$	Stokes vector
$\mathbf{S} \equiv \mathbf{S}(\Theta)$	scattering matrix
S_i	components of the scattering matrix
S_{km}	Kubelka-Munk scattering coefficient
T	transmittance
T_d	diffuse transmission
$\mathbf{T}(2\theta)$	standard rotator matrix
$\mathbf{T}(-2\theta)$	counter-rotator matrix
U	polarization at ± 45° to the scattering plane
V	left or right circular polarization
V	volume
W	weight
α	isotropic polarizability of scatterer
α	absorption coefficient
α_R	dichroism in polarizer

β	absorption per concentration coefficient	μ_t	total attenuation coefficient of unscattering medium
γ	angle between the radial direction and the direction of the initial ray	ρ	angle of fast axis of retarder
γ	leakage in polarizer	ρ	particle density (or volume density)
δ	phase of the wave scattered in direction (θ,ϕ)	ρ_n	probability that a photon gets scattered n-times
δ_p	strain in polarizer	σ	rotation angle
δx	phase angle of E_x	σ_a	absorption cross section
δy	phase angle of E_y	σ_s	scattering cross section
$\partial_{eff} = 1/\mu_{eff}$ effective penetration depth		$\tau = \omega t - kz$ propagation term (wave phase)	
ε	phase	θ	incident angle
$\Delta\varepsilon$	phase difference	θ	polar angle
φ	parameter used in the arguments of I_n	θ	scattering angle
		θ'	reflected angle
φ_P	optical activity of polarizer	ξ	randomly generated number
φ_R	optical activity of retarder	ω	frequency
ϕ	azimuthal angle	ω	effective albedo
χ	angle of ellipticity		
$\kappa(r)$	diffusion coefficient	Γ	mean number of scattering events
λ	wavelength		
λ	parameter of regularization	Δ	depolarization factor
μ_a	absorption coefficient of the medium	$\Phi(t)$	photon density
		$\Phi_i(t)$	photon density approximation
$1/\mu_a$	absorption mean free path	Θ	phase function of the angle between the incident and scattered light
μ_{eff}	effective attenuation coefficient		
μ_s	scattering coefficient		
μ'_s	reduced scattering coefficient	Ω	solid angle

Abbreviations

BSDF	Bidirectional Scatter Distribution Function
BT	biological tissue
DOP	Degree of polarization
DOP_C	Degree of circular polarization
DOP_L	Degree of linear polarization
EM	Electromagnetic
FEM	Finite Element Method
MC	Monte Carlo
NIR	Near Infrared
PDE	Partial Differential Equation
PDF	Probability Density Function
PLMC	Polarized Light Monte Carlo
RTE	Radiative Transfer Equation
TOAST	Temporal Optical Absorption and Scattering Tomography

List of figures and tables

List of tables

1 INTRODUCTION

The objects or structures existing in the nature and forming object fields can be divided into deterministic (regular), random (statistic) and fractal (self-similar) ones. As a consequence, the set of parameters used to characterize such the structures, would differ considerably. As a good example, the biological tissues or food materials display large compositional variations, inhomogeneities, and anisotropic structures. Tissue optics is a rapidly expanding field of great interest to those involved mainly in the development of optical medical technologies and food control. The composition of tissue can be affected by process conditions and material history. It is difficult to define what exactly constitutes an engineering property of a certain food. In general, however, any attribute affecting the processing or handling of a food can be defined as engineering properties [1].

Traditionally, these properties are divided into the following categories:
- **mechanical** (structural, geometrical, and strength),
- **thermal** (specific heat, thermal conductivity, and diffusivity),
- **electrical** (conductivity and permittivity),
- **optical** (color, gloss, and translucency) properties.

Most of them indicate changes in the chemical composition and structural organization of tissues or foods ranging from the molecular to the macroscopic level. A change in either composition or structure usually results in a simultaneous change in several properties.

The variety of methods and instruments for in-line process and quality control and for rapid measurements in the biomedicine and food industry has rapidly expanded [2,3,4]. Many different measuring setups, as well as sensors have been investigated. The refractive index of biological tissue is a fundamental parameter in applications of optical diagnosis and laser treatments [5]. Chemical sensors and biosensors, including semiconductor, acoustic and optical devices as well as direct electric measurement, offer considerable potential for the monitoring of food composition and the prediction of microbial and rancid degradation. The water activity of foods is one of the parameters used to predict their stability during storage. Compositional analysis with infrared, microwave and ultrasonic techniques offers the advantage of non-invasive hygienic in-line monitoring. Based on a knowledge of the dielectric and acoustic properties of foods, these techniques can be applied to a range of in-line analysis tasks [3, 6].

Since the topics of the thesis deal with optical properties of postmortem processed meat, we targeted them, particularly the scattering and polarization of light in interaction with matter.

So, the optical imaging is a powerful approach for visualizing tissue structure and function across spatial scales ranging from micrometers to centimeters. Tissue optical imaging technologies are generally discussed in two broad regimes, microscopic and macroscopic, which are based on controlling and measuring coherent and diffuse light-tissue interactions, respectively.

When an obstacle is illuminated by an electromagnetic (EM) wave, electric charges in the obstacle are set into oscillatory motion by the electric field of the incident wave [7]. The accelerated charges re-radiate EM energy in all directions. This secondary radiation is called the radiation scattered by obstacle. If the frequency of scattered light is the same as that of incident light, then the scattering event is caller as elastic scattering. If the incident EM energy is transformed into thermal energy, then the process is labeled as inelastic scattering and is called as absorption [9].

Light scattering and polarization are widely used in biological research to determine particle numbers, particle sizes, axial ratios, size distributions, particle mobility, and indices of refraction. Light scattering in biological tissues originates from the tissue inhomogeneities such as cellular organelles, extracellular matrix, blood vessels, etc [4]. This often translates into unique angular, polarization, and spectroscopic features of scattered light emerging from tissue, and therefore information about tissue macroscopic and microscopic structure can be obtained from the characteristics of scattered light [9]. Recognition of this fact has led to a long history of the studies of light scattering by biological structures such as cells and connective tissues.

Polarized light plays important roles in the understanding of the nature of electromagnetic waves [7], elucidating the three-dimensional characteristics of chemical bonds [10], uncovering the asymmetric (chiral) nature of biological molecules [11], determining sugar concentrations in industrial processes [12], quantifying protein properties in solutions [13], supplying a variety of nondestructive evaluation methods [6], developing advanced concepts such as polarization entropy [14], contributing to remote sensing in meteorology and astronomy [15], and differentiating between normal and precancerous cells in superficial tissue layers [16], as well as other biomedical applications [17].

The biological tissue is a turbid medium where significant depolarization is provided due to strong multiple scattering effects, inhomogeneities in the media cause scattering which may alter the direction of propagation, polarization and phase of the light [4]. The propagation of light through such media may be analyzed either by means of the wave or the photon theory, respectively [7]. Photons travel in straight line paths until they encounter an inhomogeneity, where they are scattered in random directions. Most of studies measure only the small-angle differential scattered light intensity even though

much more additional information is contained in the polarization states of the differentially scattered light.

Traditional optical spectroscopic techniques are rigorous and are well established in simple, homogeneous, optically thin samples. On the other hand, diffuse optical imaging and spectroscopy aims to investigate tissue physiology millimeters to centimeters below the tissue surface [2, 18]. Traditional optical spectroscopy can not be used for this purpose, since light is strongly scattered in tissue. In addition, in order to reach tissue located centimeters below the surface there must be significant light penetration. Fortunately, a spectral window exists in the near-infrared, wherein the reduced absorption coefficients of water and hemoglobins enable photons travel deep into tissue. Therefore, near-infrared photon transport in tissues is dominated by scattering rather than absorption [18].

The multiple scattering of light within a material is an area of considerable interest [4,6]. In medical diagnostics, the analysis of scattered laser light from tissue samples is increasingly being used as a diagnostic tool [19]. Some attemps in biomedical polarimetry have been made in the context of optical imaging, specifically using polarization gating to separate out and potentially remove the multiply scattered (depolarized) component of the light beam in order to enhance contrast and to improve tissue imaging resolution [20]. This has proven moderately successful in selected applications, provided that proper attention is paid to the optimal choice of incident polarization states (e.g., linear versus circular), polarization detection schemes (e.g., Stokes versus Mueller polarimetry) [21-24], geometry of detection (e.g., transmission versus reflection) [25], etc.

Early physical property analyses of food products required constant uniform values and were often oversimplified and inaccurate. Unfortunately, the biological tissue is a complex medium, so some simulation is necessary. Nowadays, computational engineering techniques, such as the finite element or Monte Carlo methods [26, 27], are much more sophisticated and can be used to evaluate non-uniform properties (for example, thermal properties) that change with time, temperature, and location in food products that are heated or cooled when stored.

Mathematical models have been fitted to data as a function of one or several experimental parameters, such as temperature, water content, porosity, or other food characteristics [28]. Both modern and more conventional measurement methods allow computation of these properties, which can provide information about the macrostructural effects of processing conditions in fresh and manufactured foods.

Nevertheless a little attention was paid to the ageing process in the meat structure.

This thesis reports the polarization curling properties of light transmitting through or back-scattered from some slices of meat for food, corresponding to the rotation angle of polarizer. This property points out to the existence of polarization shifts in function of meat ageing process.

1.1 Objectives of dissertation thesis

In this dissertation we want to characterize the bio-materials (different kinds of meat) going to the ageing with Stokes and Mueller matrix optical polarimetry. To seriously tackle the problem we need first to examine the physical nature of the scattering of polarized light and to see how multiple scattering affects the degree of polarization. Knowledge of this fact would aid in determining the validity of using scalar theories in analyzing the multiple scattering of polarized light.

The images and matrix elements with Mueller calculus provides a comprehensive information of samples due to which it is possible to combine all the necessary parameters for describing a beam of light into a single image. The resultant describing the light beam is simply the four-parameter Stokes vector and determined by measuring a flux transmitted through a set of polarization optics: polarization generating optics provide linear and/or circular polarized light to sample and polarization analyzing optics collect polarized output light from sample to detecting devices. The characteristic Mueller matrix in all experiments contains 16 elements, having total 49 intensity measurements at different polarization states. In practice, all 16 elements may not be independent. Only seven of sixteen Mueller matrix elements are independent and others depending on the symmetry and certain properties of the optical medium.

Therefore objectives of the dissertation are to provide
- better understanding of nature of various physical phenomena (polarization, scattering, birefringence) in turbid media and in biological tissue, and
- measurement of temporal changes of polarization states due to multiple scattering of light in biological tissues going to ageing.

These objectives also include a detailed study of:
1. complicated nature of polarization effects in tissue, including simultaneous multiple effects,
2. depolarization of signal generated by tissue multiple scattering,
3. difficulties in measuring typically small tissue polarization signals,
4. analysis and quantification of measured signals or images, and mainly
5. complexity in understanding and interpreting tissue polarimetry results.

1.2 Organization of thesis

Having introduced the main objectives of the project, this section will give an overview of the development of the thesis towards the goal of non-invasive tissue measurement.

Chapters 2 to 4 represent the introduction to the field. Due to the complexity of the biological tissue, they not only bring a review of state of-the-art, but also represent their modifications which we have made for our purpose.

In Chapter 2, the concept of light propagation in biological tissue is first introduced and optical properties of biological tissue are discussed, stressing the scattering and polarization of light by different tissue components and in whole tissues. Then the direct and indirect methods of optical properties measurement are schematically overviewed, and different models of light transport based on modified Beer-Lambert law, Kubelka-Munk model, radiative transfer theory are described, and their use in determining the optical properties of tissue is established.

Very short Chapter 3 describes different types of biological tissue and introduces the Rayleigh and Mie elastic scattering on small particles. Then shortly explains three basic classes of photons passing through random media.

Chapter 4 discusses the principles of scattering and polarization properties of biological tissue. The single and multiple scattering of the light in turbid medium are described by scattering matrix. Due to the measurements in forward and backward propagation direction of light, the problem of multiple scattering is introduced. First, the description of polarized light in terms of Stokes vectors is outlined. Subsequently, the interaction of polarized light with a scattering medium is characterized in terms of a Jones and Mueller matrices. The degree of polarization (DOP), which is important characteristic in ageing measurement, is also introduced.

Chapter 5 describes experimental setups used for measurements of polarization properties of light scattered in forward and backward directions, respectively, which accurately allow determine various characteristics of biological tissue.

Chapter 6 gives the results and discussion of computed and experimental results. Monte Carlo analysis of multiscattered light using introduced polarized light (PLMC) method is considered and the intensity of transmitted and back-scattered light is computed: first four elements of Mie phase matrix, then normalized intensities vs. distance of detector r for a number of size parameters x and optical thicknesses L are computed. The difference between the vector and scalar radiative transfer solutions for diffuse light field in distance r and computed Degree of linear and circular polarization for the same parameters x and L are also presented. The experimental measurements of polarization rotation in dynamic temporal and thermal changes in processed meat are shown, and the comparison of simulated and measured bask-scattered Mueller matrices for pork chop fibers is provided.

Chapter 7 summarizes obtained methods, results, shows the problems raised in the study of very complex media, which we met during the thesis work. Finally it suggests outlines for further work, highlighting the direction towards more automatic measurement of biological tissue ageing.

2   LIGHT – MATTER INTERACTION

2.1   Waves as information carriers

Light is used for sensing a variety of parameters, and its domain of applications is so vast that it pervades all branches of science, engineering, and technology, biomedicine, agriculture, etc. Devices that use light for sensing, measurement, and control are termed optical sensors. Optical sensing is generally noncontact and noninvasive, and provides very accurate measurement. In many cases, accuracy can be varied over a wide range. In these sensors, an optical wave is an information sensor and carrier of information.

Any one of the following characteristics of a wave can be modulated by the measured property (the measurand) [7]:
• Amplitude or intensity
• Phase
• Polarization
• Frequency
• Direction of propagation.

However, the detected quantity is always intensity, as the detectors cannot follow the optical frequency. The measured property modifies the characteristics of the wave in such a way that, on demodulation, a change in intensity results. This change in intensity is related to the measured property. In some measurements, the wave intensity is modulated directly, and hence no demodulation is used before detection.

2.2.   Optical properties of biological tissues

Light traveling through tissue experiences two main types of interaction: absorption and scattering. Other forms of radiation are also absorbed by tissue. Indeed it is the absorption of x-rays that enables an image to be created. Scatter, however, is a property that is far more dominant for light and so cannot be ignored as it is for other imaging modalities [4]. The principal optical properties in biological tissue to be discussed are:
    - reflection,
    - transmission,
    - absorption,
    - scattering,
    - anisotropy,
    - refractive index,
and some of them are shown schematically in Fig. 2.1.
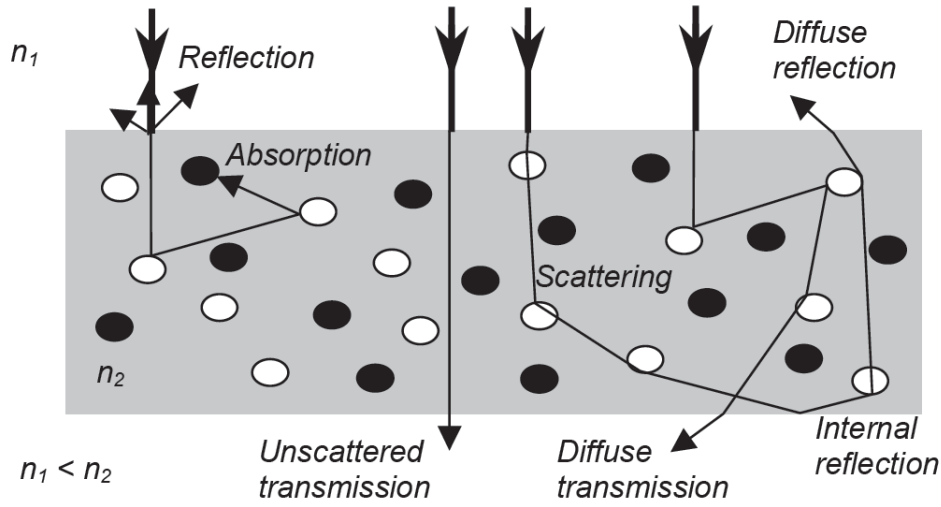
Fig. 2.1 Schematic diagram for the interaction of light with matter.

All of these properties are dependent on the wavelength of the light probing the tissue. Additional optical characteristics of tissues include their fluorescence and inelastic scatter properties.

2.2.1 Transmission

When light passes through an object, it is called transmission (Fig.2.1). Absorption, reflection, refraction, and diffusion (explained in the following sections) all affect light transmission components, thus revealing the effects of dispersion.

2.2.2 Absorption

An object can absorb part or all of incident light, usually by converting it into heat. Many materials absorb some wavelengths while transmitting others, which is called selective absorption.

Absorption is the transfer of energy from incident radiation to the surrounding tissue. If a non-scattering medium is illuminated with a collimated beam of light with intensity I_0 and wavelength λ, the intensity of the emerging light is given by Lambert´s law [29]

$$I = I_0 e^{-\mu_a d} \tag{2.1}$$

where I is the intensity of transmitted light, I_0 intensity of light entering the material, μ_a is the absorption coefficient of the medium and d is the thickness of the sample. Lambert's law of absorption states that equal thicknesses of a given homogenous material absorb the same fraction of light.

 The absorption coefficient is the number of absorption events per unit length (mm^{-1} or cm^{-1}). It follows that its reciprocal $1/\mu_a$, often called the absorption mean free path, is the distance required for the intensity to fall to *1/e* of the original value.

Beer's law further breaks down the absorption coefficient μ_a into two variables: particle density (or volume density) ρ of an absorber as the number of absorbing particles per unit volume, and the absorption cross section σ_a, as the cross section area that a perfect absorber would have to cause the equivalent attenuation to a collimated light beam, then we can also express the absorption coefficient as the cross-sectional area of absorption per unit volume medium.

$$\mu_a = \rho\sigma_a \qquad\qquad (2.2)$$

Thus by substituting equation (2.5) into equation (2.4) we obtain Beer-Lambert´s law:

$$I = I_0 e^{-\rho\sigma_a d} . \qquad\qquad (2.3)$$

Within biological tissue there are various substances that contribute to the absorption of light, known as chromophores. Figure 2.2 shows the absorption spectra of some common chromophores from the UV to the mid infrared region of the electromagnetic spectrum, as well as the absorption spectra for water [17].
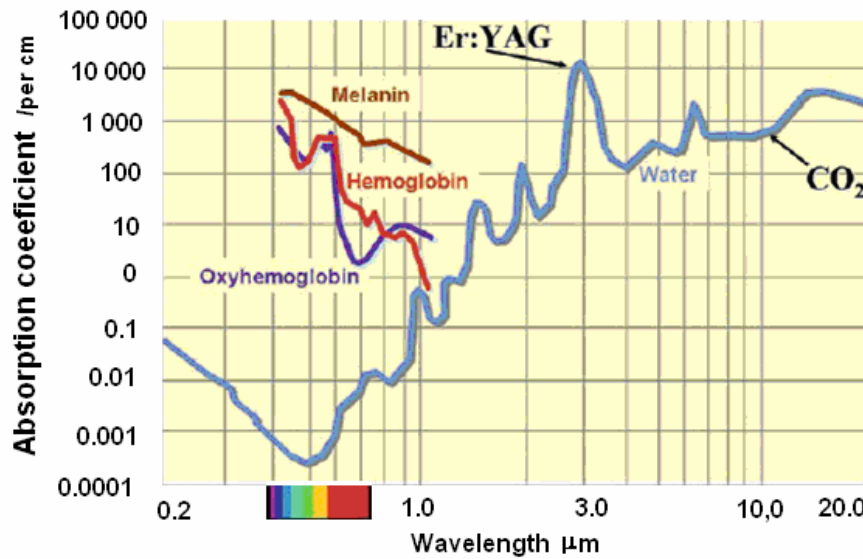
Fig. 2.2 The absorption spectra for the main chromophores found within tissue [17].

As can be seen, the water (which is contained in biological tissue) has a low absorption over the NIR range. Water can, nevertheless, strongly influence measurements due to the high concentration. In most tissues water is the major constituent with 30 - 60%, this means that the accumulative absorption effect cannot be ignored.

2.2.3 Scattering - Diffusion

When light strikes a perfectly smooth surface, the reflection is specular. When light strikes a rough surface, the light is reflected or transmitted in many different directions at once, which is called diffusion or scattering (Fig. 2.1).

The amount of diffuse transmission or reflection that occurs when light moves through one material to strike another material depends on two factors:
- the difference in refractive index between the two materials, and on
- the size and shape of the particles in the diffusing material compared to the wavelength of the light.

For example, the molecules in air happen to be the right size to scatter light with shorter wavelengths, giving us blue sky. One method of describing diffusion is the bidirectional scatter distribution function (BSDF), which quantifies scatter and its effects.

When an obstacle is illuminated by an EM wave, electric charges in the obstacle are set into oscillatory motion by the electric field of the incident wave. The accelerated charges re-radiate EM energy in all directions. This secondary radiation is called the radiation scattered by the obstacle. If the frequency of the scattered light is the same as that of the incident light, then the scattering event is called as elastic scattering. If the incident EM energy is transformed into thermal energy, then the process is called as absorption. Scattering and absorption are not mutually independent processes, though, depending on the situation, one may be more prominent than the other.

Optical scattering is caused by inhomogeneity in the refractive index n of a medium. The intensity and spatial distribution of the scattering light depends on the size and shape of the inhomogeneity relative to the optical wavelength and disparity of the refractive index. Two cases of scattering are usually considered. Rayleigh scattering relates to scattering particles whose radius a is considerably smaller than wavelength λ of the incident light. The Mie scattering occurs normally when the size of a particle illuminated by visible or near-infrared light is larger than one micrometer. The effect of scattering can be thought of as a removal of a proportion of the incident intensity from the propagating beam, in much the same way as the effect of absorption [4].

Scatter is the phenomenon that causes the direction of radiation within a medium to be changed. Just as the absorbing properties of a medium can be described by its absorption coefficient μ_a so the scattering coefficient μ_s can describe its scattering properties. In the case of a collimated source and single scattering this is given by:

$$I = I_0 e^{-\mu_s x} \tag{2.4}$$

where I is the non-scattered component of light after traversing a non-absorbing medium of thickness x. The scattering coefficient can also be described in terms of the particle density ρ and the scattering cross section σ_s such that:

$$\mu_s = \rho\sigma_s \, . \tag{2.5}$$

The scattering coefficient μ_s represents the probability per unit length of a photon being scattered.

2.2.4 Anisotropy

The scattering properties of bulk media (like biological tissue) are often described in terms of the reduced scattering coefficient μ'_s.

$$\mu'_s = \mu_s(1-g) \tag{2.6}$$

where the anisotropy function g is given as:

$$g = \int_{4\pi} p_{11}(\Theta)\cos(\theta)\cos(\varphi)d\varphi \, . \tag{2.7}$$

The phase function $p_{11}(\Theta)$ is a function of the angle between the incident and scattered light, and in the following it is known as a scalar Mie function. It is assumed that Θ is independent of θ, the orientation of the scatterer.

2.2.5 Polarization

Since the thesis deals with imaging using polarized light, we begin with the most basic notion of polarization of light, its representation and measurement. Polarization is a property which arises out of the transverse nature of the electromagnetic (EM) radiation, and is related to the orientation of the plane of vibration of its electric field. The magnetic field associated with the radiation is not taken into account to denote polarization.

All light waves are composed of electric **E** and magnetic **B** field vectors and are mutually orthogonal to each other and the direction of propagation. We take only electric field. In the electric field the polarization states (i.e. vertical or horizontal) refer to the orientation of **E**, it is assumed that the direction of propagation **k** is in the *z* direction. Polarization states arise from relationship between the magnitude and phase of the orthogonal components of **E** (i.e. E_x and E_y).

The most general form if polarized light is elliptical polarization. Linear and circular polarizations are simply special degenerate cases of elliptical polarization (Fig.2.3).
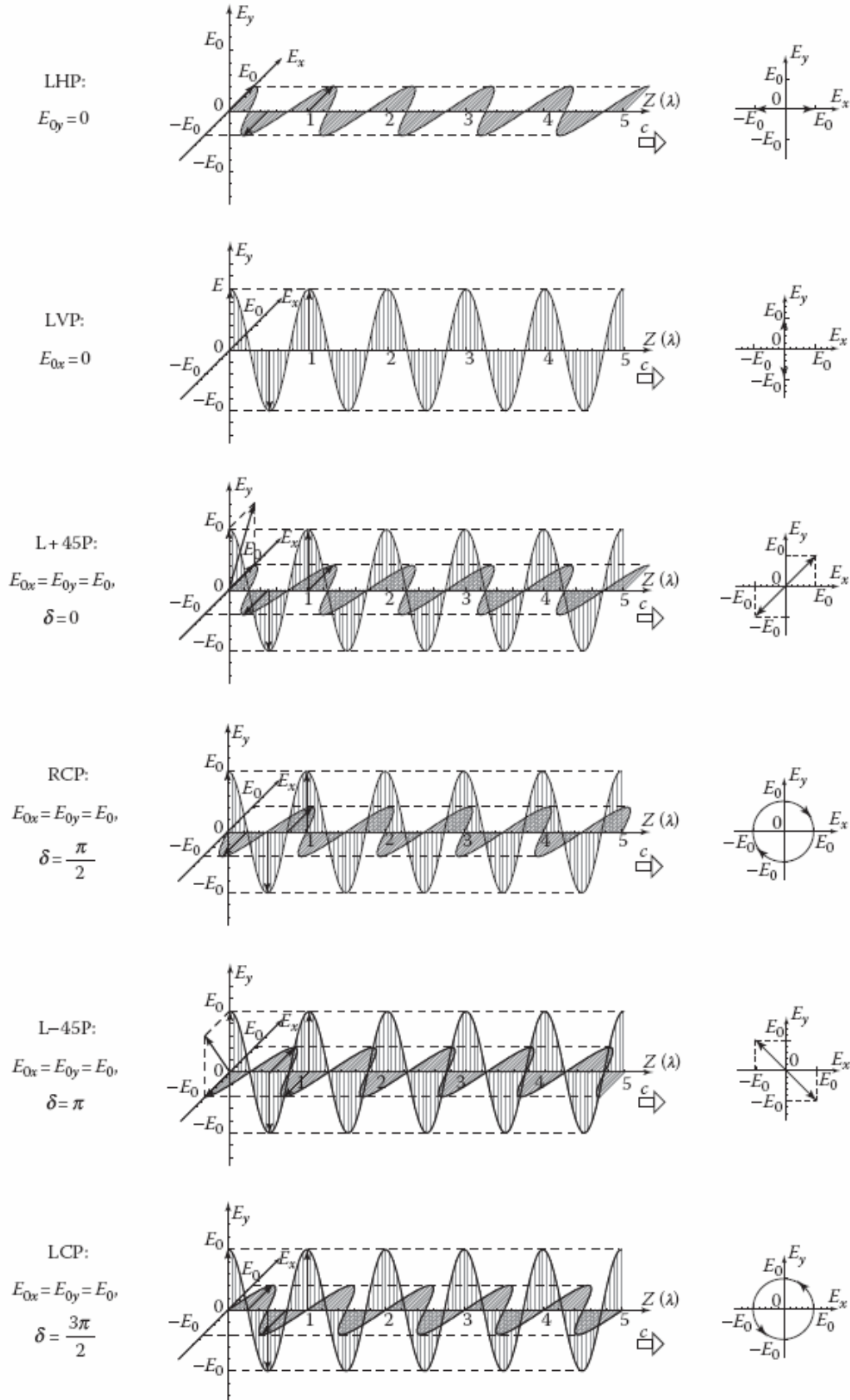
Fig. 2.3 Degenerate polarization states (from [4]).

The type of polarization is determined by the relative magnitude and phase difference between the two orthogonal components of **E**. In general, **E** can be described mathematically by [29]:

$$E = E_x(z,t) + E_y(z,t) \tag{2.8}$$

where E_x and E_y are given by

$$E_x(z,t) = E_{0x} \cos(\tau + \delta_x) \tag{2.9}$$

$$E_y(z,t) = E_{0y} \cos(\tau + \delta_y) \tag{2.10}$$

where $\tau = \omega t - kz$ is the propagation term and $\omega = 2\pi f$ is the angular frequency, and t is time, δx and δy are the phase angles of E_x and E_y respectively, and E_{0x} and E_{0y} are the peak magnitudes in the x and y directions.

Randomly polarized light refers to light whose polarization is completely symmetric about the direction of propagation. The terms unpolarized and naturally polarized are often used to refer to randomly polarized light. The simplest form of polarized light is linear polarization. Light is said to be linearly polarized, or plane-polarized, when the electric field remains in a fixed plain that contains both **E** and **k**. For light to be linearly polarized, the following has to hold true

$$\delta = \delta_x - \delta_y = 0 \tag{2.11}$$

Substituting (2.11) into (2.9) and (2.10) results in identical cosine terms for E_x and E_y we receive

$$E = (E_{0x} + E_{0y}) \cos(\tau + \delta) \tag{2.12}$$

The next simplest case is circular polarization which arises under the following conditions:

$$E_{0x} = E_{0y} = E_0$$

$$\delta = \frac{\pi}{2} + 2m\pi \text{ where } (m = 0, \pm 1, \pm 2,...) \tag{2.13}$$

For circularly polarized light, equations (2.9) and (2.10) become

$$E_x(z,t) = E_0 \cos(\tau), \ E_y(z,t) = E_0 \sin(\tau), \tag{2.14}$$

where δx has been arbitrarily set to zero without loss of generality. Combining equation (2.14) gives the following for equation (2.8)

$$E = E_0 \left[\cos(\tau) + \sin(\tau) \right] \tag{2.15}$$

Notice that in the case of circular polarization, the magnitude of **E** remains constant while the direction of **E** is time varying. This is the exact opposite of the case of linear polarization.

In fact, linear and circular polarizations are simply special cases of elliptical polarization. In the case of elliptical polarization, both the magnitude and direction of **E** are time varying. The equation for the polarization ellipse has the following form

$$\frac{E^2_x}{E^2_{0x}} + \frac{E^2_y}{E^2_{0y}} - \frac{2E_x E_y \cos\delta}{E_{0x} E_{0y}} = \sin^2\delta \tag{2.16}$$

,

which shows that the polarization can be characterized in terms of the parameters E_{0x}, E_{0y}, and δ. Collett [24] derives the following relationship between ψ and the parameters E_{0x}, E_{0y}, and δ

$$\tan 2\psi = \frac{2E_x E_y \cos\delta^2}{E^2_{0x} - E^2_{0y}} \tag{2.17}$$

.

He also derives the relationship between ψ, α, and δ

$$\tan 2\psi = (\tan 2\alpha)\cos\delta \tag{2.18}$$

.

In the case of linear polarization ($\delta = 0$ or π) equation (2.18) reduces to

$$\psi = \pm\alpha \tag{2.19}$$

.

In the case of circular polarization ($\delta = \pi$ or 3π) equation (2.16) reduces to $\psi = 0$ indicating that there is no rotation. This makes sense since a circle is rotationally symmetric. Finally, the angle of ellipticity, χ, is defined as:

$$\tan\chi = \frac{\pm b}{a}, \quad \frac{\pi}{4} \le \chi \ge \frac{\pi}{4} \tag{2.20}$$

where a and b, the major and minor axis, are given by

$$a = \sqrt{E^2_{0x}\cos\psi + E^2_{0y}\sin^2\psi + 2E_{0x}E_{0y}\cos\psi\sin\psi\cos\delta}$$

$$b = \sqrt{E^2_{0x}\sin\psi + E^2_{0y}\cos^2\psi - 2E_{0x}E_{0y}\cos\psi\sin\psi\cos\delta} \tag{2.21}$$

2.2.6 Polarization properties

2.2.6.1 Depolarization

Physically, depolarization (or degree of polarization – *DOP*) of light by a sample of matter can be a result of multiple scattering of photons, or a rapid or random change in the phase or wavelength of the emitted photons that result in a scrambling of the output polarization of the emitted light beam such that it does not favor any polarization state

over the others. Practically, all matter depolarizes light to a degree established by its asymmetric and inhomogeneous makeup.

2.2.6.2 *Dichroism*

Dichroism is the selective absorption of one of the two orthogonal polarization components (*x,y*) of an incident light wave. A dichroic polarizer is physically anisotropic; producing a preferential absorption of one field component while being essentially transparent to the other. The simplest form of a dichroic polarizer is a grid of parallel conducting wires. There are also certain materials which are inherently dichroic due to the anisotropy which exists in their crystal structure. One of the best known naturally occurring examples is the mineral tourmaline. Certainly the most famous dichroic material is the Polaroid sheet [7].

2.2.6.3 *Birefringence*

Many crystalline substances are optically anisotropic. We know that the light excites the electrons within the medium. The electrons are driven by the electric field, they re-radiate secondary wavelets, which then recombine and the resultant wave continues on. The speed of the wave, and thus the index of refraction, is determined by the difference between the frequency of the electric field and the natural, or characteristic, frequency of the electrons. An anisotropy in the binding force will therefore be manifest in an anisotropy in the index of refraction. A material of this sort, which displays two different indices of refraction, is said to be birefringent [4, 29].

2.2.6.4 *Polarizance*

For a sample to exhibit polarizance, it has to have a structural arrangement that enables it to reflect, absorb and re-emit, light at oblique angles, or one that results in either the differentially absorption of orthogonal polarization components of light or in the differentially absorption of linear versus circularly polarized light [2].

2.3   Measurements of optical properties

A number of methods have been proposed for measuring the optical properties of tissues. These can be separated into two classes: direct and indirect.

In direct techniques, optical properties are found using nothing more complicated than Beer's law. Unscattered transmission measurements [29], effective attenuation measurements [30], and goniophotometric measurements of the single scattering phase function [31, 32] are direct techniques.

In indirect techniques, a theoretical model of light scattering is used. Indirect techniques can be subdivided into interactive and non-iterative methods. A non-iterative method uses equations in which the optical properties are explicitly given in terms of the

measured quantities. The Kubelka-Munk and two or four-flux models are non-iterative indirect methods [34, 35]. In indirect iterative methods, the optical properties are implicitly related to measured quantities. The values for the optical properties are iterated until the calculated reflection and transmission match the measured values. These methods are the most cumbersome to use, but the optical model employed can be much more sophisticated than in the non-iterative methods.

2.3.1   Direct methods

Direct techniques do not depend on any specific model to obtain the optical parameter from measurements. Two optical parameters that are not dependent upon any

specific model are the total attenuation coefficient μ_2 and the effective attenuation coefficient μ_{eff}. These parameters are determined using the following methods.

1) The total attenuation coefficient μ_t is obtained from measurements of unscattered transmission, as depicted in Fig. 2.4. Thin slabs (0.1 to 1.0 mm) are generally employed. Experimental data are most affected by beam geometry, sample characteristics, detection schemes, and multiple reflections at boundaries. This measurement is conceptually simple, but difficult to implement because of problems in separating on-axis scattered light from unscattered light.
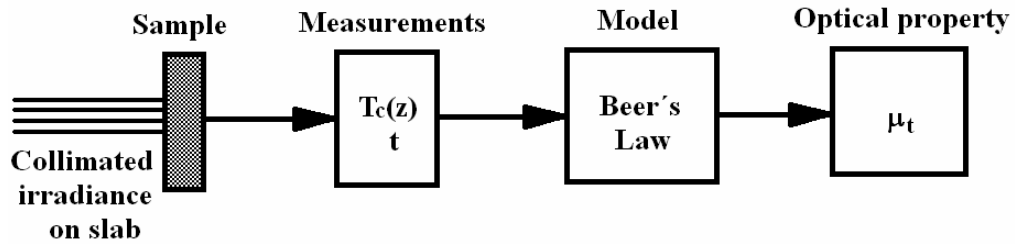
Fig. 2.4 Measured values from the unscattered transmission T_c, through a sample of thickness t are analyzed using Beer´s law to provide estimates of the total attenuation coefficient μ_t.

2) The effective scattering coefficient μ_{eff} or effective penetration depth $\partial_{\text{eff}} = 1/\mu_{\text{eff}}$, is estimated from flux measured by interstitial detectors (Fig. 2.5). This is the simplest and most commonly determined parameter. Fiber-optic detectors must be located inside the diffusion region of irradiated bulk samples, far from sources and boundaries. It is crucial that the measurement field be in the diffusion region. Otherwise the orientation of the fiber with respect to incoming beam and its numerical aperture would introduce measurement errors.
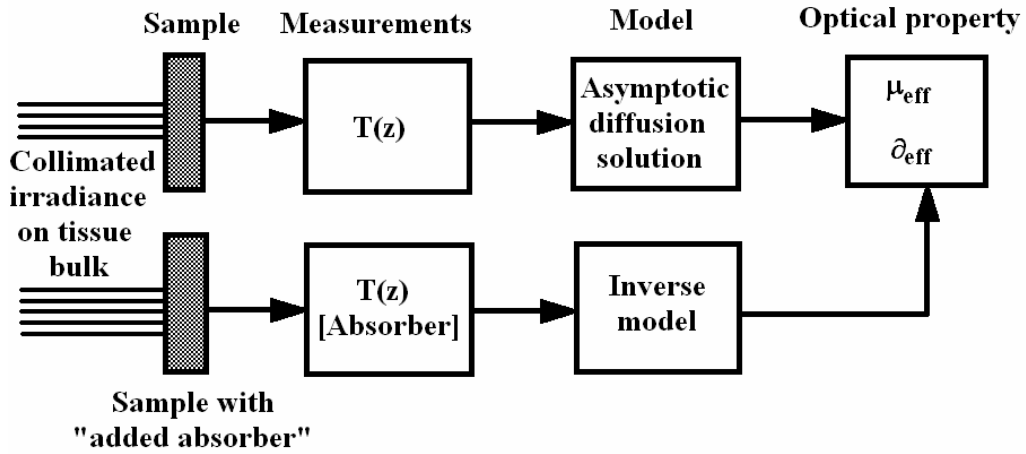
Fig.2.5 Insterstitial measurements of flux inside a sample with or without an added absorber yield an estimate of the effective attenuation coefficient μ_{eff} or the effective penetration depth $\partial_{eff} = 1/\mu_{eff}$.

2.3.2   Non-iterative indirect methods

Such approaches require simple expressions relating the optical properties to measured transmission and reflection (e.g., Kubelka-Munk equations). The first method employs calculations of Kubelka-Munk absorption and scattering coefficients (A_{km}, S_{km} from measurements of diffuse reflection and transmission for diffuse irradiance, as depicted in Fig. 2.6. This method is strongly limited because a perfectly diffuse irradiating source is not easily available.
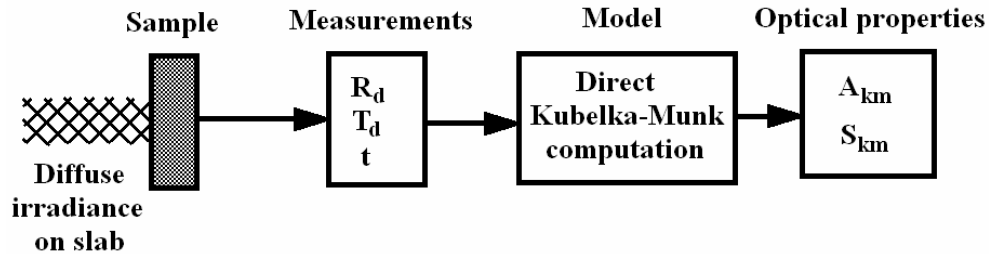
Fig.2.6 Measurements of diffuse reflection R_d, and diffuse transmission T_d, and the sample thickness x, for diffuse irradiance are used to compute Kubelka-Munk absorption A_{km} and scattering S_{km} coefficients.

The second method utilizes determination of absorption, scattering, and anisotropy coefficients from diffuse transmission and reflection measurements. Kubelka-Munk coefficients are first computed, then transformed into transport coefficients, and finally combined with a measurement of unscattered transmission to yield the three optical coefficients. The same limitations of method as for first method are applied here.

Other non-iterative methods have also been used. An example is the combination of the absorbance of a sample placed in an integrating sphere and angular phase function

measurements [35]. Similar methods [4] combine measurements of angular radiance patterns with measurements of μ_{eff} to deduce μ_a, μ_s, and g (fig.2.7).
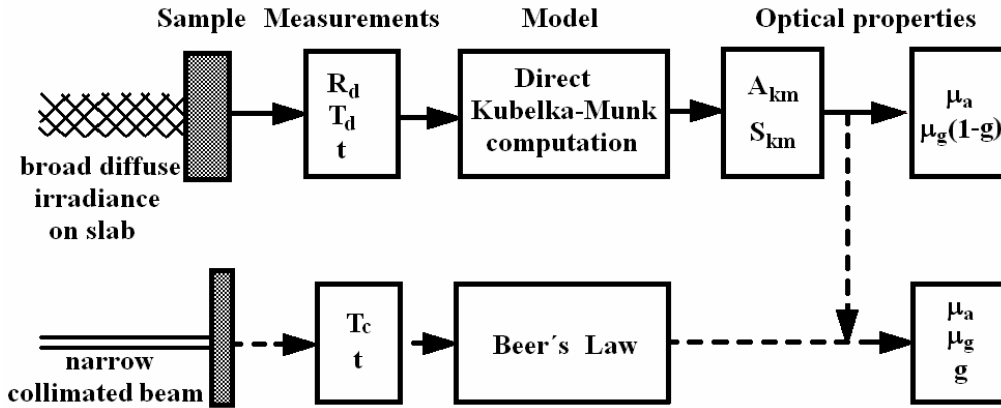
Fig.2.7 Measurements of diffuse reflection and transmission for diffuse irradiance lead to Kubelka-Munk coefficients; these are then converted to transport parameters. When collimated transmission is available, μ_a, μ_s, and g can be calculated.

2.3.3   Iterative indirect methods

Unlike noniterative techniques, iterative procedures can use complicated solutions to the transport equations. Examples are diffusion theory, adding-doubling models [36], and Monte Carlo [37]. Typically, μ_a and $\mu_s(1-g)$ can be obtained if only total reflection and transmission are measured as shown in Fig. 2.8.
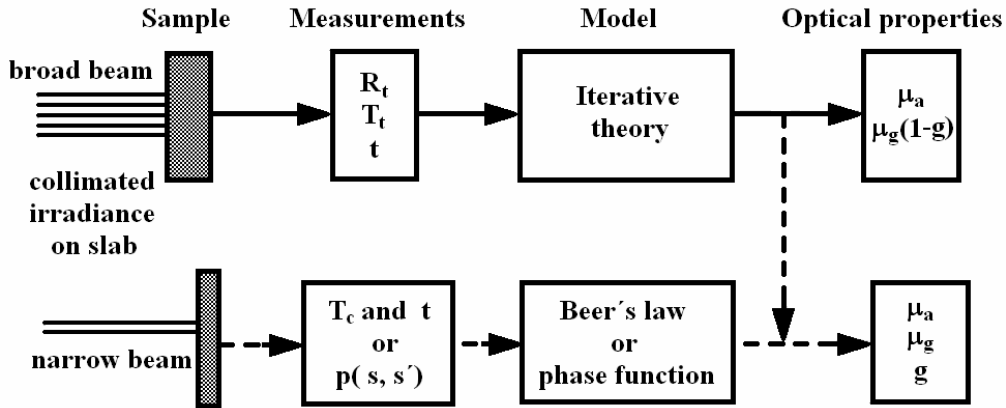
Fig.2.8 If only total reflection and transmission are available, the absorption coefficient μ_a and reduced scattering coefficient $\mu_s(1-g)$ can be determined with an iterative light transport model. An additional measurement (collimated transmission or the phase function) permits separate estimation of μ_a, μ_s, and g.

If a third measurement or either the unscattered transmission or the phase function is available, the values for μ_a, μ_s, and g [or $p(s,s')$] can be determined. Iterative solutions

usually include corrections for mismatched boundary conditions and/or for multiple layers. These methods often require two or more of the following measurements on a sample of known uniform thickness:

1) total (or diffuse) transmission for collimated or diffuse irradiance,

2) total (or diffuse) reflection for collimated or diffuse irradiance,

3) absorbance of the sample, placed inside an integrating sphere,

4) unscattered (collimated) transmission for collimated irradiation, and

5) angular distribution of emitted light from an irradiated sample.

Any three measurements from 1) to 5) would be sufficient to determine the three optical properties.

The use of electromagnetic theory with Maxwell's equations is the most mathematically rigorous and best suited method for polarimetry analysis, at least in clear media with well-defined optical interfaces. The advantage is that all effects of multiple scattering, diffraction, and interference can be included. Their disadvantage - direct solutions from Maxwell's equations have hardly been attempted for multiple scattering media like tissue. However, unlike optically clear media, tissue is a turbid medium possessing microscopically inhomogeneous complex dielectric structures (macromolecule, cell organelles, organized cell structures, blood and lymphatic networks, extra-cellular matrix, interstitial layers, etc.). Due to the ensuing complexity, the Maxwell's equations approach for polarized light propagation in such a complex turbid medium is impractical and is not presently feasible [2, 4]. Instead, light propagation through such media is often modeled using the radiative transport theory [2, 4, 38]. Although the scalar radiative transport theory and its simplified approximation, the diffusion equation, has been successfully used to model light transport in tissue (specifically light intensity distribution in tissue volume, diffuse reflectance, etc.), both are intensity based techniques, and hence typically neglect polarization [29].

2.4.1   Modified Beer-Lambert law

Scattering causes light to travel extra distance in tissue, increasing the probability of photon absorption. The differential path-length *DP*, the real optical path-length, can be obtained from the differential path-length factor *DPF*, given by:

$$DP = DPF.r \qquad\qquad (2.22)$$

where *r is a* geometrical distance between the source and detector. The differential path-length factor or scaling factor will depend on the number of scattering events that occur. The *DPF* will in practice be a function of the scattering coefficient (it will increase with increasing μ_s), the anisotropy *g*, the absorption coefficient (it will decrease with increasing μ_a), and the geometry of the medium. It must be included in the Beer-Lambert law to describe attenuation in a scattering medium. The *DPF* can be considered

approximately constant for a given tissue, since the measured difference in attenuation is small compared with the large constant background attenuation in tissue. It is also necessary to introduce an additive term G due to the scattering losses. Thus,

$$I_{(r)} = I_0 . e^{(-\mu_a . DPF . r + G)} .$$ (2.23)

This is known as the modified Beer-Lambert Law. G is dependent on the measurement geometry and the scattering coefficient of the tissue under study and is largely unknown. Consequently, spectroscopic measurements generally assume that G is constant during the measurement period and attempt to quantify changes in the absorption instead of absolute values:

$$\Delta A_{21} = A_2 - A_1 = \ln \frac{I_1}{I_2} = DPF.r.\Delta\mu_{21} = DPF.r.\alpha(\lambda).\Delta[C]_{21} .$$ (2.24)

The differences in attenuation measured between two oxygenation states is given by A_{21} corresponding to an absorption change of $\Delta\mu_{a21}$. The DPF can be measured by two methods: intensity modulated optical spectroscopy or time of flight.

2.4.2 Kubelka-Munk model

Kubelka and Munk [39] developed a simple relationship between the scattering and absorption coefficients of layers of paint and its overall reflectance.

The Kubelka-Munk (K-M) equation is expressed as follows:

$$f(R) = \frac{(1-R)^2}{2R} = \frac{A_{km}}{S_{km}},$$ (2.25)

where R is the absolute reflectance of the sampled layer, A_{km} is K-M absorption coefficient and S_{km} is K-M scattering coefficient. This relationship, applies energy transport equations to describe the radiation transfer in diffuse scattering media. Two parameters are used in the description: scattering and the absorption coefficients. The absorption and scattering coefficients represent the product of the actual absorption (or scattering) cross section by the density of the absorbers (or scatterers). The absorption and scattering cross sections of a particle have the dimension of area, and, generally, they are functions of the orientation of the particle and the state of polarization of the incident light.

The K-M theory, as originally stated, is considered to be a two-flux theory, since only two types of diffuse radiant flux are involved: a diffuse downward flux and a diffuse upward flux. The relationship between the fluxes are expressed by two simultaneous linear differential equations

$$\frac{dI^+}{dz} = -A_{km}I^+ - S_{km}I^+ + S_{km}I^-$$

$$-\frac{dI^-}{dz} = -A_{km}I^- - S_{km}I^- + S_{km}I^+$$ (2.26)

Here I^+ is intensity in forward direction z, while I^- in backward direction. The first term on the right hand side is absorption, second is intensity scattered into opposite direction, and third term is a contribution to the intensity, scattered from the opposite direction.

The original K-M theory also assumes that the medium presents inhomogeneities which are small compared to its thickness. The K-M theory based models used in tissue optics, also called flux models [34], use K-M equations relating tissue optical properties to measured reflectance R and transmittance T.

2.4.3   Radiative transfer equation

In the Radiative transfer equation (RTE) [2, 38] approach light is treated as composed of distinct particles (photons) propagating through a medium. The model is restricted to interactions between light particles themselves and is derived by considering changes in energy flow due to incoming, outgoing, absorbed and emitted photons within an infinitesimal volume dV in the medium (energy balance).

The model considers a small packet of light energy defined by its position **r**, direction of propagation $\hat{s}$, over a time interval dt, and with propagation speed c (Fig. 2.9).
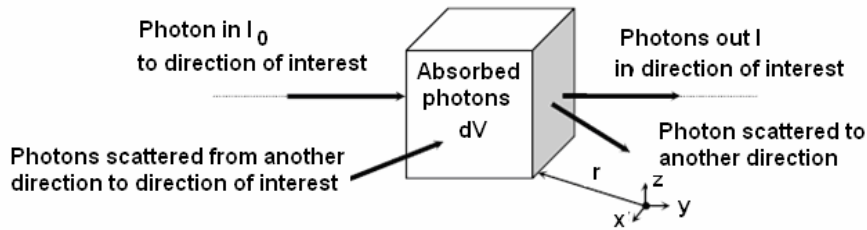
Fig. 2.9 Model for RTE.

The change in energy radiance $I(r,t,\hat{s})$ is equal to the loss in energy due to absorption and scattering out of $\hat{s}$, plus the gains in energy from light scattered into the $\hat{s}$-directed packet from other directions and from any local source of the light at r. This energy balance is represented by the individual terms in the RTE:

$$\frac{1}{c}\frac{\partial I(r,t,\hat{s})}{\partial t} + \hat{s}\nabla I(r,t.\hat{s}) =$$

$$= -\left[(\mu_a + \mu_s').I(r,t,\hat{s})\right] + \mu_s'\int_{4\pi} p(\hat{s},\hat{s}').I(r,t,\hat{s}').d^2\hat{s}' + q(r,t,\hat{s})$$ (2.27)

Each term in equation (2.27) represents in time domain a certain quantity (Figs. 2.11). So

$$\frac{1}{c}\frac{\partial I(r,t,\hat{s})}{\partial t} + \hat{s}\nabla I(r,t.\hat{s}) \tag{2.28}$$

is the difference between the number of photons entering the volume and the number of photons leaving it per unit time (Fig. 2.10),
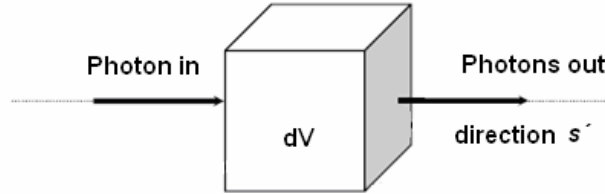
Fig. 2.10 Difference between the number of photons entering the volume and the number of photons leaving it per unit time.

$$(\mu_a + \mu'_s).I(r,t,\hat{s}) \tag{2.29}$$

is attenuation given to light due to absorption and scattering (Fig. 2.11),
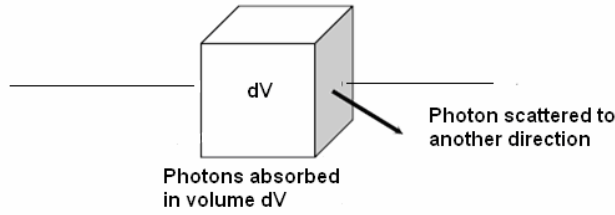
Fig. 2.11 Attenuation of light due to absorption and scattering.

$$\mu'_s \int\limits_{4\pi} p(\hat{s},\hat{s}').I(r,t,\hat{s}').d^2\hat{s}' \tag{2.30}$$

is increase in the light due to scatter from all directions to the final direction given by unity vector $\hat{s}'$ (Fig. 2.12)
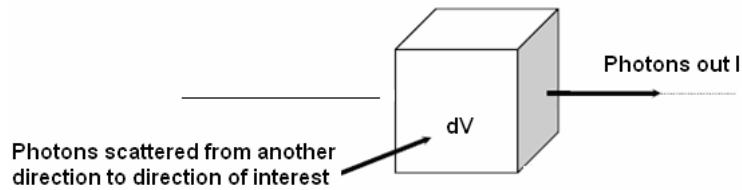
Fig. 2.12 Increase in the light due to scatter from all directions to the final direction.

and $q(r,t,\hat{s}')$ is a local source of light in material (*i.e.* fluorescence) (Fig. 2.13).
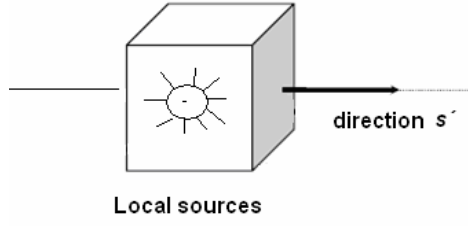
Fig. 2.13 Local sources of light in material.

Here, two important parameters are $\Phi(r,t)$ which represents photon density or diffuse photon fluence (inside the element), and $J(r,t)$ which is the photon flux or current (at its boundary). The latter is a measurable parameter and allows equation (2.27) to be solved for μ_s' and μ_a, respectively [40]

$$\Phi(r,t) = \int_{4\pi} I(r,t,\hat{s}').d\hat{s}' \tag{2.31}$$

$$.J(r,t) = \int_{4\pi} \hat{s}.I(r,t,\hat{s}').d\hat{s}' \tag{2.32}$$

Exact solutions for the RTE exist for simple cases such as isotropic scattering in simple geometries.

2.4.3.1 *The diffusion approximation*

Three variables in the RTE depend on direction $\hat{s}$: the radiance $I(r,t,\hat{s})$, the phase function $p(\hat{s},\hat{s}')$ and the source term $q(r,t,\hat{s})$. If these are expanded into spherical harmonics, an infinite series of equations which approximate to the RTE is obtained. The PN approximation is obtained by taking the first N spherical harmonics, of which the simplest is the time-dependent P1 approximation. If the following assumptions are made:

- scatter is the dominant interaction: μ_s' $>> \mu_a$,

- phase function $p(\hat{s},\hat{s}')$ is independent of the absolute angle,

- photon flux $J(r,t)$ changes slowly d$J(r,t)/dt = 0$ and

- all sources are isotropic, the result is the time-dependent **diffusion equation**:

$$\frac{1}{c}\frac{\partial\Phi(r,t)}{\partial t} - \nabla\kappa(r)\nabla\Phi(r,t) + \mu_a(r)\Phi(r,t) = q(r,t) \tag{2.32}$$

where

$$J(r,t) = -\kappa(r)\nabla\Phi(r,t) \tag{2.33}$$

is first Fick's Law, and $\kappa(r)$ is the diffusion coefficient defined as:

$$\kappa(r) = \frac{1}{3.\left[\mu_a(r) + \mu_s'(r)\right]}. \tag{2.34}$$

The diffusion equation (2.33) has been widely used to model light transport in tissue, although it is necessary to assume that light propagates diffusively (which is generally the case in bulk tissue), and the source and detector are separated in space and time, to ensure that the light is diffuse when it reaches the detector. By contrast, these assumptions generally do not hold near the source, near the surface and internal boundaries and in anisotropic tissues, and in regions of either high absorption or low scatter (voids regions). For these cases, higher order approximations to the RTE may be required [41], and models which incorporate void regions within a diffusing model.

2.4.4 Green's functions

A general method for solving partial differential equations (PDE) such as the diffusion equation is the application of Green's functions, where the source term $q(r,t)$ consists of an infinitely short pulse or δ-function (any other source can be obtained by convolution [42]. An example of analytical solution was developed for a homogeneous slab where boundaries are described using the so-called method of images. This yields time-resolved reflectance and transmittance equations, and least-squared fitting to experimental data allows the optical coefficients to be determined. For instance, during the determination of the optical properties of a liquid slab of intralipid solution, a rectangular transparent receptacle is filled with the homogenous solution (nominal properties of the mixture are $\mu_s' = 1$ mm^{-1}, $\mu_a = 0.01$ mm^{-1}). A connector for a light source is attached on one of the faces, and another for a detector is attached on the opposite face. Both connectors are at the same height and located in the middle of each face. A representation of the experiment is shown in Fig. 5.3. A short pulse from a laser source is applied and the time-resolved transmitted intensity across the solution is detected (50 mm of thickness). The values of the absorption and scattering coefficients are obtained from the temporal distribution of transmitted light due by fitting with the corresponding Green function.

Other analytical solutions for simple geometries, such as spheres and cylinders, as well as the frequency domain equivalents of the equations, are given in [43]. For more complex geometries, the solutions are solved numerically.

2.4.5 Finite element method

The finite element method (FEM) can be applied in order to solve numerically the partial differential equations (such as diffusion equation) for arbitrary and complex geometries. FEM can be applied anywhere where a differential equation formulation is available for the transport model [44]. The method involves dividing a region of interest (or domain) into a finite number of volume or area elements.
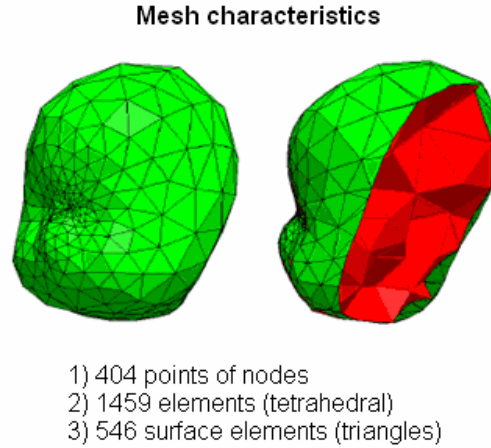
Fig. 2.14 Head-shaped finite element mesh (left) and the surface cut away to show internal structures (right).

The boundary of one element consists of discrete points called nodes (or connecting points). Surface domains may be subdivided into triangles and volumes may be subdivided into tetrahedral (polyhedrons) shapes. Each element has its individual set of optical properties (μ_a and μ_s'). The shape and distribution of the elements is ideally defined by automatic meshing algorithms (e.g. NETGEN [45]). Figure 2.14 shows a finite element (volume) mesh generated using automatic meshing algorithms (NETGEN).

The photon density approximation $\Phi_i(t)$ is then calculated at each node i, and summed over all N nodes in the region. It can be expressed using the piecewise polynomial function:

$$\Phi^h(r,t) = \sum_i^N \Phi_i(t)u_i(r).$$ (2.35)

The *h* superscript denotes the iterative process that is calculated at the nodes and which provides an approximate solution for photon density $\Phi(t)$. The $u_i(r)$ is a basis function and it describes the way that the function $\Phi_i(t)$ is allowed to vary over an element (between nodes). Its simplest form is to be a constant, although a variety of basis functions can be used The advantages of this method are its computational speed, the high flexibility (as for the Monte Carlo method) when applied to complex geometries and it can model photon density and flux everywhere. The disadvantages are that there is no means of deriving individual photon histories and it is subject to the same limitations as the diffusion equation [44].

2.4.6   Monte Carlo based models

The Monte Carlo method was originally proposed by Metropolis and Ulam [46] to simulate radiative transfer which was accomplished by a stochastic model keeping track

of photon trajectories. Since then, many simulation problems have been studied using Monte Carlo techniques, including the transport of light in tissue [47, 48].

Many problems of practical interest often involve a range of light sources, multiple tissues types, and complex geometries. The essence of the Monte Carlo approach is to launch a photon at an interface, and once launched, the photon is continually propagated and scattering until it is either absorbed by the tissue or escapes from the tissue from some boundary. Analytical solutions for realistic scenarios are complicated, even when possible. These more realistic cases are instead solved with numerical techniques.

The Monte Carlo (MC) method, as applied to the transport of light radiation, is based on the RTE and involves computer-simulated calculations of photon propagation in scattering media. As with radiative transfer theory, MC simulations treat the photons as particles, ignoring their wave-like nature. Therefore, parameters such as the phase and polarization of the light are usually omitted, mainly due to the multiple scattering of the photons, the results is that these properties are quickly randomized. In the simplest of MC simulations photons are injected into a medium individually and their paths traced until they are either absorbed or permanently scattered out of the region of interest. The rules of photon propagation are expressed as probability distributions (hence the name 'Monte Carlo'), which are based on the geometry and optical properties of the medium.

Monte Carlo models have been used extensively in the simulation of biological tissues. The models are easy to implement and provide rigorous solutions for even complex tissues. Since Monte Carlo methods converge to a solution within some acceptable error definition, theoretically, any level of accuracy can be achieved [49]. However, in practice, the accuracy of a model is limited by the accuracy and validity of the input parameters as well as the mechanisms for accounting for scattering and absorption. To the best of our knowledge, Monte Carlo models in biomedicine.

The advantages of MC simulation over the diffusion approximation are that MC simulations do not require that μ_s, μ_a, and accurate results can be obtained close to sources and boundaries. In addition, complicated geometries and multi-layered tissues in which the optical properties vary spatially can be modeled easily [37].

However, although potentially highly accurate, the simulations can be expensive due to the long computational times required to achieve such accuracy. For example, for a 1% accuracy the paths of 10,000 photons must be detected.

There are two methods in which to perform this process. The first, called *fixed* step-size, evaluates whether a photon is absorbed, scattered or propagated with no interaction at fixed intervals through the medium. Prahl [2] suggests one-tenth of a mean free path as a good step-size. At each step in the evaluation, the events of absorption and scattered are assumed to be independent and thus only one such event can occur. The second method, called *variable* step-size, forces a photon to be either absorbed or scattered at each interaction.

The basic steps of a single photon through this type of MC simulation are as follows [49]:

1. The photon is incident on the tissue boundary at an angle of θ and with a weight of $W = 1$.

2. The photon weight is reduced by an amount equivalent to the reflected component at the boundary, ΔW.

3. The new direction of the photon is calculated from the incident angle α and the refractive index at the tissue boundary.

4. The photon step size l is calculated as follows:

$$l = -\frac{\ln(\xi)}{\mu_t} \tag{2.36}$$

where ξ is a randomly generated number between 0 and 1 and μ_t is the total attenuation coefficient. It can be shown that on average the step size l is equal to the mean free path, μ_t^{-1}, as expected.

5. The photon weight is reduced again, due to absorption, by an amount

$$\Delta W = W \frac{\mu_a}{\mu_t} \tag{2.37}$$

where W is now the weight at the end of step 2.

6. A random number, 0 or 1, is then generated to determine if the photon will be scattered. If the number generated is 0 then no scatter occurs and the procedure is repeated from step 3. For a value of 1 the photon is scattered.

7. The new direction of the scattered photon is calculated using two angles:
   -the deflection angle θ, which has values between 0 and π, and
   - the azimuthal angle ϕ with values between 0 and 2π. The deflection angle is calculated from the normalized, cumulatively integrated scattering phase function using ξ. The azimuthal angle is uniformly distributed over the interval 0–2π and is therefore calculated by $\phi = 2\pi\xi$.

Steps 3–6 are repeated for the desired number of photons. If the simulation involves a more complex heterogeneous model the process returns to step 1 when a tissue boundary is reached, proceeding in the same manner but using the optical properties for the new region.

3 BIOLOGICAL TISSUE

Biological or living tissue is made up of cells. There are many different types of cells, but all have the same basic structure. Tissues are layers of similar cells that perform a specific function. The different kinds of tissues are grouped together to form organs.

There are four basic types of biological tissue:
- **Connective tissue** supports other tissues and binds them together. This includes bone, blood, and lymph tissues, as well as the tissues that give support and structure to the skin and internal organs.
- **Epithelial tissue** provides a covering for deeper body layers. The skin and the linings of the passages inside the body, such as the gastrointestinal system, are made of epithelial tissue.
- **Nerve tissue** is made up of nerve cells (neurons) and is used to carry messages to and from various parts of the body. The brain, spinal cord, and peripheral nerves are made of nerve tissue.
- **Muscle tissue** includes three types of tissue:
o Striated muscles, such as those that that move the skeleton (also called voluntary muscle).
o Smooth muscles (also called involuntary muscle), such as the muscles contained in the stomach and other internal organs.
o Cardiac muscle, which makes up most of the heart wall (also an involuntary muscle).

Among these basic types of tissue the muscle tissue is best for investigation and measurement of the ageing process [3, 6]. More precisely, among three types of muscles tissues – striated, smooth and cardiac – only first ones that move the skeleton are appropriated for this kind of investigation due to their fibrous nature.

Due to the fact that biological tissue is complex random material showing inhomogeneity, anisotropy and nonlinearity in the structure, its rigorous characterization is almost impossible. On the other hand, this complexity involves an important amount of information. Therefore, the research of polarization states of scattered light is one of emerging novel techniques in biomedical science and food control.

Inhomogeneities in the media cause scattering which may alter the direction of propagation, polarization and phase of light. While the propagation of light through such media may be analyzed either by means of the wave picture or the photon picture, the latter is more appealing. Photons travel in straight line paths until they encounter an inhomogeneity, when they are scattered in random directions.

The light scattered by a tissue has interacted with the ultrastructure of the tissue, and tissue ultrastructure extends from membranes to membrane aggregates to collagen fibers to nuclei to cells. Size range of tissue ultrastructure will determine if it is a Mie or Rayleigh scatterer.

The scattering parameters of such media depend on
• refractive index fluctuations
• used wavelength
• particle size and shape.

The scattering is said to be in the Rayleigh regime when the radius *a* of the scatterer is less than the wavelength of light (small size particles: Rayleigh theory $a < \lambda/10$).

The intensity of detected light in the direction θ is expressed by

$$I = I_0 \frac{8\pi^2 N\alpha}{\lambda^4 r^2}(1+\cos^2\theta) \qquad (3.1)$$

where *I* is the intensity of the scattered light, λ wavelength of incident light I_0, N number of scatterers, α their polarizability, *r* distance from scatterer, θ scattering angle. Rayleigh scattering is inversely related to fourth power of the wavelength of the incident light.

Gustav Mie in 1908 published a solution to the problem of light scattering by homogeneous spherical particles of any size. Mie theory describes the way in which spherical, homogeneous particles interact with electromagnetic radiation (Fig. 3.1).

Here, the particle means material that constitutes a region with refractive index n_2 that differs from the refractive index of its surroundings n_1. Mie scattering is not strongly wavelength dependent, therefore it is possible to use it in the calculus of biological tissue.

In the case, the intensity of scattered light is equal in both the forward and backward directions. As the size of the particle increases, the scattering is more peaked in the forward direction. The case of $a > 1$, known as the Mie regime, (matching size particles: Mie theory $\geq \lambda$) shows peaking in some angles (Fig. 3.1) [2, 4].
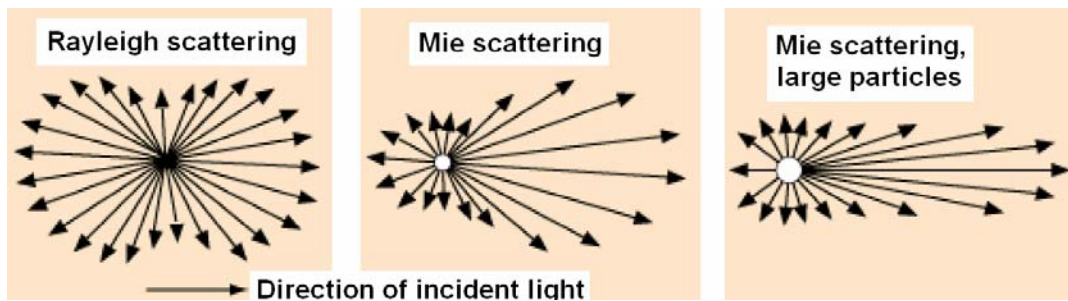

Fig. 3.1 Rayleigh and Mie scattering.

Which are sources of scattering in tissue?

Refractive index mismatch between lipid and surrounding aqueous medium (Fig. 3.2).
– Soft tissues are dominated by lipid contents
– Cellular membranes, membrane folds, and membranous structure, $d \sim 0.1$ μm
• Mitochondria, $d \sim 1$ μm
– Intracelluar organelle composed of many folded membrane, cristae
• Collagen fibers, $d \in (2 \text{ to } 3)$ μm
– Collagen fibrils, $d = 0.3$ μm
– Periodic fluctuation in collagen ultrastructure $\rightarrow$ source of Rayleigh scattering in UV and visible range ($d \sim 70$ nm)
• Cells.
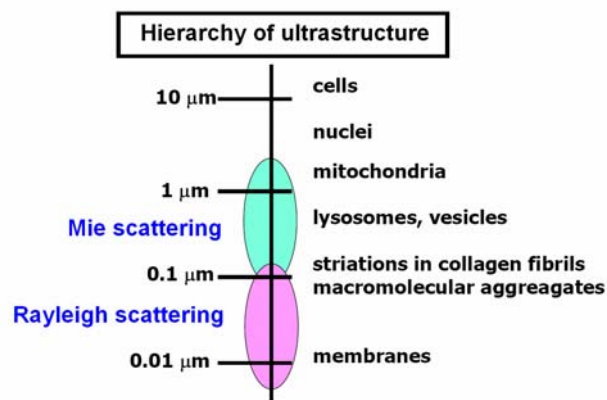
Fig. 3.2 Review of elastic scattering on biological scatterers.

Hence in a turbid medium made up of a random aggregate of scatterers, the photons undergo repeated multiple scattering in forward and backward directions. The turbid medium is characterized by the scattering mean free path, l_s, which is the mean distance the photons travel before getting scattered, and the transport mean free path l^* which is the mean distance photons travel before the direction of propagation is randomized. Since it is quite possible that photons are forward scattered (and continue to travel in the same direction), $l^* > l_s$. The transport mean free path depends upon the number density of scatterers, refractive index contrast between the medium and the scatterers, and the anisotropy factor, i.e. a factor quantifying the directional distribution of scattering. Typical value of l^* for infrared light in tissues are 1-2 mm. The light emerging from a turbid medium consists of three components: the unscattered - ballistic, the slightly scattered - snake and scattered - diffusive photons (Fig 3.3). These differ in their paths through the medium, and consequently in their imaging properties. The unscattered or forward scattered photons travel un-deviated and emerge the first, having traveled the shortest distance through the medium. These preserve the characteristics of the incident light, namely direction of propagation, polarization and are hence best for imaging. However, they are few in number, their intensity falling off as

$$I = I_0 \exp\left(\frac{-x}{l^*}\right) \qquad\qquad (3.2)$$

where I_0 is the input intensity, and x is the distance traveled.

Fig. 3.3 Trajectories of photons in a random medium.
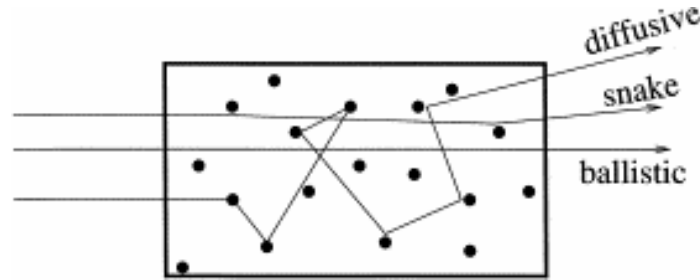
The diffuse component, which forms the bulk of the emergent light in turbid media is made up of photons that have undergone random multiple scattering, and these emerge later than the ballistic photons because of their increased path lengths. Their polarization, direction of propagation and phase are completely randomized. Snake photons are those that travel in near-forward paths, having undergone few scattering events, all of which are in the forward or near-forward direction. Consequently, they retain the image bearing characteristics to some extent. Due to the scattering a pulse of light incident on a turbid medium emerges elongated. Typically, a femtosecond pulse is stretched to a picoseconds or a nanosecond pulse on traveling through a turbid medium. The duality of light, the fact that it exhibits both wave and particle nature, it explains light interactions at the macroscopic level, using geometric or ray optics, and accounts for phenomena such as shadow formation while the wave nature of light explains light interactions at the micro and sub-micro level and accounts for photon interference and diffraction phenomena. In general, for the propagation of light we use Maxwell's equation, and for the interaction of the light with matter, where the absorption and emission of light involves, we use the quantum theory.

In order to have a clear understanding on the use of polarized light for biomedical applications, it will be essential to investigate both the wave and particle nature of light. The knowledge of this theory pertains to the measurements that will be necessary to enable the discrimination of the properties of matter that we are interested in.

Visible light and near-infrared (NIR) light interact with biological tissue predominantly by absorption and elastic scattering. Unfortunately, while most of the physiological information is contained in the absorption coefficient (the number of absorption events per unit length, μ_a), the scatter coefficient (the number of scattering events per unit length, μ_s) in tissue is generally considerably larger, so that signals measured over distances of a few milimeters or larger are dominated by diffuse light.

4 LIGHT SCATTERING AND POLARIZATION

In this chapter, a notion of basic theory used in the thesis to describe the multiple scattering process is presented. First, the description of polarized light in terms of Stokes vectors will be outlined. Subsequently, the interaction of polarized light with a scattering medium will be characterized in terms of a matrix.

4.1 Light field

The formal theory of elastic light scattering [4, 29] deals with
- Maxwell's equations,
- boundary conditions and
- idealized physical models for the scatterers, as well as with
- matrix algebra, which manipulates the interaction matrices, and with
- light vectors, which describe the optical system, ignoring the exact mechanism causing the scattering.

The fundamental problem of deriving structural features of the scatterer from scattering information is presently unsolvable for most biophysical cases. However, the matrix algebra can be used to catalog the scattering signals, which are related to the matrix elements involved in the scattering process.

The state of polarization and intensity of a light beam incident on the medium is specified by the 4×1 Stokes vector **S** in the following form:

$$\mathbf{S} = \begin{bmatrix} I \\ Q \\ U \\ V \end{bmatrix} = \begin{bmatrix} S_0 \\ S_1 \\ S_2 \\ S_3 \end{bmatrix}. \tag{4.1}$$

Here $I \equiv S_0$ is total intensity, $Q \equiv S_1$ − polarization at 0° or 90° to the scattering plane, $U \equiv S_2$ − polarization at ±45° to the scattering plane, and $V \equiv S_3$ − left or right circular polarization, and S_0, S_1, S_2, S_3 represent four elements of Stokes vector **S.**

Another quantity of interest in radiative transfer of polarized light is the degree of polarization DOP of the light. This is defined as

$$DOP = \frac{\sqrt{Q^2 + U^2 + V^2}}{I} = \frac{\sqrt{S_1^2 + S_2^2 + S_3^2}}{S_0}, \tag{4.2}$$

and indicates the fraction of the light intensity that is polarized regardless of whether it is linear and/or circular. Similarly, the degree of *linear* polarization DOP_L is defined by

$$DOP_L = \frac{\sqrt{Q^2 + U^2}}{I} = \frac{\sqrt{S_1^2 + S_2^2}}{S_0}. \tag{4.3}$$

The quantity $\sqrt{Q^2 + U^2}$ represents the magnitude of linear polarization in the light field. However, it does not specify the orientation of the electric vector. Further, the degree of *circular* polarization (DOP_c,) is defined by

$$DOP_C = \frac{V}{I} = \frac{S_3}{S_0}. \tag{4.4}$$

Also note that $DOP = \sqrt{(DOP_L)^2 + (DOP_C)^2}$.

4.2   Scattering medium

The scattering properties of a medium are defined by a *scattering matrix* **S**(Θ)**.** A detailed discussion of the general scattering matrix is given in van de Hulst [8]. We will review the role of Rayleigh and Mie particles and their relationships to biological particles, and then give an example of the matrix multiplication implied by a particular arrangement of the optical components to show how matrix elements are measured. We will then discuss some matrix element signals we measured to show their significance to biological systems.

All polarization states could be described using the Jones vector and the Stokes parameter. As shown in Fig.4.1, once the incident light and the output light's polarization states are identified, the polarization elements of an optical device, which is a black box, can be determined subsequently.
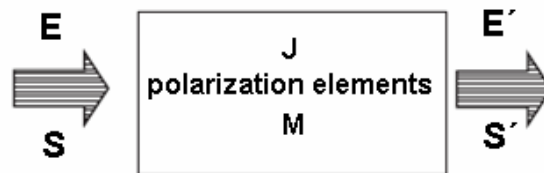

Fig 4.1 Jones matrices and Mueller calculus.

At present, popular theories of polarized radiation interaction with optical elements or scattering media may be divided into two groups:
- Jones calculus, which assumes a coherent addition of waves [8]; and
- Stokes-Mueller calculus, which assumes an incoherent addition of waves [49, 50].

However, in both approaches one usually starts a theoretical analysis with severely restrictive assumptions. In the Jones calculus, one starts out with Maxwell's equations describing electric field **E**, whereas in the Mueller calculus, it starts by postulating a linear relation between the input Stokes vector **S** and the output Stokes vector **S**´emerging from the optical medium.

The development of the Mueller analysis is heuristic and lacks the mathematical rigor of the Jones calculus. However, the Mueller formalism has an advantage in that it deals with intensities rather than field vectors.

If un-polarized light is incident on one or more particles, the Stokes parameters of the scattered light can be shown to be in general, partially polarized. This result shows that scattering is a mechanism for polarizing light. The degree of polarization of the scattered light depends on the scattering direction and some time has been found to be a maximum, when the scattered direction is normal to the incident direction. With this, we come to the conclusion of all the preliminaries needed to deal with studies on scattering of polarized light through turbid medium, which is the main work reported in this thesis.

The Jones calculus is written as

$$\mathbf{J}.\mathbf{E} = \mathbf{E'} \text{ or } \begin{bmatrix} J_{xx} & J_{xy} \\ J_{yx} & J_{yy} \end{bmatrix} \begin{bmatrix} E_x \\ E_y \end{bmatrix} = \begin{bmatrix} E'_x \\ E'_y \end{bmatrix}. \tag{4.5}$$

The Mueller calculus is indicated as

$$\mathbf{M}.\mathbf{S} = \mathbf{S'} \text{ or } \begin{bmatrix} M_{00} & M_{01} & M_{02} & M_{03} \\ M_{10} & M_{11} & M_{12} & M_{13} \\ M_{20} & M_{21} & M_{22} & M_{23} \\ M_{30} & M_{31} & M_{32} & M_{33} \end{bmatrix} \begin{bmatrix} S_0 \\ S_1 \\ S_2 \\ S_3 \end{bmatrix} = \begin{bmatrix} S'_0 \\ S'_1 \\ S'_2 \\ S'_3 \end{bmatrix}. \tag{4.6}$$

A scatterer changes the state of the incoming polarized light by mixing the initial polarization states of the incident electric field vectors $E_{\|0}$, and $E_{\perp 0}$. Here $E_{\|0}$, and $E_{\perp 0}$ are the initial components parallel and perpendicular to the scattering plane, respectively. The new parallel and perpendicular electric field components $E_{\|}$ and $E_{\perp}$ arise through an interaction represented by mixing coefficients a_i.

$$\begin{aligned} E_{\|} &= A_2 E_{\|0} + A_3 E_{\perp 0} \\ E_{\perp} &= A_4 E_{\|0} + A_1 E_{\perp 0} \end{aligned} \quad \text{or} \quad \begin{vmatrix} E_{\|} \\ E_{\perp} \end{vmatrix} = \begin{bmatrix} A_2 & A_3 \\ A_4 & A_1 \end{bmatrix} \begin{vmatrix} E_{\|0} \\ E_{\perp 0} \end{vmatrix}. \tag{4.7}$$

The Stokes vector **S**, which completely characterizes the intensity and polarization of a light ray, is defined in terms of time averages of the electric field components of an electromagnetic wave:

$$
\begin{aligned}
S_0 &= I = \left\langle E_\parallel E_\parallel^* + E_\perp E_\perp^* \right\rangle = A_x^2 + A_y^2 \\
S_1 &= Q = \left\langle E_\parallel E_\parallel^* - E_\perp E_\perp^* \right\rangle = A_x^2 - A_y^2 \\
S_2 &= U = \left\langle E_\parallel E_\perp^* + E_\perp E_\parallel^* \right\rangle = 2 A_x A_y \cos \Delta\varepsilon \\
S_3 &= V = \left\langle i(E_\parallel E_\perp^* - E_\perp E_\parallel^*) \right\rangle = 2 A_x A_y \sin \Delta\varepsilon
\end{aligned}
\quad \text{or} \quad
\begin{vmatrix} I \\ Q \\ U \\ V \end{vmatrix}
=
\begin{vmatrix}
\left\langle E_\parallel E_\parallel^* + E_\perp E_\perp^* \right\rangle \\
\left\langle E_\parallel E_\parallel^* - E_\perp E_\perp^* \right\rangle \\
\left\langle E_\parallel E_\perp^* + E_\perp E_\parallel^* \right\rangle \\
\left\langle i(E_\parallel E_\perp^* - E_\perp E_\parallel^*) \right\rangle
\end{vmatrix}
= \mathbf{S}. \quad (4.8)
$$

The transformation of an incident four-component Stokes vector $\mathbf{S}_0$ by a scattering matrix $\mathbf{S}(\Theta)$ gives a final Stokes vector $\mathbf{S}_f$ where $\mathbf{S}_f = \mathbf{S}(\Theta).\mathbf{S}_0$ or

$$
\begin{vmatrix} I_f \\ Q_f \\ U_f \\ V_f \end{vmatrix}
=
\begin{vmatrix}
S_{11} & S_{12} & S_{13} & S_{14} \\
S_{21} & S_{22} & S_{23} & S_{24} \\
S_{31} & S_{32} & S_{33} & S_{34} \\
S_{41} & S_{42} & S_{43} & S_{44}
\end{vmatrix}
.
\begin{vmatrix} I_0 \\ Q_0 \\ U_0 \\ V_0 \end{vmatrix}.
\qquad (4.9)
$$

When the values of the Stokes vector $\mathbf{S}$ are inserted into the matrix representation (4.9) one gets the general form of the scattering matrix [4]. Any component of the electric field vector $\mathbf{E}$ can be written explicitly in terms of its phase ε, amplitude A, wavenumber k, and frequency ω. We have

$$
\mathbf{E}(r) = A \exp(-i\varepsilon) \exp[-i(kr - \omega t)]. \qquad (4.10)
$$

This vector is used to get the matrix that gives a direct relationship between the amplitudes A_i ($i = j$ or k) and the phase difference $\Delta\varepsilon = \varepsilon_\varphi - \varepsilon_k$. Then

$$
A_k A_k^* = |A_k|^2 ; \quad \left\langle A_j A_k^* + A_k A_j^* \right\rangle = |A_j||A_k|\sin \Delta\varepsilon \qquad (4.11)
$$

and

$$
i/2(A_j A_k^* - A_k A_j^*) = |A_j||A_k|\cos \Delta\varepsilon, \qquad (4.12)
$$

and we get:

$$
\mathbf{S} =
\begin{bmatrix}
\frac{1}{2}(A_1^2 + A_2^2 + A_3^2 + A_4^2) & \frac{1}{2}(-A_1^2 + A_2^2 - A_3^2 + A_4^2) & (A_3 A_2 - A_4 A_1)\cos\Delta\varepsilon & -(A_2 A_3 + A_4 A_1)\sin\Delta\varepsilon \\
\frac{1}{2}(-A_1^2 + A_2^2 + A_3^2 - A_4^2) & \frac{1}{2}(A_1^2 + A_2^2 - A_3^2 - A_4^2) & (A_3 A_2 - A_4 A_1)\cos\Delta\varepsilon & -(A_2 A_3 + A_4 A_1)\sin\Delta\varepsilon \\
(A_2 A_4 + A_3 A_1)\cos\Delta\varepsilon & (A_2 A_4 - A_3 A_1)\cos\Delta\varepsilon & (A_2 A_1 + A_3 A_4)\cos\Delta\varepsilon & -(A_2 A_1 - A_3 A_4)\sin\Delta\varepsilon \\
(A_2 A_4 + A_3 A_1)\sin\Delta\varepsilon & (A_2 A_4 - A_3 A_1)\sin\Delta\varepsilon & (A_2 A_1 + A_3 A_4)\sin\Delta\varepsilon & (A_2 A_1 + A_3 A_4)\cos\Delta\varepsilon
\end{bmatrix}. \; (4.13)
$$

The general scattering matrix given above applies to any system of particles. However, it is convenient to divide the particles into two rather broad ranges depending on the ratio of wavelength λ to particle size D. The two classes of scattering particles are called Rayleigh and Mie particles.

Additionally, the light intensity obtained at the end in the case of Jones matrix is

$$
I = \left\langle E_x + E_y \right\rangle^2. \qquad (4.10)
$$

In the case of Mueller matrix, the light intensity is directly given by S_0.

To conclude, the polarization degrees of freedom of the Jones and the Mueller matrices are as shown in Fig 4.1. Both the Jones method and the Mueller method give double refraction, double absorption (dichroism), circular double refraction (optical rotating power), circular double absorption (circular double dichroism), and others.

Their major difference is that as opposed to the Jones vector **J** treating only totally polarized lights, in the Mueller calculus, the Stokes vector **S** is used to describe the polarization state of a light beam, and the Mueller matrix **M** to describe the polarization-altering characteristics of a sample. This sample may be a surface, a polarization element, an optical system, turbid medium, biological tissues, and any other light-matter interaction which produces a reflected, refracted, diffracted, absorption, and scattering of light beam.

The Mueller matrix can deal with all polarization states including depolarization, which is important in the study of biological samples.

4.2.1   Scattering matrix

The 4×4 scattering matrix **S**(Θ) transforms the Stokes vector of an incident light beam to the Stokes vector of a scattered light beam (Fig.4.1). The scattering matrix can be obtained experimentally, or derived in a rigorous manner. For scattering by a medium composed of spherical scatterers, this matrix can be derived rigorously by use of the Maxwell equations with appropriate boundary conditions. The form of this matrix is given by

$$\mathbf{S}(\Theta) = \begin{bmatrix} p_{11}(\Theta) & p_{21}(\Theta) & 0 & 0 \\ p_{21}(\Theta) & p_{11}(\Theta) & 0 & 0 \\ 0 & 0 & s_{21}(\Theta) & -d_{21}(\Theta) \\ 0 & 0 & d_{21}(\Theta) & s_{21}(\Theta) \end{bmatrix} \qquad (4.11)$$

where **S**(Θ) is a function of the included angle Θ between the incident and scattered light beams. $p_{11}(\Theta)$, $p_{21}(\Theta)$, $s_{21}(\Theta)$ and $d_{21}(\Theta)$ are independent parts of Mie phase function representing four elements of the matrix.

All the elements of the scattering matrix **S**(Θ) are real. The scattering matrix **S**(Θ) operates on the incident Stokes vector (the S-axis is assumed to be parallel to the scattering plane as shown in Fig. 4.1). Note that the shaded region is the scattering plane. Each of the four independent functions in (4.11) is a function of the size parameter ($x = n_{\mathrm{m}}\pi D/\lambda$, where D is the geometric diameter of the single scatterer and n_{m} is the refractive index of the medium surrounding the scatterers) and the relative complex index of refraction ($m = n - i\kappa$) of the spherical scatterer. It should be noted that $p_{11}(\Theta)$ is normalized as

$$\frac{1}{4\pi} \int_{4\pi} p_{11}(\Theta) d\Omega = 1.$$ (4.12)

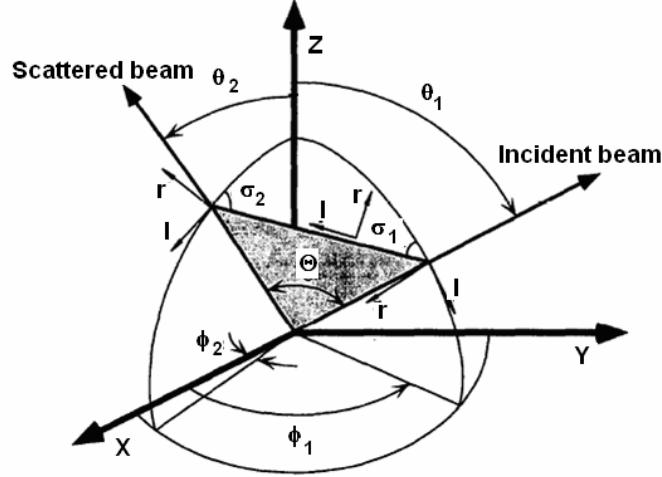where Ω is the solid angle and $p_{11}(\Theta)$ is the **scalar** Mie phase function.

Fig. 4.2 Geometry of the rotation angles necessary in the phase matrix. Shaded plane is the scattering plane. Light beams propagate in the direction r×I.

4.3   Multiple scattering problem

In multiple scattering problems, the I axes of the Stokes vectors, both incident and scattered, are assumed to be parallel to the meridional planes (planes of constant ϕ as seen in Fig. 4.2), and designated ϕ_1 and ϕ_2 respectively. To compute the scattered Stokes vector at a particular location, the coordinate frame of the incident light beam must be **rotated** by an angle $\pi - \sigma_1$ (see Fig. 4.2) such that the I axis is parallel to the scattering plane. The scattering matrix then operates on this rotated Stokes vector. A subsequent rotation by - σ_2 brings the I axis parallel to the meridional plane of the scattered light beam. The above rotations are mathematically equivalent to pre- and post-multiplying the scattering matrix by rotation matrices. Various papers outline this operation [22, 51] hence only the final result will be given here. If the rotation operator is denoted by $\mathbf{L}(\sigma)$, for a rotation of σ, then the **phase** matrix is given by

$$\mathbf{P}(\mu_2, \phi_2; \mu_1, \phi_1) = \mathbf{L}(-\sigma_2)\mathbf{S}(\Theta)\mathbf{L}(\pi - \sigma_1)$$ (4.13)

In the above equation, σ can be found by using spherical trigonometry. So, if $C_1 = \cos 2\sigma_1$, $C_2 = \cos 2\sigma_2$, $S_1 = \sin 2\sigma_1$, and $S_2 = \sin 2\sigma_2$,

$$\mathbf{P}(\mu_{2,}\phi_2;\mu_1,\phi_1) =$$

$$= \begin{bmatrix} p_{11}(\Theta) & C_1 p_{21}(\Theta) & -S_1 p_{21}(\Theta)S_1 & 0 \\ C_2 p_{21}(\Theta) & C_2 p_{11}(\Theta)C_1 - S_2 s_{21}(\Theta)S_1 & -C_2 p_{11}(\Theta)S_1 - S_2 s_{21}(\Theta)C_1 & S_2 d_{21}(\Theta) \\ C_2 p_{21}(\Theta) & S_2 p_{11}(\Theta)C_1 + C_2 s_{21}(\Theta)S_1 & -S_2 p_{11}(\Theta)S_1 + C_2 s_{21}(\Theta)C_1 & S_2 d_{21}(\Theta) \\ 0 & S_1 d_{21}(\Theta) & C_1 d_{21}(\Theta) & s_{21}(\Theta) \end{bmatrix} \quad (4.14)$$

For Rayleigh scattering, the d_{21} term is zero, which results in the decoupling of the circular polarized component. The phase matrix is the vector analog of the phase function used in the scalar radiative transfer theory [52].

4.4   Stokes vectors calculus

When light in an arbitrary state of polarization propagates though a scattering medium or interacts with some optical element, its polarization properties are modified [2, 4]. We may categorize the physical mechanism that can change the state of polarization of light into four areas:
-    propagation through anisotropic media,
-    scattering by a system of particles,
-    oblique reflection and refraction at interfaces, and
-    diffraction by apertures.

Here we put most of the emphasis on the first two types of interaction. The effect of non-image-forming optical instruments and scattering media on an incident electromagnetic plane wave is to transform the Jones vector and the Stokes vector so that the medium can be represented by a transformation matrix. All these problems involve sets of linear equations, and matrix methods provide an appropriate and compact way to deal with these problems. The polarization of light is fully described by the four elements of the Stokes vector, the measurement of which has become possible because of advances in experimental technology.

The contemporary description of polarized light in terms of Stokes vector (4.1) is particularly interesting technique. Its four components describe the intensity and polarization of incoming beam of light. It provides an extremely effective computational technique in the form of the Mueller matrix methods. A natural starting point for characterizing the turbid media through polarized light is Stokes vectors calculus. The beam may be polarized completely, partially, or not at all, it may be monochromatic or polychromatic.

Operational approach makes use of a set of four filters. Any of several different sets could be used, but to make our account specific we shall assume a set of four filters F_1, F_2, F_3, F_4 that have the following properties, each has a positive transmittance for

incident un-polarized light, each is oriented so that its faces are vertical and are perpendicular to the beam, F_1 has the same effect on any incident beam, irrespective of the beam's polarization; in short, it is isotropic, F_2 is opaque to light polarized with its electric vibration direction at 90°, that is, vertical, F_3 is opaque to light polarized at -45°, F_4 is opaque to left-circularly polarized light. Obviously the filters represent non-polarizing, linearly (horizontally) polarizing, linearly (+45°) polarizing and right-circularly polarizing filters respectively, as implied by the polarization forms produced by the four filters used in determining the Stokes parameters of beam shown in Fig. 4.3.
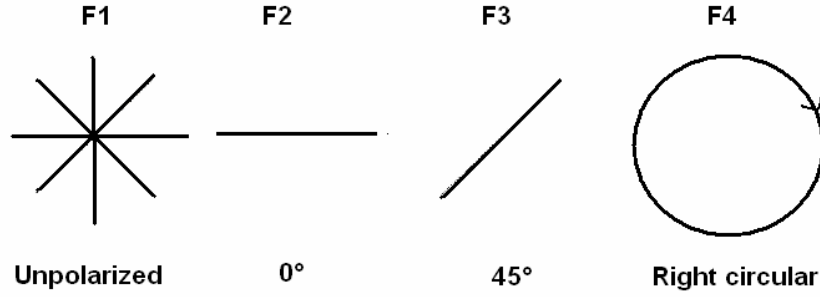

Fig. 4.3 Polarization forms determining four Stokes parameters of a laser beam.

The importance of the Stokes parameters is that they can be formulated using directly measurable quantities. The operational definition of the Stokes parameters is then

$$\begin{aligned}
S_0 &= 2I_0 \\
S_1 &= 2I_1 - 2I_0 \\
S_2 &= 2I_2 - 2I_0 \\
S_3 &= 2I_3 - 2I_0
\end{aligned} \tag{4.15}$$

Let's now relate these parameters to the expressions, for the electric field of a quasi-monochromatic light wave propagating in the z direction,

$$E_x(t) = E_{0x}(t)\cos\left\{(kz - \omega t) + \Delta\varepsilon_x\right\} \tag{4.13}$$

$$E_y(t) = E_{0y}(t)\cos\left\{(kz - \omega t) + \Delta\varepsilon_y\right\} \tag{4.14}$$

where $E(t) = E_x(t) + E_y(t)$ and k, ω are the mean values of wave traveling in z direction and $\Delta\varepsilon$ is phase difference. Then

$$\begin{aligned}
S_0 &= \left\langle E_{0x}^2 + E_{0y}^2 \right\rangle \\
S_1 &= \left\langle E_{0x}^2 - E_{0y}^2 \right\rangle \\
S_2 &= \left\langle 2E_{0x}E_{0y}\cos\Delta\varepsilon \right\rangle \\
S_3 &= \left\langle 2E_{0x}E_{0y}\sin\Delta\varepsilon \right\rangle
\end{aligned} \tag{4.15}$$

or given in the vector form by:

$$\mathbf{S} = \begin{bmatrix} S_0 \\ S_1 \\ S_2 \\ S_3 \end{bmatrix} = \begin{bmatrix} \langle E_{0x}^2 \rangle + \langle E_{0y}^2 \rangle \\ \langle E_{0x}^2 \rangle - \langle E_{0y}^2 \rangle \\ 2\langle E_{0x} E_{0y} \cos \Delta\varepsilon \rangle \\ 2\langle E_{0x} E_{0y} \sin \Delta\varepsilon \rangle \end{bmatrix}. \tag{4.16}$$

The different polarization states can also be described in term of phase and amplitudes (Tab. 4.1).

Table 4.1 The polarization states and their representing equations.

Polarization state [symbol]	Phase	Amplitude	Equation
Horizontal [H]	$\Delta\varepsilon = \pm n\pi$ $n = 0,1,...$	$E_{0y} = 0$ $E_0 = E_{0x}$	$E = E_x + E_y = E_x$ $E_x(z,t) = iE_0 \cos(kz - wt)$
Vertical [V]	$\Delta\varepsilon = \pm n\pi$ $n = 0,1,...$	$E_{0x} = 0$ $E_0 = E_{0y}$	$E = E_x + E_y = E_y$ $E_y(z,t) = jE_0 \cos(kz - wt)$
+ 45° [P]	$\Delta\varepsilon = \pm n\pi$ $n = 0,1,...$	$E_{0y} = E_{0x} = E_0$	$E = E_x + E_y = E_y$ $E(z,t) = (i + j)E_0 \cos(kz - wt)$
- 45° [M]	$\Delta\varepsilon = \pm n\pi$ $n = 0,1,...$	$E_{0y} = E_{0x} = E_0$	$E = E_x + E_y$ $E(z,t) = (i - j)E_0 \cos(kz - wt)$
Right circular [R]	$\delta = \pm n\pi/2$ $n = 1,2,...$	$E_{0y} = E_{0x}$	$E = E_0 \left[iE_0 \cos(kz - wt) + \right.$ $\left. + jE_0 \sin(kz - wt) \right]$
Left circular [L]	$\Delta\varepsilon = \pm n\pi$ $n = 1,2,...$	$E_{0y} = E_{0x}$	$E = E_0 \left[iE_0 \cos(kz - wt) - \right.$ $\left. - jE_0 \sin(kz - wt) \right]$

4.5   Jones calculus and polarization of light

The electric field of any polarized beam propagating along the z-axis may be written as

$$E = E_x i + E_y j \tag{4.17}$$

where $E_x = A_x \exp(kz - wt + \varphi_x)$, $E_y = A_y \exp(kz - wt + \varphi_y)$.

We can write the components as a column vector, which is called a Jones vector.

$$\mathbf{E} = \begin{bmatrix} E_x \\ E_y \end{bmatrix} = \begin{bmatrix} A_x e^{i(kz-wt+\phi_x)} \\ A_y e^{i(kz-wt+\phi_y)} \end{bmatrix}. \tag{4.18}$$

We may factor out and the dependence on *z* and *t* and just write

$$\mathbf{E} = \begin{bmatrix} E_x \\ E_y \end{bmatrix} = \begin{bmatrix} A_x e^{i\varphi_x} \\ A_y e^{i\varphi_y} \end{bmatrix}.$$

(4.19)

The intensity of the beam is proportional to $A_x^2 + A_y^2$. The most general Jones vector of a polarized beam propagating along the z-axis is given by the above equation.

If a polarized beam with field vector **E** is incident on a polarization-changing medium such as a polarizer or a wave plate, and the result is a beam in another polarization state given as:

$$\begin{bmatrix} E_x' \\ E_y' \end{bmatrix} = \begin{bmatrix} m_{11} & m_{12} \\ m_{21} & m_{22} \end{bmatrix} \begin{bmatrix} E_x \\ E_y \end{bmatrix}.$$

(4.20)

Here the 2×2 transformation matrix is called the Jones matrix [8]. Table 4.2 lists the Jones matrices for common optical elements used in the experiments. If we require the Jones matrix for an optical element which has been rotated through an angle *θ* with respect to the direction given in the table above, we must multiply the above matrix by the usual matrices for rotation **R(Θ)**, i.e.

$$\mathbf{M}(\Theta) = \mathbf{R}(\Theta)\mathbf{M}\mathbf{R}(-\Theta)$$

(4.21)

where

$$\mathbf{R}(\Theta) = \begin{bmatrix} \cos\theta & -\sin\theta \\ \sin\theta & \cos\theta \end{bmatrix}.$$

(4.22)

Table 4.2 Jones matrices for some optical elements.

Optical Element	Jones matrix
Horizontal linear polarizer	$\begin{bmatrix} 1 & 0 \\ 0 & 0 \end{bmatrix}$
Vertical linear polarizer	$\begin{bmatrix} 0 & 0 \\ 0 & 1 \end{bmatrix}$
Linear polarizer at 45°	$\begin{bmatrix} \cos^2\theta & \cos\theta\sin\theta \\ \cos\theta\sin\theta & \sin^2\theta \end{bmatrix}$
Quarter wave plate (fast axis vertical)	$e^{i\pi/4}\begin{bmatrix} 1 & 0 \\ 0 & -i \end{bmatrix}$
Quarter wave plate (fast axis horizontal)	$e^{i\pi/4}\begin{bmatrix} 1 & 0 \\ 0 & i \end{bmatrix}$

To find the Jones matrix for a sequence of polarization transformations, for example a linear polarizer followed by a quarter wave plate, we simply multiply the individual Jones matrices together in the correct order. If an incident beam of light with field vector **E** passes through a sequence of four polarizing elements, **M**$_1$ followed by **M**$_2$, **M**$_3$ and **M**$_4$, then the resultant field vector **E'** is given by **E' = M**$_1$.**M**$_2$.**M**$_3$.**M**$_4$. **E**.

So Jones calculus deals with polarized beam of light passing through optical devices.

4.6   Mueller matrix

Mueller developed a matrix that relates the Stokes vector of the light incidented on a sample to the Stokes vector leaving the sample [4, 52]. Using the method with the input and output polarization states (Stokes vectors) known, the 4×4 Mueller matrix can be used to describe the polarization properties of a sample. The Mueller matrix has the general form:

$$\mathbf{M} = \begin{bmatrix} m_{11} & m_{12} & m_{13} & m_{14} \\ m_{21} & m_{22} & m_{23} & m_{24} \\ m_{31} & m_{32} & m_{33} & m_{34} \\ m_{41} & m_{42} & m_{43} & m_{44} \end{bmatrix} \tag{4.23}$$

This is a 4×4 matrix, and thus contains 16 elements. The individual matrix is indicative not only of the composition of the device but also of its orientation; thus the matrix of a linear polarizer whose transmission axis is horizontal is different from the matrix of a similar polarizer that has been turned so that its axis is at, say, 40°. The main rules used in performing the multiplications are the standard rules of matrix algebra. One must also observe the following convention, the vector representing the incident beam must be written at the right, and the successive matrices representing the successively encountered devices must be arranged in order, the matrix of the last-to-be-encountered device being written at the left [45].

The Mueller matrix can be calculated using 16, 36, or 49 polarization images, with 36 and 49 images corresponding to an over determined system (tab.4.3). Sometimes it is necessary to use more than 16 images to reduce the error due to noise associated with the Mueller matrix calculation [52].

Table 4.3 Mueller matrix equations for acquisition of a) 16, b) 36, and c) 49 polarization images.

a)

M$_{11}$=HH+HV+VH+VV	M$_{12}$=HH+HV-VH-VV	M$_{13}$=2PH+2PV-M$_{11}$	M$_{14}$=2RH+2RV-M$_{11}$
M$_{21}$=HH-HV+VH-VV	M$_{22}$=HH-HV-VH+VV	M$_{23}$=2PH-2PV-M$_{21}$	M$_{24}$=2RH-2RV-M$_{21}$
M$_{31}$=2HP+2VP-M$_{11}$	M$_{32}$=2HP-2VP-M$_{12}$	M$_{33}$=4PP-2PH-2PV-M$_{31}$	M$_{34}$=4RP-2RH-2RV-M$_{31}$
M$_{41}$=2HR+2VR-M$_{11}$	M$_{42}$=2HR-2VR-M$_{12}$	M$_{43}$=4PR-2PH-2PV-M$_{41}$	M$_{44}$=4RR-2RH-2RV-M$_{41}$

b)

M$_{11}$=HH+HV+VH+VV	M$_{12}$=HH+HV-VH-VV	M$_{13}$=PH+PV-MH-MV	M$_{14}$=RH+RV-LH-LV
M$_{21}$=HH-HV+VH-VV	M$_{22}$=HH-HV-VH+VV	M$_{23}$=PH-PV-MH+MV	M$_{24}$=RH-RV-LH+LV
M$_{31}$=HP-HM+VP-VM	M$_{32}$=HP-HM-VP+VM	M$_{33}$=PP-PM-MP+MM	M$_{34}$=RP-RM-LP+LM
M$_{41}$=HR-HL+VR-VL	M$_{42}$=HR-HL-VR+VL	M$_{43}$=PR-PL-MR+ML	M$_{44}$=RR-RL-LR+LL

c)

M$_{11}$=OO	M$_{12}$=HO-VO	M$_{13}$=PO-MO	M$_{14}$=RO-LO
M$_{21}$=OH-OV	M$_{22}$=HH-HV-VH+VV	M$_{23}$=PH-PV-MH+MV	M$_{24}$=RH-RV-LH+LV
M$_{31}$=OP-OM	M$_{32}$=HP-HM-VP+VM	M$_{33}$=PP-PM-MP+MM	M$_{34}$=RP-RM-LP+LM
M$_{41}$=OR-OL	M$_{42}$=HR-HL-VR+VL	M$_{43}$=PR-PL-MR+ML	M$_{44}$=RR-RL-LR+LL

The Mueller matrices are shown in Tab. 4.3, where the first and second terms represent the input and output polarization states, respectively. The polarization states are defined as: H = Horizontal, V = Vertical, P = +45°, M = -45°, R = Right circular, L = Left circular and O = Open (i.e. no polarization).

For example, the Mueller matrix of material irradiated with Stokes vectors is given as:

$$\mathbf{S}_f = \mathbf{M.S} = \begin{bmatrix} m_{11} & m_{12} & m_{13} & m_{14} \\ m_{21} & m_{22} & m_{23} & m_{24} \\ m_{31} & m_{32} & m_{33} & m_{34} \\ m_{41} & m_{42} & m_{43} & m_{44} \end{bmatrix} \begin{bmatrix} S_0 \\ S_1 \\ S_2 \\ S_3 \end{bmatrix} \qquad (4.24)$$

and according to the usual rules of the matrix multiplication, the product has the form,

$$\mathbf{S}_f = \begin{bmatrix} m_1 S_0 & m_{12} S_1 & m_{13} S_2 & m_{14} S_3 \\ m_{21} S_0 & m_{22} S_1 & m_{23} S_2 & m_{24} S_3 \\ m_{31} S_0 & m_{32} S_1 & m_{33} S_2 & m_{34} S_3 \\ m_{41} S_0 & m_{42} S_1 & m_{43} S_2 & m_{44} S_3 \end{bmatrix}. \qquad (4.25)$$

It is to note that each row of the product contains terms that are connected by plus signs. Accordingly each row consists, essentially, of a single element. Thus the expression is a column vector, not a 4×4 matrix. When, say, four optical devices are inserted in the beam, four matrices must be used and four multiplications are called for. If the four matrices are called $\mathbf{M}_1$, $\mathbf{M}_2$, $\mathbf{M}_3$, $\mathbf{M}_4$, and if $\mathbf{S}$ represents the Stokes vector of the incident beam, the procedure for finding the specification $\mathbf{S}_f$ of the emerging beam is indicated schematically thus

$$\mathbf{M}_1.\ \mathbf{M}_2\ .\ \mathbf{M}_3\ .\ \mathbf{M}_4\ .\ \mathbf{S}\ =\mathbf{M}_t\ .\ \mathbf{S}=\mathbf{S}_f. \qquad (4.26)$$

4.6.1　Derivation of Mueller matrix for polarizer

The matrices of the Mueller calculus are not derived from the electromagnetic theory of light or any other theory [22]. Rather, they rest on a phenomenological foundation. They were initially discovered by experimentation, or by reliance on previous experimentation. One makes a guess as to what the elements of 4×4 matrixes must be, then tries out the matrix to see whether it performs satisfactorily. To be deemed fully satisfactory, it must lead to results that are known to be correct for four independent types of incident beam, for example,
(1) unpolarized light,
(2) light that is horizontally polarized,
(3) light that is linearly polarized at 45°, and
(4) light that is right-circularly polarized.

The task of finding the matrix $\mathbf{P}(\theta)$ of a polarizer at some general azimuth θ is easy, once one knows the matrix $\mathbf{P}_0$ of the polarizer in its principal orientation, that is, with its transmission axis horizontal. Using a convention procedure of matrix algebra, one computes the product, which is standard and is:

$$\mathbf{P}(\theta) = \mathbf{T}(-2\theta)\cdot\mathbf{P}_0\cdot\mathbf{T}(2\theta) \qquad (4.27)$$

where $\mathbf{T}(2\theta)$ is the standard rotator matrix [2],

$$\mathbf{T}(2\theta)=\begin{bmatrix} 1 & 0 & 0 & 0 \\ 0 & C_2 & S_2 & 0 \\ 0 & -S_2 & C_2 & 0 \\ 0 & 0 & 0 & 1 \end{bmatrix} \qquad (4.28)$$

where $C_2 = \cos 2\theta$, $S_2 = \sin 2\theta$, and $\mathbf{T}(-2\theta)$ is the counter-rotator matrix, the same as $\mathbf{T}(2\theta)$, except that the signs of the sine elements S_2 are changed.

As standard Mueller matrix for polarizer is given by

$$\mathbf{P}_0 = \begin{bmatrix} 1/2 & 1/2 & 0 & 0 \\ 1/2 & 1/2 & 0 & 0 \\ 0 & 0 & 0 & 0 \\ 0 & 0 & 0 & 0 \end{bmatrix}. \tag{4.29}$$

So performing the indicated multiplication one finds, for the matrix $\mathbf{P}(\theta)$ of an ideal homogeneous linear polarizer with transmission axis at angle θ

$$\mathbf{P}(\theta) = \begin{bmatrix} 1 & 0 & 0 & 0 \\ 0 & C_2 & -S_2 & 0 \\ 0 & S_2 & C_2 & 0 \\ 0 & 0 & 0 & 1 \end{bmatrix} \begin{bmatrix} 1/2 & 1/2 & 0 & 0 \\ 1/2 & 1/2 & 0 & 0 \\ 0 & 0 & 0 & 0 \\ 0 & 0 & 0 & 0 \end{bmatrix} \begin{bmatrix} 1 & 0 & 0 & 0 \\ 0 & C_2 & S_2 & 0 \\ 0 & -S_2 & C_2 & 0 \\ 0 & 0 & 0 & 1 \end{bmatrix} \tag{4.30}$$

$$\mathbf{P}(\theta) = \frac{1}{2} \begin{bmatrix} 1 & C_2 & S_2 & 0 \\ C_2 & C_2^2 & C_2 S_2 & 0 \\ S_2 & C_2 S_2 & S_2^2 & 0 \\ 0 & 0 & 0 & 0 \end{bmatrix}. \tag{4.31}$$

The same procedure applies to a retarder: the matrix of a device at a non-principal azimuth is computed from that of the device at the principal azimuth with the aid of the rotator matrix and counter-rotator matrix.

4.6.2 General Mueller matrix for retarder

If ρ is the angle of axis (fast axis) of retarder with respect to the x-axis, then $a_x = \cos\rho$ and $a_y = \sin\rho$, as shown in Fig. 4.4. The standard Mueller matrix for the retarder at fast axis is given by [45].

$$\mathbf{M}_R = \begin{bmatrix} 1 & 0 & 0 & 0 \\ 0 & D^2 - E^2 + G^2 & 2DE & -2EG \\ 0 & 2DE & -D^2 + E^2 + G^2 & 2DG \\ 0 & 2EG & -2DG & 2G^2 - 1 \end{bmatrix}. \tag{4.32}$$

Here $D = S_1 \sin\dfrac{\Delta\varepsilon}{2}$, $E = S_2 \sin\dfrac{\Delta\varepsilon}{2}$, $F = S_3 \sin\dfrac{\Delta\varepsilon}{2}$ & $G = \cos\dfrac{\Delta\varepsilon}{2}$ and $\Delta\varepsilon$ is the phase difference (required to produce for rotation of polarization of light for two components of light beam passing through the retarder and S_1, S_2, S_3 are the 2nd, 3rd and 4th components of the Stokes vector respectively. That is

$$S_1 = a_x^2 - a_y^2, \ S_2 = 2a_x a_y \cos\Delta\varepsilon, \ S_3 = 2a_x a_y \sin\Delta\varepsilon \tag{4.33}$$
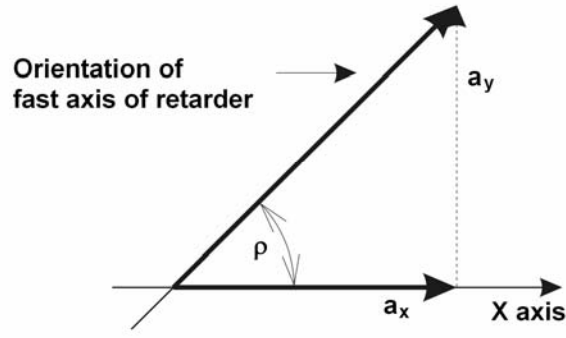
Fig. 4.4 The orthogonal components due to orientation of retarder.

4.7   Biological particles

Using previous equations (4.9) and (4.13) we can characterize a biological particles which are generally complex arrangements of various shaped structures [52], often having large size distributions resulting in relatively little structure in the differential scattered light intensity S_{ii}. However, complex structure does occur on other S_{ij} signals, as shown by our preliminary work with selected biological systems. The matrix elements of (4.9) and (4.13) we studied in this experiment are:

$$S_{11} = \frac{1}{2}(A_1^2 + A_2^2 + A_3^2 + A_4^2),$$ (4.34)

$$\frac{S_{12}}{S_{11}} = \frac{\frac{1}{2}(-A_1^2 + A_2^2 - A_3^2 + A_4^2)}{\frac{1}{2}(A_1^2 + A_2^2 + A_3^2 + A_4^2)} = \frac{-A_1^2 + A_2^2 - A_3^2 + A_4^2}{A_1^2 + A_2^2 + A_3^2 + A_4^2},$$ (4.35)

$$\frac{S_{13} + S_{33}}{S_{11} + S_{31}} = \frac{(A_3 A_2 - A_4 A_1 + A_2 A_1 + A_3 A_4)\cos\Delta\varepsilon}{\frac{1}{2}(A_1^2 + A_2^2 + A_3^2 + A_4^2) + (A_2 A_4 - A_3 A_1)\cos\Delta\varepsilon},$$ (4.36)

$$S_{34}^* = \frac{S_{14} + S_{34}}{S_{11} + S_{13}} = \frac{(A_2 A_3 + A_3 A_4)\cos\Delta\varepsilon - (A_2 A_3 + A_4 A_1)\sin\Delta\varepsilon}{\frac{1}{2}(A_1^2 + A_2^2 + A_3^2 + A_4^2) + (A_2 A_3 + A_4 A_1)\cos\Delta\varepsilon}.$$ (4.37)

Theoretically, the S*$_{34}$ matrix combination is unique in comparison to other matrix elements. The presence of the phase terms $\cos\Delta\varepsilon$ and $\sin\Delta\varepsilon$ can cause a sign change in S*$_{34}$ for very small changes of $\Delta\varepsilon$. The larger number of possibilities for zeros and oscillations about zero contribute to the larger structure on the S*$_{34}$ signal as compared to the other matrix elements and matrix element combinations listed above. The S*$_{34}(\theta)$ signal can be zero at various θ even if no coefficients are zero. Among other matrix elements the S*$_{34}$ is highly structured and thus can be an excellent probe of scatterers.

4.8   Degree of polarization

The degree of polarization (DOP), which is important characteristics in ageing measurement, can be calculated through output intensities and the values of measured intensities lie between -1 and 1, and they represent the tendency of the measured light to be polarized linearly, ±45°, and right or left-handedness.

DOP is a measure of the polarization purity of light. $DOP = 1$ means that light is completely polarized; $DOP = 0$ means the light is completely depolarized; $DOP < 1$ means the light is partially polarized.

If an incident state is 100% polarized and the exiting state has a *DOP* < 1, then the system is said to possess depolarization property. Depolarization is usually encountered due to multiple scattering of photons (although randomly oriented uniaxial birefringent domains can also depolarize light); incoherent addition of amplitudes and phases of the scattered field results in scrambling of the output polarization state. The general form of a pure depolarization Mueller matrix is

$$\mathbf{M}_\Delta = \begin{bmatrix} 1 & 0 & 0 & 0 \\ 0 & a & 0 & 0 \\ 0 & 0 & b & 0 \\ 0 & 0 & 0 & C \end{bmatrix}, \ |a|,|b|,|c| \leq 1. \tag{4.38}$$

Here $1-|a|$ is depolarization factor for linear polarization (horizontal/vertical), $1-|b|$ for +45°/−45° linear polarization, and $1-|c|$ for circular polarization. The net depolarization factor is usually defined as

$$\Delta = 1 - \frac{|a|+|b|+|c|}{3} = 1 - \frac{\left[TR(M_\Delta)-1\right]}{3}, \ 0 \leq \Delta \leq 1, \tag{4.39}$$

where *T* is transmittance and *R* reflectance of the tissue slab.

Note that this definition of depolarization factor of the medium is different from the conventional Stokes parameter-based definition of degree of polarization of the light [Eqs. (4.2) and (4.3)]. The latter represents the degree of polarization resulting from all depolarization effects encountered by the beam, and also depends on the incident Stokes vector. In contrast, the depolarization factors of (4.39) represent the pure depolarizing transfer function of the medium [53].

Another quantity of interest is the mean number of scattering events Γ undergone by a photon.

Since $I_n(x,y,z;\mu,\phi)$ is the intensity (note that this represents the first element of the Stokes vector) of light which has undergone n scattering events, and $\sum_{n=1}^{\infty} I_n(x,y,z;\mu,\phi)$ is the intensity of light which has been scattered *at least* once (i.e., n ≥ 1), the probability that a photon gets scattered n times (where n ≥ 1), ρ_n is

$$\rho_N = \frac{I_N(x,y,z;\mu,\phi)}{\sum_{n-1}^{\infty} I_N(x,y,z;\mu,\phi)} \tag{4.40}$$

Thus the mean number of scattering events $\Gamma(x,y,z;\mu,\phi)$ undergone by a photon at a particular location of interest is the estimated value of n, and is evaluated with the equation

$$\Gamma(x,y,z;\mu,\phi) = \sum_{n=1}^{\infty} \rho_n = \frac{\sum_{n=1}^{\infty} n I_n(x,y,z;\mu,\phi)}{\sum_{n=1}^{\infty} I_n(x,y,z;\mu,\phi)} \ . \tag{4.41}$$

5   EXPERIMENTAL

The tissue polarimetry of scattered light ends in two major directions, tissue imaging and tissue characterization. For our purpose only the second item is useful. In the checking of ageing state of meat tissue control, accurate measurement of the polarization retaining signal is extremely important. In this regard, many of the traditional polarimetry systems are not suitable for biological tissue examination [54-57]. Resultant multiple scattering in thick tissues leads to depolarization of light, creating a large depolarized source of noise that makes a detection of the small remaining information-carrying polarization signal very difficult.

A variety of experimental tools schematically described in Chapter 2 has therefore been developed to maximize measurement sensitivity, so that reliable measurements and analyses of the tissue polarimetry data can be performed. These methods can be employed to perform measurement of both Stokes vector of the light upon interacting with the sample, and/or of the Mueller matrix of the sample itself, as will be described in next Chapter 6.

5.1   Samples

For the purpose of our investigation, different kinds of biological tissue and media have been used, as follows:
- pork chop meat [58, 59],
- chicken breast meat [60],
- milk [61], and
- polystyrene bills as phantom for the computation of scattering [61].

The samples from porcine or chicken meat were cut in slices with thickness of 1.0-5.0 mm in a parallel or perpendicular way to the muscle fibers (Fig. 5.1). Their surface area has been 1×1 cm^2 for transmitted light, and greater then one square centimeter for backscattering experiments.

Measurements were provided in three different temperatures. The meat samples were hold in ambient room temperature (20°C), in the cooler (4°C) and ice-box (-8°C) for three days.
There are various experimental systems capable of detecting weak polarization signals in the presence of large diffusive background for light scattered from a random biological medium [4, 17].

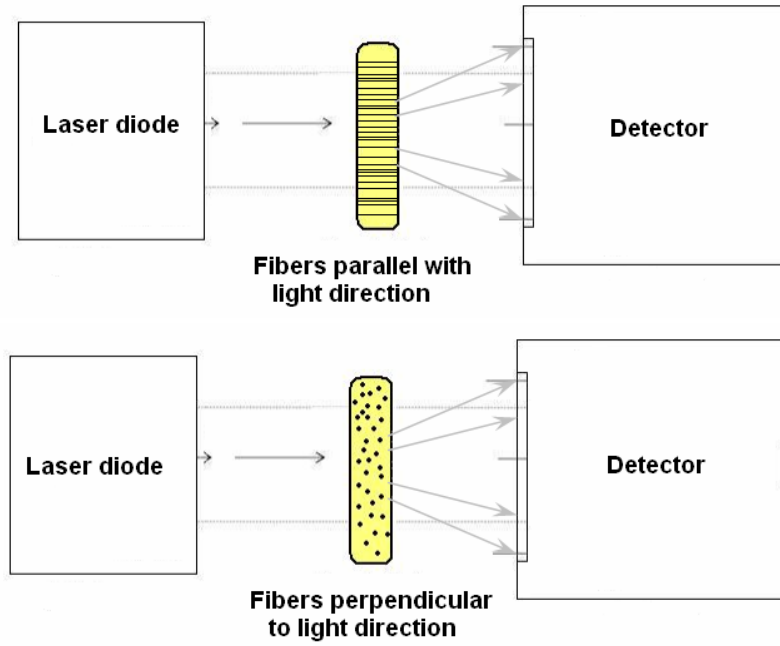We have tried several of them in transmitted and reflected (back-scattered) light.

Fig. 5.1 Orientation of muscle fibers during investigation.

5.2 Transmitted light

The optical setup for measuring coordinate distributions of parameters of biological tissue (BT) (i.e. meat) object fields with transmission mode is shown in Fig. 5.2. Here 1 – laser diode, 2 - collimator, 3 – object between cover glasses, 4 – lens, 5 – analyzer, 6 – PIN detector, 7 – PC.
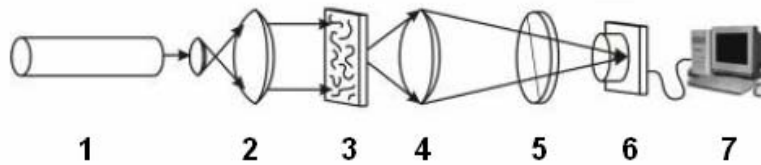

Fig. 5.2. Experimental set-up for the measurement of polarization variations of light transmitted through the sample.

Collimated linearly polarized laser light from most frequently used He-Ne laser ($\lambda = 632.8$ nm) or laser diode ($\lambda = 635$ nm) with a power up to 5 mW illuminates a sample and is scattered on it [61]. The transmitted scattered light passes through a polarization analyzer attached with a rotating mount and a computer controlled stepping motor drive unit. The polarization is controlled by quarter-wave plates, while polarizer is used to form a laser beam with polarization azimuths $0 \leq \alpha \leq \pi$ and the ellipticities $0 \leq \beta \leq \pi/2$.

Polarization images of BT obtained by means of microobjective were projected onto the PIN photodiode with square surface of 25.0 mm^2. The coordinate distribution of the intensities of the BT laser image was first measured by means of the Si PIN detector, without the analyzer. Then the analyzer was inserted, whose transmission axis was sequentially rotated from $\alpha = 0$ to 360° and the intensity values for these angles were measured. After changing orientation of the transmission axis of analyzer within the range 0-360°, the minimal and maxima levels of the image intensities. The precision of analyzer rotation stage is better than 0.1 degree, but the step of 1 degree was used in the range of 360° (Fig. 5.3).
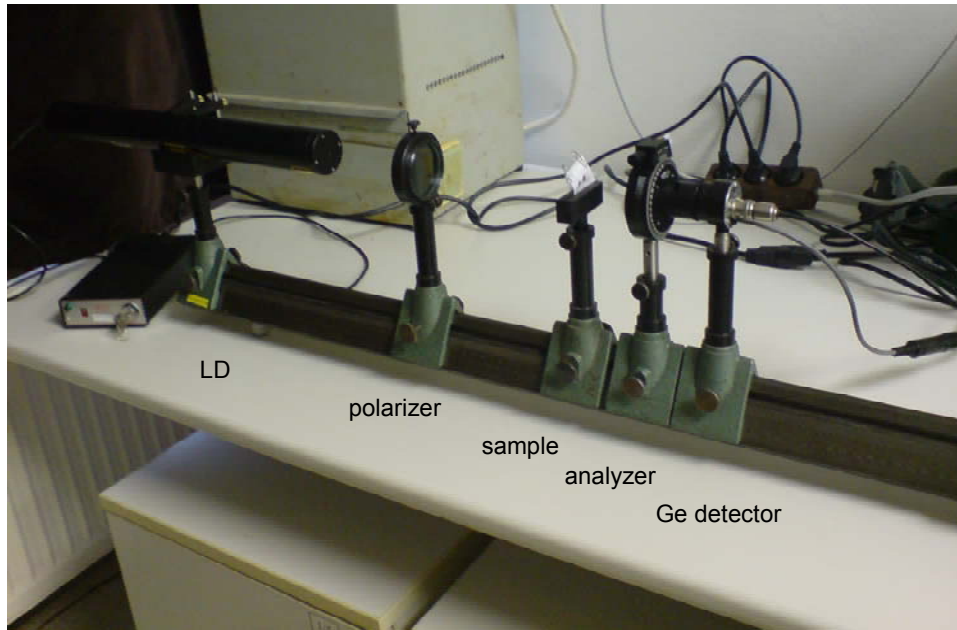
Fig. 5.3. Experimental set-up for forward transmitted light.

5.2.1 Stokes vector polarimeter

Multiple scattering measurement in thick tissues leads to depolarization of light, creating a large depolarized source of noise that hinders the detection of the small remaining information-carrying polarization signal.

Hence a schematic of the experimental polarimetry system employing polarization modulation and synchronous lock-in-amplifier detection is shown in Fig.5.4.

Light from a He-Ne laser ($\lambda = 632.8$ nm) first passes through a mechanical chopper operating at a frequency $f_c \sim 500$ Hz; this is used in conjunction with lock-in amplifier detection to accurately establish the overall signal intensity levels. The input optics enables generation of any of the four input Stokes polarization parameters of light which can be determined by performing six intensity measurements involving linear and circular polarization states [57].
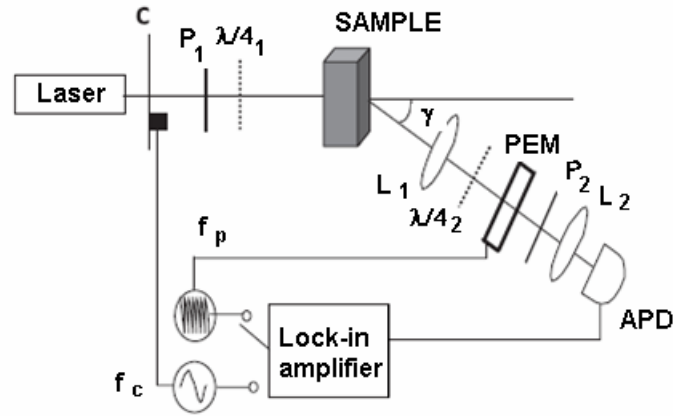
Fig. 5.4. Scheme of the experimental polarimetry system employing polarization modulation and synchronous lock-in-amplifier detection [57].

The detected signal is sent to a lock-in amplifier with its reference input switching between the frequencies of the chopper (500 Hz) and the PEM controller (50 kHz and harmonics) for synchronous detection of their respective signals.

5.3　Back-scattered light

The experimental scheme to obtain the Mueller matrix of the biological tissue from back-scattered light measurement is shown in Fig. 5.5 and Fig. 5.6. [60]. Similarly to transmitted light set-up its optical part consists of a He–Ne laser source ($\lambda = 632.8$ nm), a linear polarizer, and an analyzer/photodetector combination to measure the scattered light intensity and the polarization properties of the scattered light. Electrical part then consists of the lock-in and transimpedance amplifiers enable sensitive synchronous measurement of the resultant photocurrent. A mechanical chopper in optical path operating at ∼ 150 Hz is also used; when tuned to its rotation frequency, the lock-in measures the overall light intensity, and when tuned to the PEM's oscillation frequency (and its harmonics), the lock-in signal is sensitive to the polarization fraction that has survived the sample interactions. The beam splitter is present to enable detection of light that emerges from the sample centered on the exact backscattering direction.
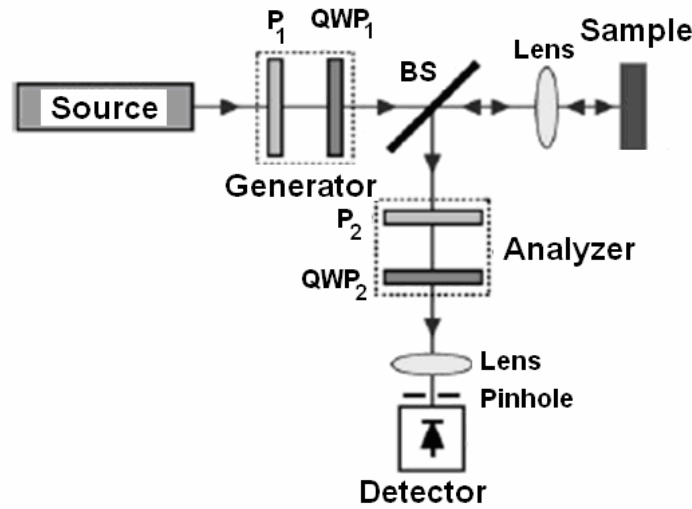
Fig. 5.5 Schematic of experimental setup for back-scattering polarimetry measurements.

Fig. 5.6 Experimental setup for back-scattering measurements.

In the measurement system, including both the input and output polarization devices employed to obtain the Mueller matrix **M** of the depolarizing medium, light coming from an input source is introduced into a polarizer and a quarter-wave plate serving both as generator (Fig. 5.4), and its output is sent to a beam splitter (BS). This BS transmits the light on the sample, focusing it onto it through an optical lens. The reflected signal is conducted by the BS to an output analyzer, that consists of a linear polarizer and a quarter wave plate, and finally to the detector.

In the similar set-up, the photoelastic modulator (oriented at 6° off normal incidence with respect to the incident beam direction, to negate the effects of modulated specular interference) oscillates in the plane of the optical table. The polarizer is at 45° with

respect to the plane of the optical table, and the orientation of analyzer is set to rotate in the 0–360° range. D1 and D2 are pinhole diaphragms (Fig. 5.7 and Fig. 5.8.) [58, 61].
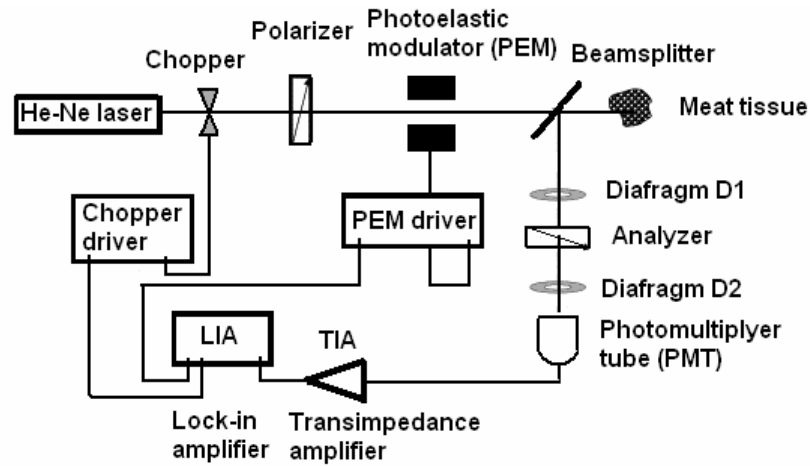
Fig.5.7 Schematic of modified experimental system for measuring back-scattered diffusely reflected light from a turbid biological sample.
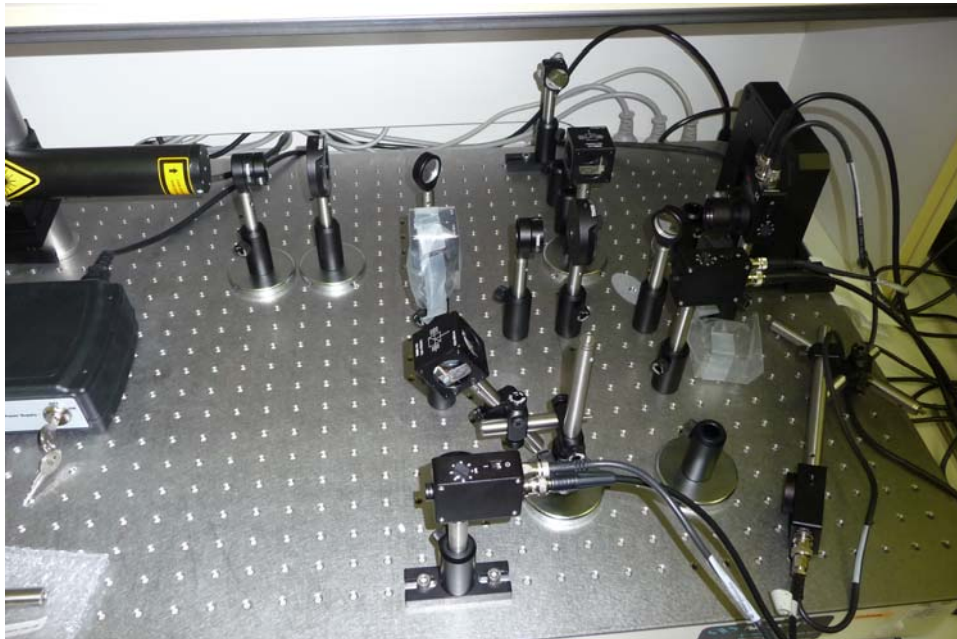

Fig.5.8 Experimental system for measuring polarization properties of back-scattered diffusely reflected light.

Finally the modified experimental system capable of detecting weak polarization signals in the presence of large diffusive background for light scattered from a random biological tissue is illustrated in Fig.5.9.
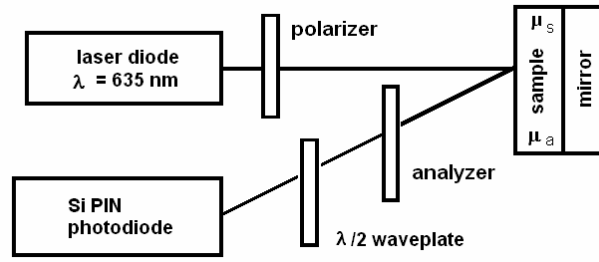
Fig. 5.9 Schematic of experimental set-up for the measurement of polarization variations of light backscattered from the sample.

Here a collimated linearly polarized light from red laser diode ($\lambda = 635$ nm) with an optical output power of 5 mW illuminated a thin slices of meat was reflected and back-scattered on it [59]. The slice was fastened on the mirror which serves to enhance the output signal. Transmitted light passing through the sample was reflected on the sample holder mirror, reflected back through the meat again, and combined with the simply reflected and back-scattered light inside the sample. Then the signal was passing through an analyzer (quarter-wave plate) attached with a rotating mount. The analyzer transmission axis has been sequentially rotated from 0 to 360°. The analyzer and detector were placed at an angle of $\leq 15°$ from the optical axis at distance of 100 mm from the surface of the sample.

In addition, a half-wave plate was inserted to compensate a rotation, because carbohydrates in the muscles have chiral carbon atoms, so the structure is optically active. Analyzed signal was projected onto the PIN Si-photodiode detector with square surface of 25.0 mm², and minima and maxima of polarization intensity were measured.

Optical devices introduced in the measurement system in order to extract out the Mueller matrix of an optical media can produce depolarization and the introduction of error factors in the measurements because of their imperfections. These errors are optical activity φ_P, strain δ_P and leakage γ in the linear polarizer and optical activity φ_R and dichroism α_R in the linear retarder. Therefore, the Mueller matrices with the error factors for the linear polarizers and retarders are calculated and the influence of these error-terms on the elements of the Mueller matrix is suppressed.

6 RESULTS

In this Chapter we use the theory outlined above to analyze the multiple scattering of a narrow, linearly polarized light beam by a plane-parallel medium composed of spherical dielectric scatterers (latex particles suspended in water) and then we shall study a real situation of the polarization state of multiple scattered light due to the meat sample ageing.

6.1 Monte Carlo analysis of multiscattered light

The proposed Monte Carlo analysis of multiple scattering events of light in turbid biotissue media is based on the radiative theory [4, 49, 60]. It is assumed that the scattering event of light is independent and has no coherence effects. In addition, we assume that all of the linearly birefringent tissue can be looked on as a uniaxial material with the slow axis (the orientation with higher refractive index) along the direction of the muscle fibers and the fast axis (the orientation with lower refractive index) along the cross section. Thus a scattering is assumed to be caused by the spherical particles that randomly suspend among the birefringent media.

The geometry of a multiple scattering event is shown in Fig. 6.1 [62].
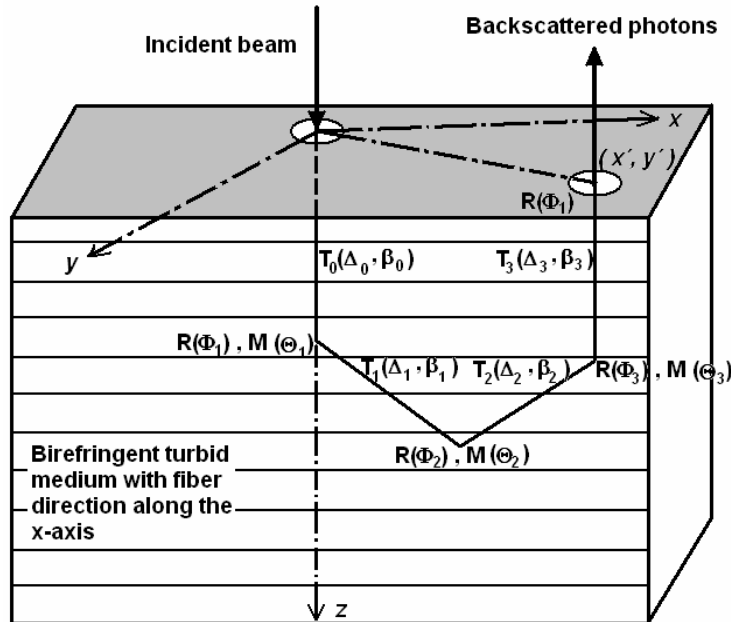

Fig. 6.1 Geometry of a multiple scattering event in a linearly birefringent turbid medium.

In this figure, we assume that the direction of the slow axis of the linear birefringence is along the *x* axis. Photons are scattered in the medium by spherical particles, therefore Mie theory can be used to describe the scattering events. Diffusely backscattered photons are recorded as a function of (*x´,y´*) on the upper surface of the medium.

Simulation of the photon trajectories in Monte Carlo method consists of the following key stages:

- injection of the photon in the medium, generation of the photon path-length,
- generation of a scattering event,
- definition of reflection/refraction at the medium boundaries,
- definition of detection and
- accounting for the absorption.
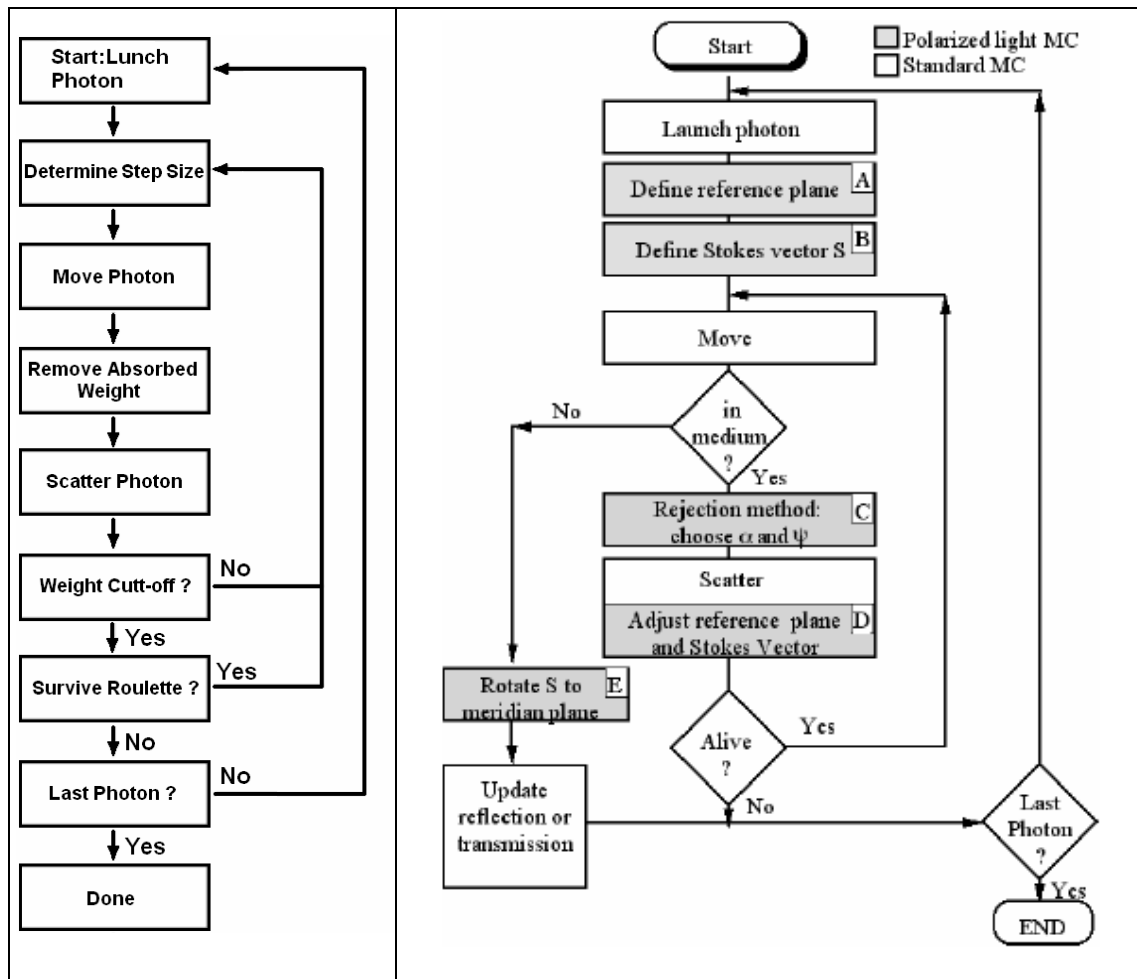
Fig. 6.2 Standard Monte Carlo program and proposed Polarized Light Monte Carlo program (PLMC) flow charts.

The polar angle θ and the azimuthal angle ϕ are not uniformly distributed between $(0, \pi)$ and $(0, 2\pi)$. Sampling of θ and ϕ depends on the probability density function (PDF) of θ and ϕ that is a function of the incident Stokes vector. Figure 6.2 shows the difference between Standard Monte Carlo program (white cells) [49] and proposed Polarized Light Monte Carlo program

(PLMC) involving polarized light into the system (additional grey cells specific for PLMC). [62].

Inside this system a backscattered component of the radiation is investigated. The spherical scatterers were assumed to have a relative refractive index of $m = 1.197 + 0i$. A variety of studied situations is shown in Table 6.1.

Table 6.1 Number of orders of scatterers as a function of size parameter x and optical thicknesses L.

x	L			
	0.1	**0.5**	**1.0**	**5.0**
0.430	25	50	50	100
0.813	25	50	50	100
1.592	25	50	50	100
2.379	25	50	50	100
3.264	25	50	50	100

For each size parameter, the back-scattered Stokes vector (4.15) was obtained for four optical thicknesses L of the slab. The four elements of the Mie phase matrix (4.11) for $m = 1.197 + 0i$, are plotted in Fig. 6.3 for the size parameters of interest in this study.


a)

b)

c)

d)
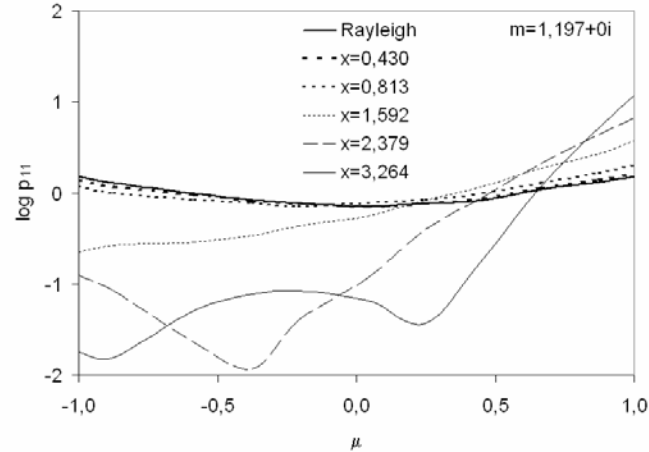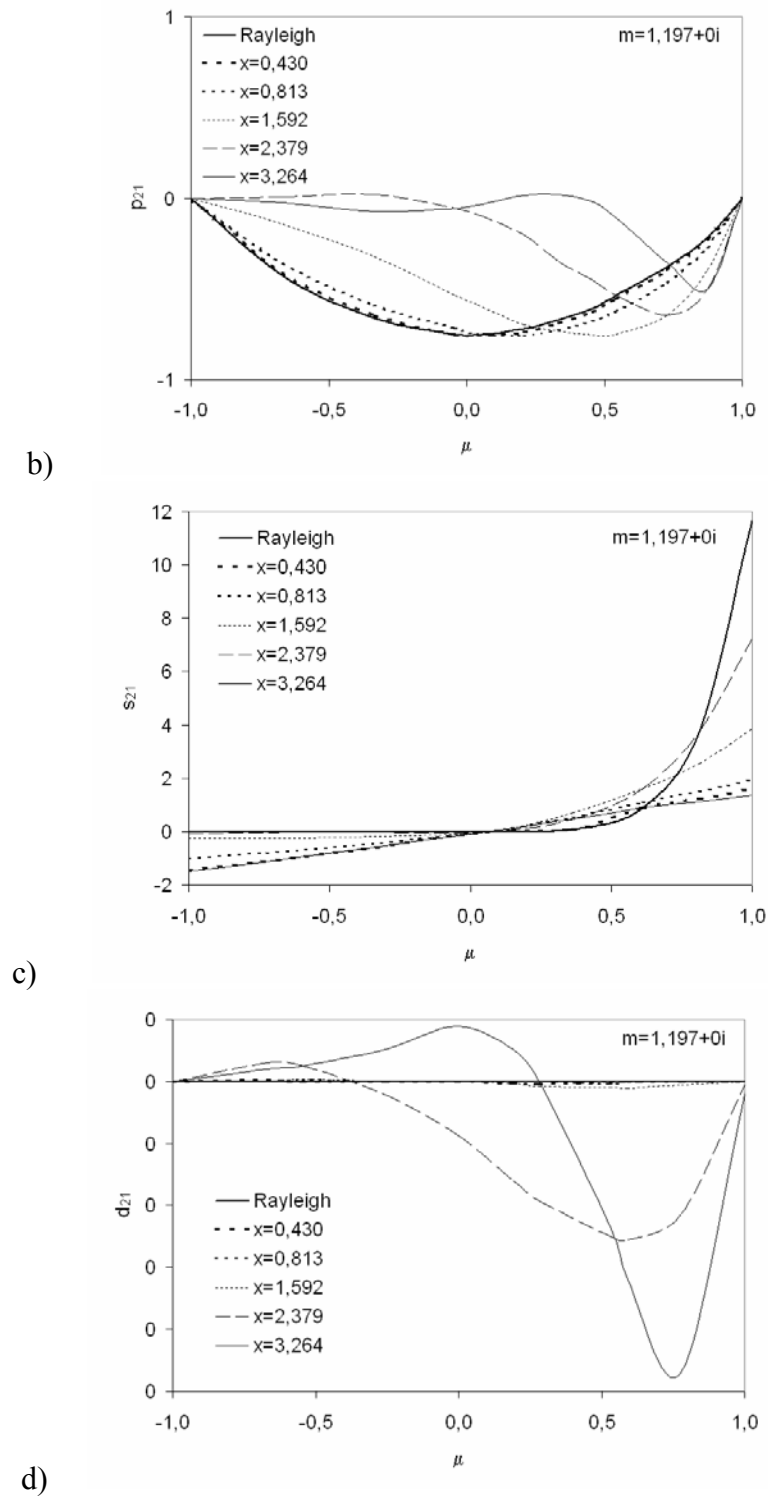
Fig. 6.3 Computed four elements of Mie phase matrix (Eq. 4.11).

The quantities of interest are the elements of the Stokes vector, the degree of linear polarization DOP_L, and the degree of circular polarization DOP_c. Another quantity of

interest is the mean number of scattering events Γ undergone by a photon and the probability ρ_n that a photon gets scattered n times (where n $\geq$ 1).

6.1.1 Intensity

The radial (see Fig. 6.1) variation of the backscattered polarized intensity appears to have the same form as that observed for the scalar problem [62, 63]. This can be seen in Fig. 6.4, where the normalized intensity increases and then decreases with an increase in the optical diameter $D = 2a$. Some interesting features can be noted. For increasing particle size parameters, the backscattered intensity decreases.
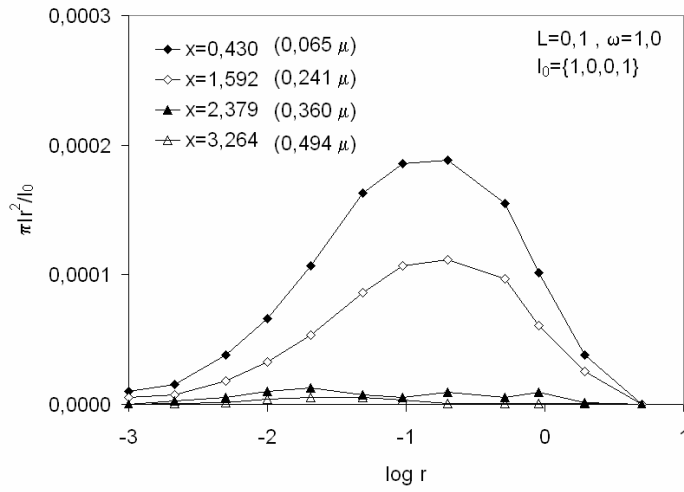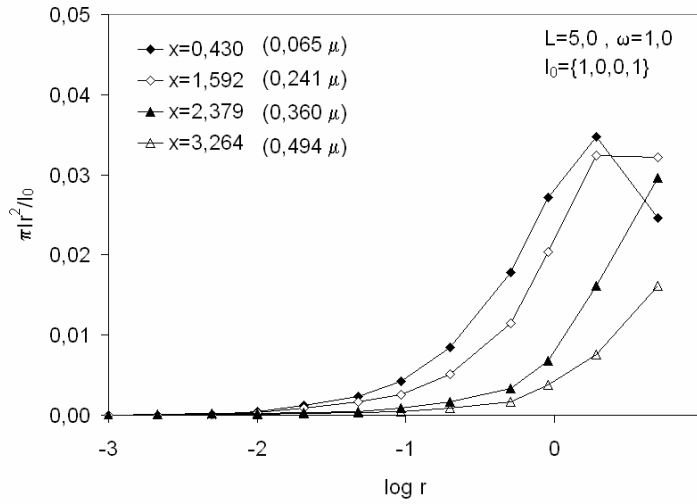

a)
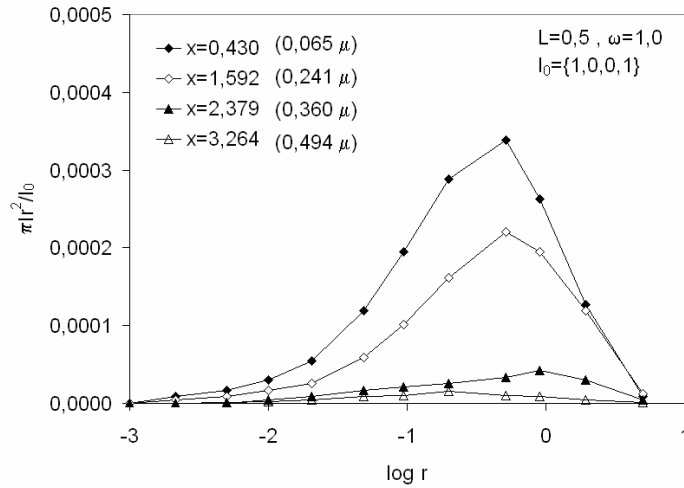
b)
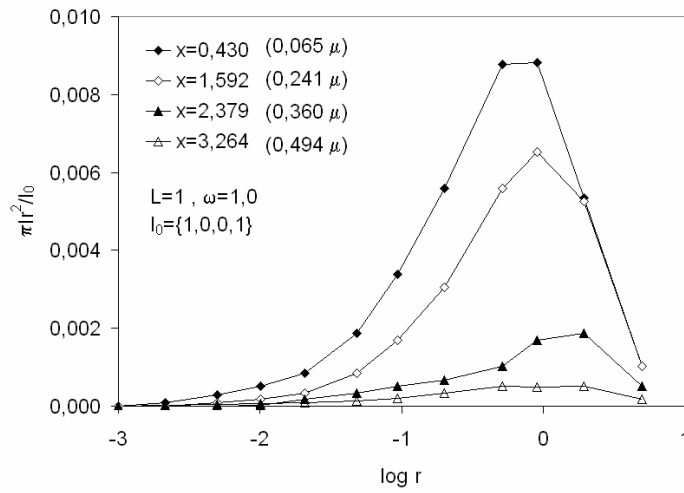
c)

d)

Fig. 6.4 Normalized intensities vs. distance of detector r for a number of size parameters x and optical thicknesses L = 0.1 mm, 0.5 mm, 1.0 mm, 5.0 mm.

This can be attributed to the fact that larger particles have a larger asymmetry factor which implies that a greater portion of the energy of the incident beam is scattered in the forward direction. For larger optical depths (see Fig. 6.4d), the backscattered intensity increases because a larger proportion of the energy of the incident beam is backscattered.
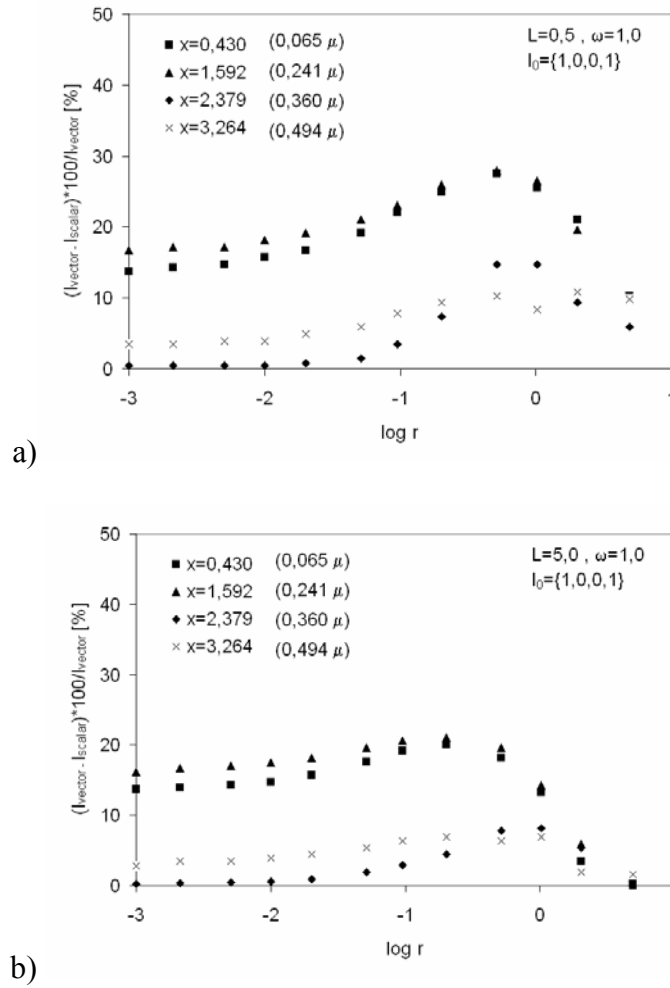
a)

b)

Fig. 6.5 Difference between the vector and scalar radiative transfer solutions for diffuse light field in distance *r* for a number of size parameters *x* and optical thicknesses $L = 0.5$ mm and L = 5.0 mm.

In Fig. 6.5 the vector and scalar estimates of the intensity for two optical thicknesses *L* are compared. Clearly, for smaller size parameters, the difference between the vector and scalar theories is significant whereas it is smaller for larger size parameters. Also, it appears that for very large optical radii the difference between vector and scalar solutions decreases. However, this does not necessarily imply that the diffuse light field at large optical radii or small size parameters is unpolarized. Quite the contrary is observed in experiments.

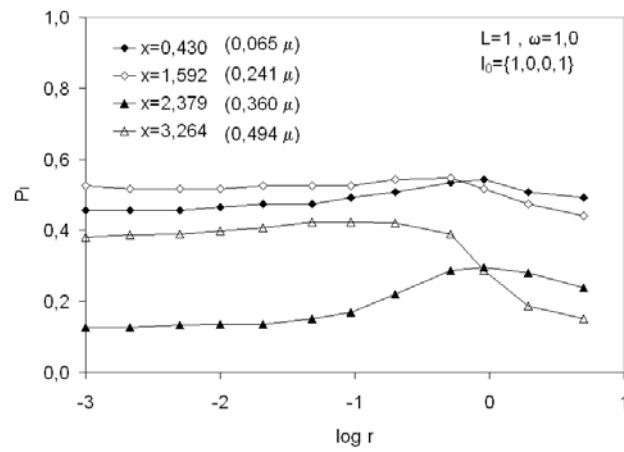## 6.1.2   Degree of linear polarization

In Fig. 6.6 computed degree of linear polarization (DOP_L) (Eq.4.3) for the above cases is shown. The behavior here is very interesting.
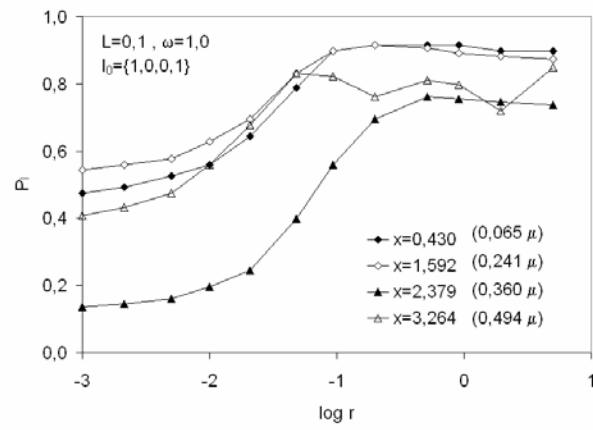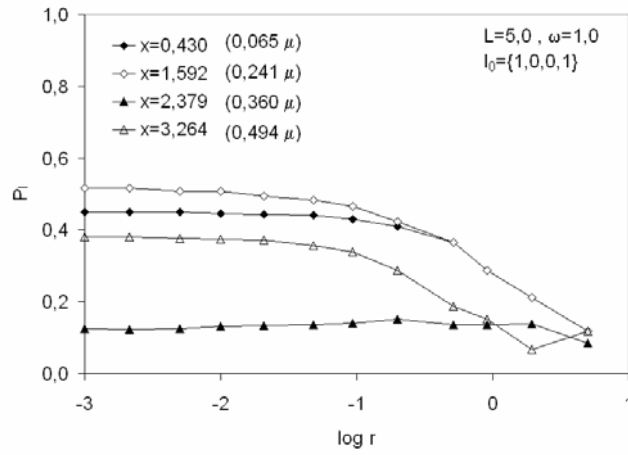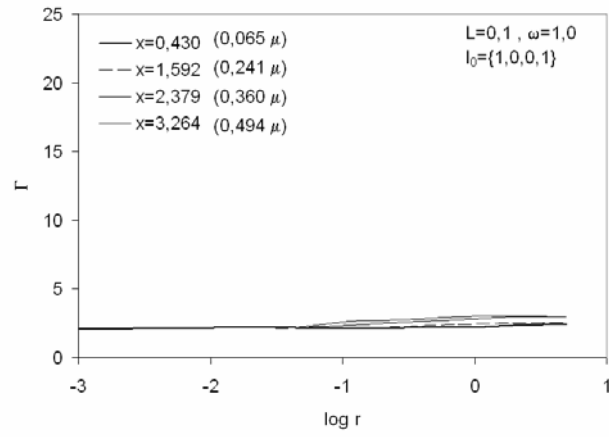
a)
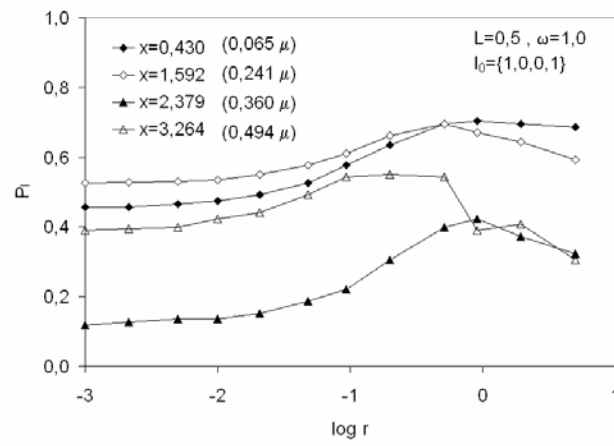
b)

c)

d)

Fig. 6.6 Computed DOP$_L$ in distance of detector r for a number of size parameters x and optical thicknesses $L = 0.1$ mm, 0.5 mm, 1.0 mm, 5.0 mm.

The DOP$_L$ (4.3) at small optical radii is the same irrespective of optical depth. This is because at small optical depths, the multiple scattering is primarily second-order (see Fig. 6.7). Thus the double scattered Stokes matrix for backscatter, which is important for biological tissue measurement, becomes essentially independent of optical depth. However, the variation with respect to particle size is harder to explain, particularly at small radii.

For an optical depth of 0.1, the DOP$_L$ at large optical radii exhibits a behavior that is monotonic with respect to particle size. The degree of linear polarization decreases with an increase in particle size. The case of x = 3.264, however, shows an anomalous behavior in the sense that the data are highly oscillatory at even small optical radii. This is because the intensity is very low in this region for x = 3.264. Thus when the DOP_L is computed by dividing by the intensity, the errors in this quantity lead to unpredictable results.

Similar trends are observed for larger optical thicknesses. However, the degree of linear polarization decreases for a given size parameter with an increase in the optical thickness. The interesting feature in Fig. 6.6 is due to the fact that, even at reasonably large optical radii, the light field exhibits a high degree of linear polarization. In Fig. 6.7, the mean number of scattering events (4.41) for a medium with an optical thickness of 5.0 mm at an optical radius of 1.0, $\Gamma > 5$. Thus even for quite a large number of scattering events (see Fig. 6.7), the light field retains its polarized character (Fig.6.6).
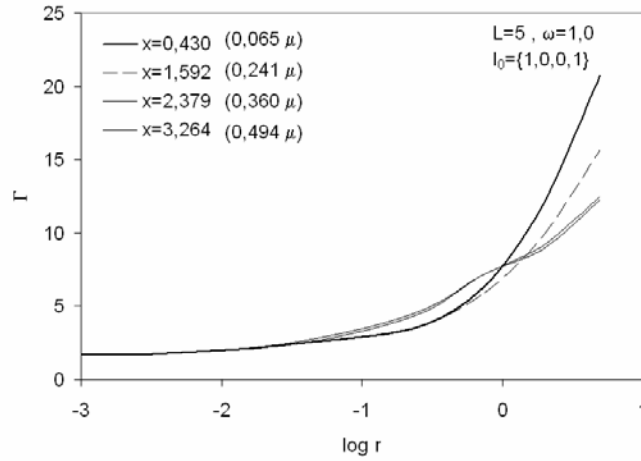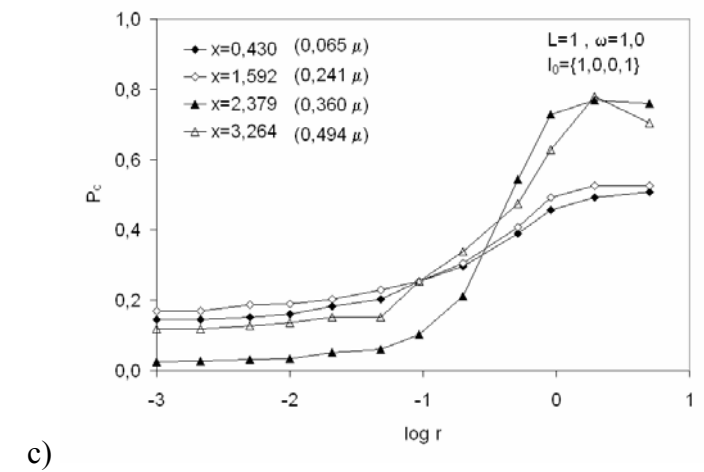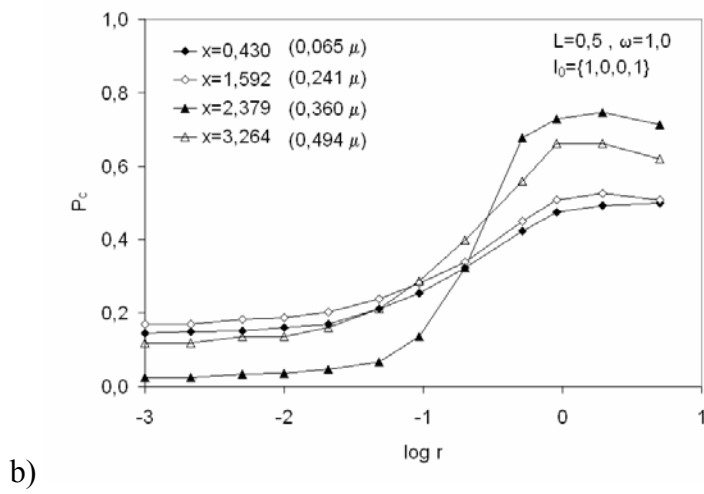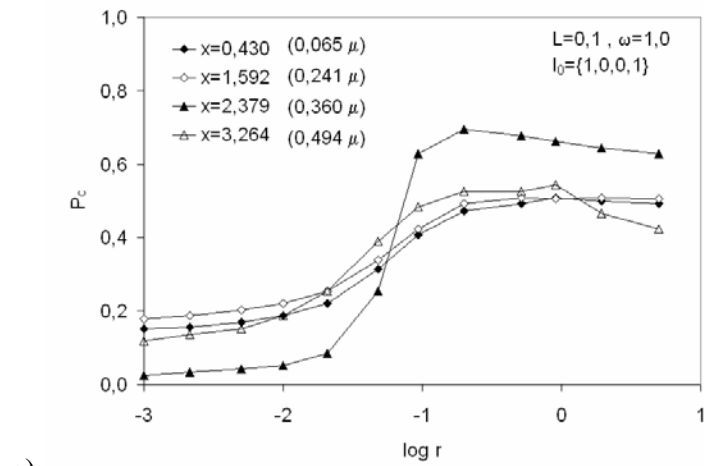
a)
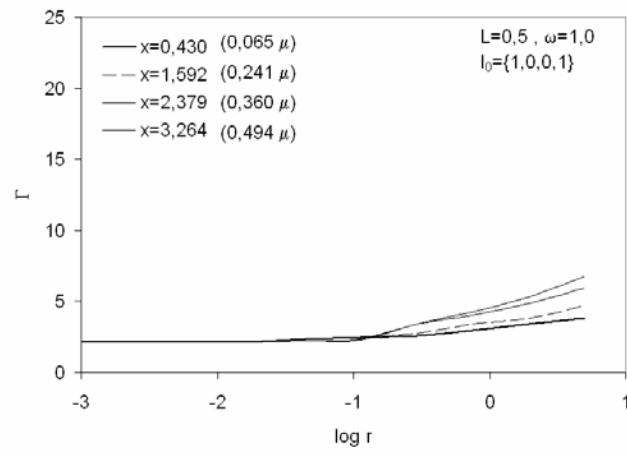
b)
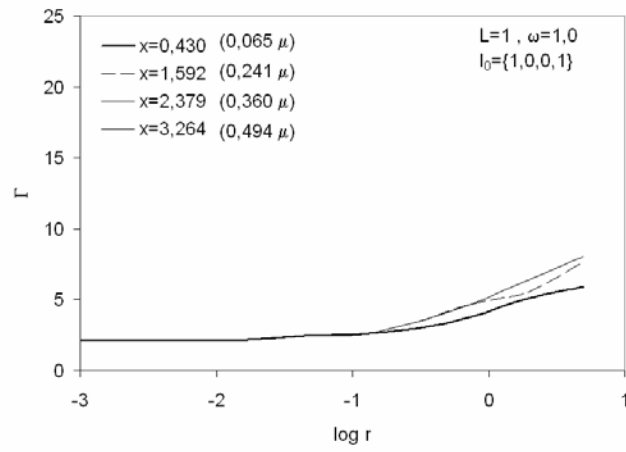
c)

d)

Fig. 6.7 Mean number of scattering events Γ in distance of detector r for a number of size parameters x and optical thicknesses $L = 0.1$ mm, 0.5 mm, 1.0 mm, 5.0 mm.

.

6.1.3 Degree of circular polarization

In Fig. 6.8, the degree of circular polarization DOP_C (4.4) is shown. In this case DOP_C is identical for all optical depths at small optical radii. The anomalous behavior for a size parameter of x = 3.264 can be explained in a similar manner to the previous paragraph. At large optical radii, the trend is an increase in the degree of circular polarization for larger size parameters. This can be explained as follows: for small size parameters, the d_{21} term in the scattering matrix (4.11) is negligible, and often = 0. This implies that the circular component of the vector radiative transfer equation (2.27) is essentially decoupled. Thus the circular component V of the vector radiative transfer equation behaves as a scalar intensity with an effective albedo $\omega < 1$. It thus approaches zero much faster than the actual intensity I. However, with an increase in the size parameter, the quantity d_2, becomes more significant. The physical effect of d_{21} is the coupling of the circular and linear components of the light field.

Thus, for a larger size parameter, an increase in the conversion of linear light to circular light can be expected.

Another interesting feature to be observed is that the sign of the degree of circular polarization goes negative as the optical radius is increased. In other words, the direction of rotation of the electric vector changes at larger optical radii. However, the degree of circular polarization does not seem to decrease appreciably at large optical radii for increased optical depths of the medium. Again, the interesting physical effect is that the light field is polarized at large optical radii.

a)

b)

c)
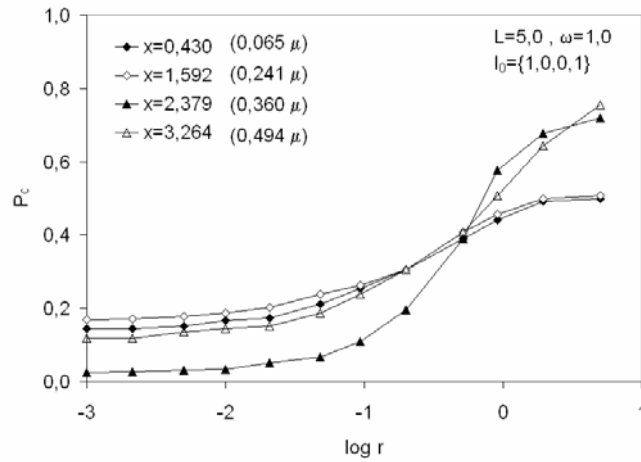
d)

Fig. 6.8. Degree of circular polarization (DOP$_C$) in distance of detector r for a number of size parameters and optical thicknesses (L = 0.1 mm, 0.5 mm, 1.0 mm, 5.0 mm).

6.2   Ageing process

Due to the fact that meat as biological tissue is a chiral medium, it is optically active and curls a linear polarization plane. Therefore this rotation is one of the characteristics of ageing process within muscle fibers.

Two types of measurements were provided [63]:

1. Measurement of polarized light transmitted through the biological tissue sample.

2. Measurement of polarized light reflected and twice transmitted forward and backward through the biological tissue sample – meat slice attached on sample holder mirror (Fig.5.9).

First for a purpose of our investigation, we have used a pork chop meat as a sample, cut in slices of 1.0-5.0 mm thick and sandwiched by a pair of microscope cover glasses. The slices were cut parallel or perpendicularly to the muscle fibers (Fig. 5.1).
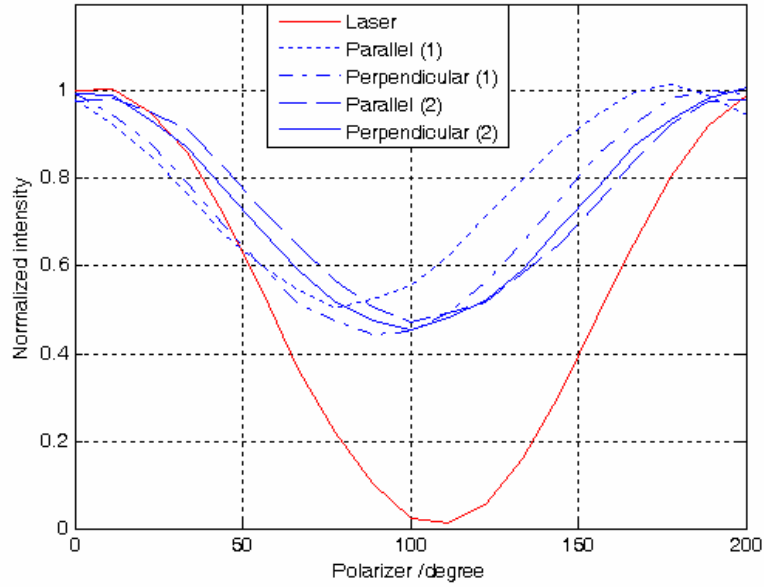
Fig.6.9 Angular dependence of polarization directions of diffused light for two meat samples sliced along the muscle fibers and orthogonally to them.

Figure 6.9 displays an angular dependence of polarized light for samples of thickness 2.0 mm for measurement without turbid scattering sample and two parallel and perpendicular muscle orientations to the cutting plane.

Following Fig. 6.10 represents calculated DOP in on a thickness of the meat layers. Next we have examined how polarization degree was related to the thickness of the sample. Figure 6.11 shows the result for slices with thickness of 3.0 mm where muscle fiber directions were aligned perpendicularly to the cover glass. The quantity of DOP was calculated from (4.2).
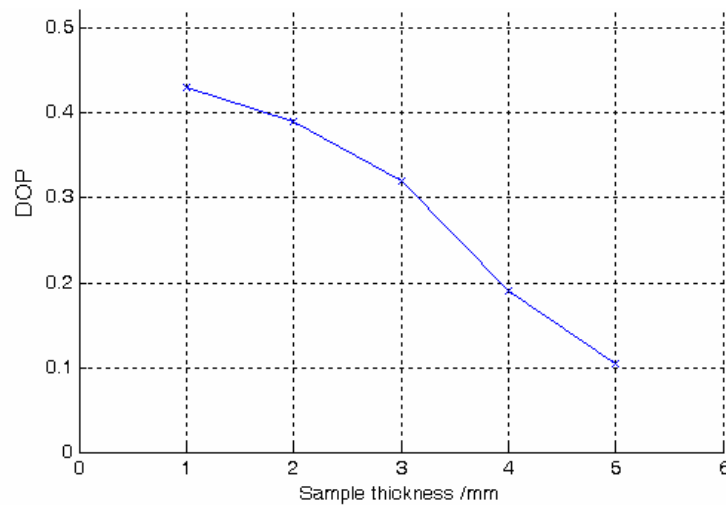

Fig. 6. 10 Dependence of degree of polarization (DOP) (Eq.4.2) on optical thicknessess of meat slices (L = 1.0 mm, 2.0 mm, 3,0 mm, 4,0 mm and 5.0 mm).

Obviously, it is recognized that the polarization is changed with the meat thickness. This is caused by the multiple scattering which makes the polarization states more uniform. But it is surprising that although scattered light has almost random characteristics, the DOP > 40% at the thickness of 1.0 mm is maintained.

We have investigated the relationship between the polarization changes and meat ageing. Figure 6.11a shows the result obtained in transmitted light during first 180 minutes with a sample thickness of 4.0 mm. Here, the chiral characteristics of the light polarization were measured every 5 minutes during first 180 minutes for a commercial meat sample with the muscle fiber orientation perpendicular to the background nontransparent plate. We can see that after approx. 20 minutes the degree of polarization decreases linearly with time after meat slicing. Figure 6.11b gives the result obtained in backscattered light with mirror and opaque plates as sample holders. This measurement was provided after storing the meat 3, 6 and 72 hours in temperature 20°C [64].
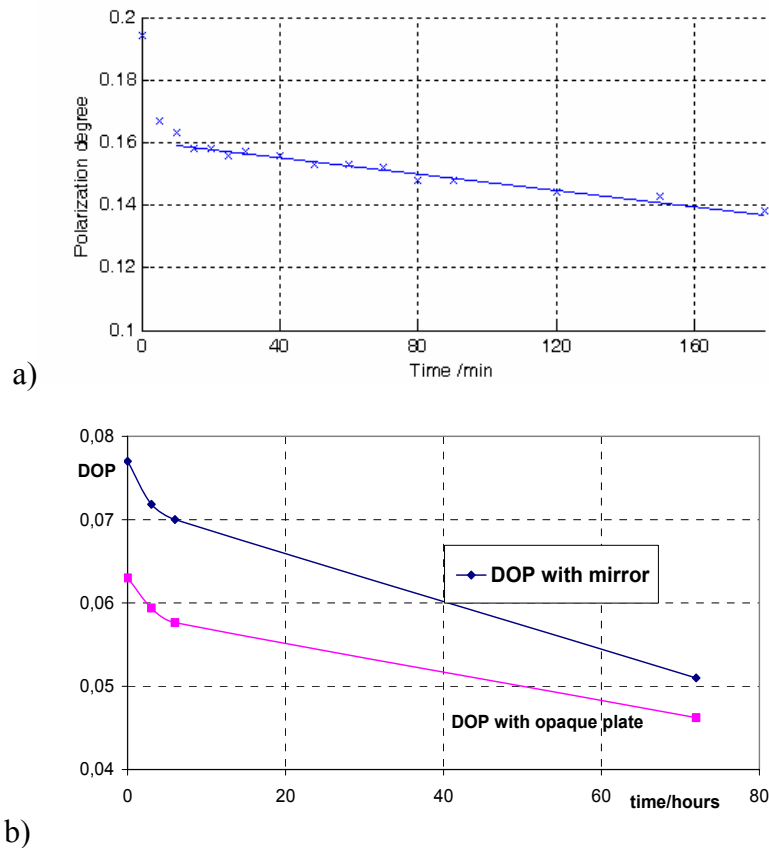

a)

b)

Fig. 6. 11 Dynamics of DOP vs. meat aging time after slice processing. a) in transmitted light, b) in backscattered light with mirror and opaque plate.

Figure 6.12 represents results of temporal dependence of linear polarization, due to the water evaporation at room temperature +20°C. In this case the sample was fixed on the mirror. Similar results, but with lower reflected intensity, was then obtained using opaque background plate instead mirror. In both cases a slight drift of polarization maxima to the left is evident.
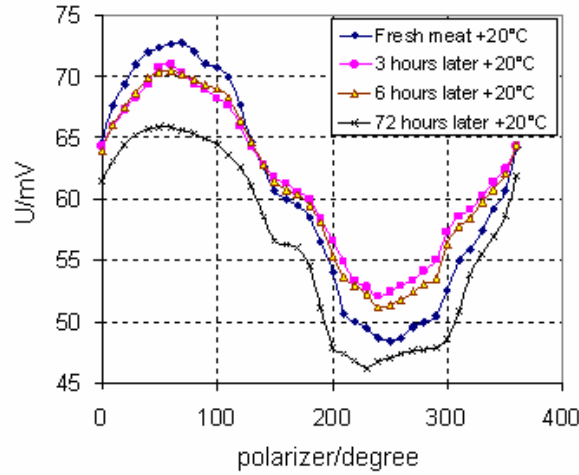
Fig. 6.12 Dynamic shift of polarization maxima due to the ageing.

Figure 6.13. represents a result of temperature influence on polarization state for three temperature (+20°C, +5°C and -8°C) after 72 hours of ageing.
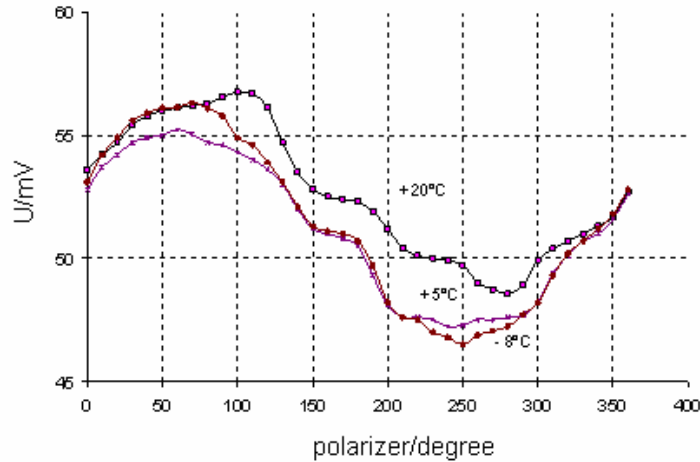
Fig. 6.13 Thermal polarization dynamics (after 72 hours) when samples were stored at +20°C, + 5°C (cooler) and -8°C (ice-box).

Finally, we have considered the meat sample as a linearly birefringent turbid medium consisting of a stack of horizontal fibers with diameter of 2 μm. Using the PLMC

method it was possible to compare results of simulated back-scattering Mueller matrix for suspension of linear detectors with diameter of 2 μm (Fig. 6.14a) with experimental back-scattering Mueller matrix measurement for fresh pork chop fibers of similar diameter (Fig. 6.14b) [62].
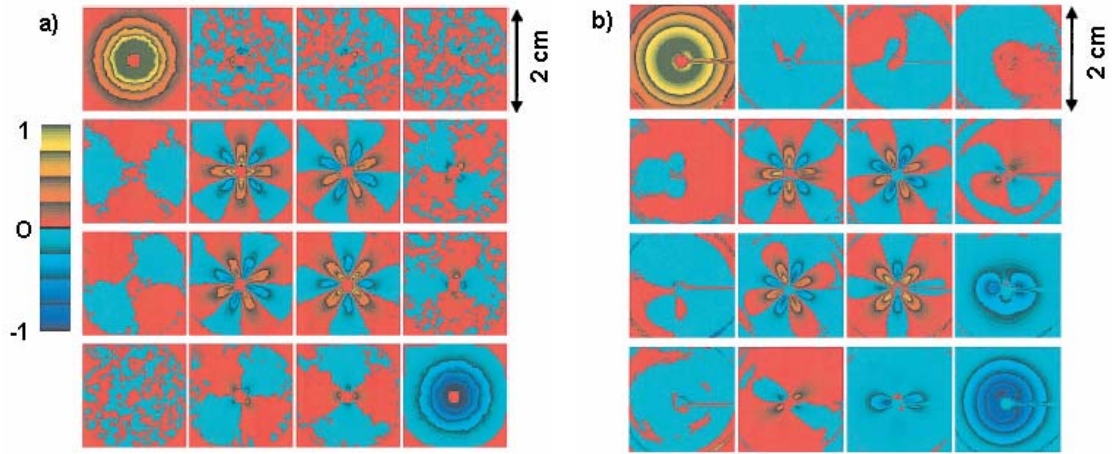
Fig. 6.14 a) Simulated back-scattering Mueller matrix for suspension of linear detectors with diameter of 2 μm.
b) Experimental back-scattering Mueller matrix for fresh pork chop fibers.
Each image displays a 2×2 cm area of the surface.

7   CONCLUSIONS

Optical inspection of biological tissues is essential tool for the medical and food quality control investigations. So the study of the light propagation in biological tissue, where cell dimensions are larger than the wavelength of the used light, is growing in importance. As a result of interaction of light and the matter, the Mie scattering of transmitted or reflected light arises and thus produces various polarization states. Thus, it is possible to take advantage of changes in polarization state of light to measure the freshness or ageing of processed food.

Having this in mind, the principal **objectives** of this dissertation thesis were to **provide**
- **better understanding** of nature of **various physical phenomena** (polarization, scattering, birefringence) in turbid media, *i.e.* biological tissue, and
- **measurement of temporal variations of polarization states due to multiple scattering** of light in biological tissue (processed meat) **going to the ageing**.

These objectives also include a **study** of:
1. **complex nature of polarization effects** in tissue,
2. **depolarization** of signal as a result of tissue **multiple scattering**,
3. **difficulty** in measuring typically s**mall tissue polarization signals**,
4. **analysis and quantification** of measured signals or images, and mainly
5. **complexity** in understanding and **interpreting tissue polarimetry results**.

To achieve these objectives, we have chosen, from enormous variety of properties and measuring techniques, a study of optical properties, and more precisely polarization, scattering in the tissues, and their behaviors during the tissue ageing.

However, it is still not clear what specific muscle properties are responsible for optical scattering. As an effort to answer these questions, we conducted several controlled experiments in which we studied the changes of scattering coefficient with muscle length (or sample thickness), temperature and ageing time. The optical scattering coefficient of pork and chicken muscles were measured based on a diffusive fitting of spatially resolved reflectance measurements. Samples with different thickness were prepared from freshly slaughtered animals. Our results indicated that muscle scattering coefficient increased with ageing time and sample thickness. This study suggests that muscle structural properties have significant impact on muscle optical scattering coefficients. These experimental observations can be confirmed and explained based on simulation using Stokes vector and Mueller matrix calculus on the basis of Radiate Transfer Equation and modified Monte Carlo method for polarized light.

Our novel approach to this field was based on the hypothesis that a state of polarization changes in meat with time. The results of thesis with personal contribution to the field are as follows:

1) Scattering – polarization properties of tissue ageing

Most of this work has involved a characterization of biological tissue optical properties as a function of ageing time [52, 57, 58, 59, 60, 63].

If the thick layer of meat sample is illuminated, the multiple scattering occurs, and this phenomenon varies accordingly. In the case of the postmortem tissue (meat) the changes caused by ageing are not caused not only by a chemical process, but also by drying of the sample leading to the variation of polarization state of the light.

Two kinds of experimental measurement were performed: scattering of polarized light passing forwards and backwards in the sample and only transmitted light.

Our measurements show a significant curl of polarized light. This depends on the orientation of the muscle fibers and ageing process of meat. The correlation of polarization changes of light in meat vs. meat ageing shows that the dynamic angular behavior of the polarization could be used as a predictor for meat ageing.

2) Simulation of polarized light photon transport in multiscattered media whose characteristics dependent on several factors [52, 57, 61, 62, 64]:

Experimental observations shown that the problem, due to its complexity, is not easy to explain, therefore it was necessary to simulate photon transport, in the case when light changes its polarization state in turbid biological tissue.

So the modified polarized light Monte Carlo method (PLMC) allows compute the photon forward and backward transfer in the tissue. The comparison of simulated back-scattering Mueller matrix for suspension of linear detectors with diameter of 2 μm and experimental back-scattering Mueller matrix for fresh pork chop fibers shows a high correlation.

Finally, to conclude we can assert that our hypothesis was partially confirmed and approved, mainly in red meats which need some time to their maturity and tenderness. We are basically able to evaluate, under normal condition of cooling, the state of meat freshness.

A non-negligible result of this thesis is also its pedagogical aspect. Therefore, the present text can be considered as a useful textbook for our students in Libya.

8   REFERENCES

[1]   BARBOSA-CANOVAS, G.V., JULIANO, P., PELEG, M., *Engineering properties of foods*, In Food Engineering, Ed. G..V. BARBOSA-CANOVAS, in Encyclopedia of Life Support Systems (EOLSS), Developed under the Auspices of the UNESCO, EOLSS Publishers, Oxford, UK, (2004/Rev.2006) http://www.eolss.net

[2]   CHEONG, W.F., PRAHL, S.A., WELCH, A.J.: A review of optical properties of biological tissues, *IEEE Journal of Quantum Electronics*, 1990, vol. 26, No. 12, 2166-2185.

[3]   DAMEZ, J-L., CLERJON, S., Meat quality assessment using biophysical methods related to meat structure, *Meat Science*, 2008, vol. 80, pp. 132–149.

[4]   TUCHIN, V.V., *Tissue Optics: Light scattering methods and instruments for medical diagnosis*, 2nd edition, SPIE Press, Bellingham, 2007, ISBN: 978-0-8194-6433-0.

[5]   JACQUES, S. L., Laser-tissue interactions. Photochemical, photothermal, and photomechanical, *Surgical Clinics of North America*, 1992, vol. 72, No. 3, pp. 531-558.

[6]   TOMÁNEK, P., MIKLÁŠ, J., BAJGAR, A., GRMELA, L., DOBIS, P., BRÜSTLOVÁ, J., Sensor of back-scattered light polarization in body cells, *Proceedings of SPIE,* 2009, vol. 7356, paper ID 735685, 9 p.

[7]   SALEEH, B.E. A, TEICH, M. C., *Fundamental of Photonics*, vol. 2, John Wiley and Sons, New York, 1991, ISBN: 0-471-83965-5

[8]   HULST, van de, H.C., *Light scattering by small particles*, Dover Publications, New York, 1981, ISBN: 0-486-64228-3

[9]   FIRDOUS, S, IKRAM, M., Polarized laser beam scattering through turbid medium for application in tissue imaging, *Science Asia*, 2005, vol. 31, p. 167-172,

[10]   SAAR, B.G., PARK, H-S., XIE, S., LAVRENTOVICH, O.D., Three-dimensional imaging of chemical bond orientation in liquid crystals by coherent anti-Stokes Raman scattering microscopy, *Optics Express,* 2007, vol. 15, No. 21, p. 13585 – 13596.

[11]   VITKIN, I.A., HOSKINSON, E., Polarization studies in multiply scattering chiral media, *Optical Engineering*, 2000, vol. 39, p. 353-362.

[12]   LIU, Y., HERING, P., SCULLY, M.O., An integrated optical sensor for measuring glucose concentration, *Applied Physics B*, 1992, vol. 54, Issue 1, p. 18-23

[13]   MATTHEYSES, A. L., KAMPMANN, M., ATKINSON, C. E., SIMON, S.M., Fluorescence anisotropy reveals order and disorder of protein domains in the nuclear pore complex, *Biophysical Journal*, 2010, vol. 99, p. 1706–1717.

[14]   CLOUDE, S.R., POTTIER, E., Concept of polarization entropy in optical scattering, *Optical Engineering,* 1995, vol. 34, No.6, p. 1599-1610.

[15] TYO, S.J., GOLDSTEIN, D.L., CHENAULT, D.B., SHAW, J.A., Review of passive imaging polarimetry for remote sensing applications, *Applied Optics*, 2006, vol. 45, No. 22, p. 5453 – 5469.

[16] YAROSLAVSKY, A.N., BARBOSA, J., NEEL, V., Di MARZIO, Ch., ANDERSON, R.R., Combining multispectral polarized light imaging and confocal microscopy for localization of nonmelanoma skin cancer, *Journal of Biomedical Optics*, 2005, vol. 10, No. 1, paper ID 014011.

[17] GHOSH, N.; VITKIN, I. A. Tissue polarimetry: concepts, challenges, applications, and outlook. *Journal of Biomedical Optics,* 2011, vol. 16, No.11, paper ID: 110801, e-ISSN: 1560-2281.

[18] GIBSON, A.P., HEBDEN, J.C., ARRIDGE S.R. Recent advances in diffuse optical imaging. *Physics in Medicine and Biology.* 2005, vol. 50, p. R1-R43.

[19] MAKSIMOVA, I.L., TARTARINTSEV, S.N., SHUBOCHKIN, L.P., Multiple scattering effects in bio-objects with laser diagnostics, *Proceedings of SPIE*, 1993, vol. 1981, Optical methods of biomedical diagnostics and therapy, p. 88-95.

[20] DEMOS, S., RADOUSKY, H., ALFANO, R., Deep subsurface imaging in tissues using spectral and polarization filtering, *Optics Express*, 2000, vol. 7, Issue 1, p. 23-28.

[21] BICKEL, W. S. BAILEY, W.M., Stokes vectors, Mueller matrices, and polarization of scattered light, *American Journal of Physics,* 1985, vol. 53, p. 468-478.

[22] HIELSCHER, A.H., BARTEL, S., Diffuse backscattering Mueller matrix analysis for tissue diagnostics with polarized light, *Proceedings of SPIE,* 2000, vol. 3917, p. 43-53.

[23] HONGHUI H., NAN Z., WEI L., TIANLIANG Y., RAN L., YONGHONG H., HUI M., Two-dimensional backscattering Mueller matrix of sphere-cylinder scattering medium, *Optics Letters*, 2010, vol. 35, No. 14, p. 2323-232.

[24] COLLETT, E., Measurement of the four Stokes polarization parameters with a single circular polarizer, *Optics Communications*, 1984, vol. 52, p. 77- 80.

[25] SANKARAN, V., WALSH, J. T.. Jr., MAITLAND, D. J., Comparative study of polarized light propagation in biological tissues, *Journal of Biomedical Optics*, 2002, vol. 7, p. 300- 306.

[26] AMBIRAJAN, A., LOOK, D. C. Jr., A backward Monte Carlo study of the multiple scattering of a polarized laser beam, *Journal of Quantum Spectroscopy and Radiation Transfer*, 1997, vol. 58. No. 2, pp. 171-192.

[27] GANGNUS, S. V., MATCHER, S. J., MEGLINSKI, I.V., Monte Carlo modeling of polarized light propagation in biological tissues, *Laser Physics,* 2004, vol. 14, No. 6, p. 886–891.

[28] RAMELLA-ROMAN, J.C., PRAHL, S.A., JAQUES, S.L. Three Monte Carlo programs of polarized light transport into scattering media: part I, *Optics Express,* 2005, vol. 13, No. 12, p. 4420-4438.

[29] MENZEL, R., *Photonics. Linear and nonlinear interactions of laser light and matter*, 2nd Edition, Springer Verlag, Berlin, 2007, ISBN: 978-3-540-23160-8.

[30] TUCHIN, V.V., Light scattering study of tissues, *Uspekhi Fizicheskikh Nauk,*1997, vol. 40, No. 5, p. 495-515.

[31] GHOSH, N., WOOD, M., VITKIN, A., Polarized light assessment of complex turbid media such as biological tissues using Mueller matrix decomposition, *Handbook of Photonics for Biomedical Science*, Chapter 9, TUCHIN, V.V. (Ed.), CRC Press, Taylor and Francis Publishing, London, 2010, p. 253–282, ISBN: 978-1-4398-0628-9

[32] FANJUL-VÉLEZ, F., ARCE-DIEGO, J-L., Polarimetry of birefringent biological tissues with arbitrary fibril orientation and variable incidence angle, *Optics Letters*, 2010, vol. 35, Issue 8, p. 1163-1165.

[33] MURPHY, A.B., Modified Kubelka–Munk model for calculation of the reflectance of coatings with optically-rough surfaces, *Journal of Physics D: Applied Physics,* 2006, vol. 39, p. 3571-3581.

[34] ROZÉ, C., GIRASOLE, T., TAFFORIN, A-G., Multilayer four-flux model of scattering, emitting and absorbing media, *Atmospheric Environment*, 2001, vol. 35, Issue 30, 5125-5130.

[35] MOURANT, J. R., BOYER, J., HIELSCHHER, A.H., BIGIO, I.J., Influence of the scattering phase function on light transport measurements in turbid media performed with small source–detector separations, *Optics Letters*, 1996, vol. 21, No. 7, p. 546-548.

[36] LEYRE, S., DURINCK, G., van GIEL, B., SAEYS, W., HOFKENS, J., DECONINK, G., HANSELAER, P., Extended adding-doubling method for fluorescent applications, *Optics Express*, 2012, vol. 20, Issue 16, p. 17856-17872.

[37] WOOD, M. F. G., GUO, X., VITKIN, I.A., Polarized light propagation in multiply scattering media exhibiting both linear birefringence and optical activity: Monte Carlo model and experimental methodology, *Journal of Biomedical Optics,* 2007, vol. 12, paper ID 014029.

[38] LIEMERT, A., KIENLE, A., Comparison between radiative transfer theory and the simplified spherical harmonics approximation for a semi-infinite geometry, *Optics Letters*, 2011, vol. 36, Issue 20, p. 4041-4043.

[39] KUBELKA, P., MUNK, F., Ein Beitrag zur Optik der Farbanstriche, *Zeitschrifts für Technische Physik*, 1931, vol. 12, p. 593–601.

[40] KALTENBACH, J.M., KASCHKE, M., Frequency- and time-domain modeling of light transport in random media, *SPIE Series ISII*, 1993, p.65-86.

[41] GIBSON, R. R., MARSHALL, H. L.,, CANIZARES, C. R., LEE, J.C., The high-resolution X-ray spectrum of MR 2251–178 obtained with the *Chandra* HETGS, *The Astronomical Journal,* 2005, vol. 627, p. 83-92.

[42] COURJON, D., BAINIER, C., *Le champ proche optique. Théorie et applications*, Springer Paris, 2001, ISBN: 2-287-59720-4.

[43] HEBDEN, J.C., ARRIDGE, S.R., DELPY, D.T., Optical imaging in medicine: 1. Experimental techniques, *Physics in Medicine and Biology,* 1997, vol. 42, p. 825–840.

[44] ARRIDGE, S. R., SCHWEIGER, M., HIRAOKA, M., DELPY, D.T., A finite element approach for modeling photon transport in tissue, *Medical Physics*, 1993, vol. 20, No. 2, p. 299-309.

[45] SCHÖBERL, J.: NETGEN - An advancing front 2D/3D-mesh generator based on abstract rules. *Computing and Visualization in Science*, 1997, vol. 1, No. 1, p. 41-52.

[46] METROPOLIS, N., ULAM, S., The Monte Carlo method, *Journal of the American Statistical Association*, 1949, vol. 44, No. 247, p. 335-341.

[47] XU, M., Electric field Monte Carlo for polarized light propagation in turbid media, *Optics Express,* 2004, vol. 12, p. 6530–6539.

[48] COTÉ, D., VITKIN, I. A., Robust concentration determination of optically active molecules in turbid media with validated three-dimensional polarization sensitive Monte Carlo calculations, *Optics Express,* 2005, vol. 13, p. 148-163.

[49] WANG, L., JACQUES, S. L., ZHENG, L., MCML—Monte Carlo modeling of light transport in multi-layered tissues, *Computing Methods and Programs in Biomedicine,* 1995, vol. 47, p.131–146.

[50] FANJUL-VÉLEZ, F., SAMPERIO-GARCÍA, D., PEREDA-CUBIÁN, D., ARCE-DIEGO, J-L., Mueller matrix group theory formalism for tissue imaging polarimetry contrast increase, in *Proceedings of the 29th Annual International Conference of the IEEE EMBS,* Lyon, France, 2007, p. 3339-3342.

[51] SWAMI, M.K., MANHAS, S., PATEL, H., GUPTA, P.K., Mueller matrix measurements on absorbing turbid medium, *Applied Optics*, 2010, vol. 49, No. 18, p. 3458-3464.

[52] ABUBAKER, H.M., Use of scattering matrix in body tissue investigation, *Proceeding of 16th Conference STUDENT EEICT 2010,* 2010, vol. 5, p.54-58, ISBN: 978-80-214-4080-7.

[53] GHOSH, N., PATEL, H. S., GUPTA, P.K., Depolarization of light in tissue phantoms – effect of a distribution in the size of scatterers, *Optics Express,* 2003, vol. 11, No. 18, p. 2198-2205.

[54] MORGAN, S.P., KHONG, M.P., SOMEKH, M.G., Effects of polarization state and scatterer concentration on optical imaging through scattering media, *Applied Optics,* 1997, vol. 36, No. 7, p. 1560-1565.

[55] RAMACHANDRAN, H. NARAYANAN, A., Two-dimensional imaging through turbid media using a continuous wave light source, *Optics Communications*, 1998, vol..154, p. 255–260.

[56] ALEXANDER, M., DALGLEISH, D.G., Dynamic light scattering techniques and their applications in food science, *Food Biophysics*, 2006, vol.1, No.1, p.2-13.

[57] ABUBAKER, H.M., TOMÁNEK, P., Stokes scattering polarimetry of biological tissues, In *Proceedings of New trends in Physics* (NTF 2012). P. KOKTAVÝ, J. BRÜSTLOVÁ (Eds.), Brno University of Technology, 2012, p.145-148, ISBN:978-80-214-4594-9.2

[58] ABUBAKER, H.M., TOMÁNEK, P., GRMELA, L., Measurement of dynamic variations of polarized light in processed meat due to aging, *Proceedings of SPIE,* 2011, vol. 8306, paper ID 8036O01.

[59] TOMÁNEK, P., MIKLÁŠ, J., ABUBAKER, H. M., GRMELA, L., Optical sensing of polarization states changes in meat due to the ageing. *AIP Conference Proceedings*, 2010, vol. 1288, No. 1, p. 127-131.

[60] ABUBAKER, H., Back-scattered polarized light and its application in tissue aging investigation. In *Student EEICT Proceedings of the 17th conference, vol. 3.* Brno, Novpress, s.r.o. Brno. 2011. p.306-310.

[61] ABUBAKER, H., TOMÁNEK, P., Backward multiscattering and transport of photons in biological tissue: Experiment and simulation, *Advances in Electrical and Electronic Engineering* - internetový časopis (http://advances.utc.sk). 2012, vol. 10, No.2, p.115-119.

[62]   ABUBAKER, H., Multiple scattering of polarized light in birefrengent turbid media: A Monte Carlo simulation, In *Proceedings of the 18th Conference STUDENT EEICT 2012,* vol. 3 Brno, Litera Brno. 2012. p.214-218.

[63]   ABUBAKER, H., Back-scattered polarized light and its application in tissue aging investigation. In *Student EEICT Proceedings of the 17th conference,* vol. 3. Brno, Novpress, s.r.o. Brno, 2011, p.306-310.

[64]   ABUBAKER, H., TOMÁNEK, P., Polarization of scattered light in biological tissue, *Proceedings of SPIE*, 2011, vol. 8306, paper ID.08306OO1 (8p.).